Insulin-like Growth Factor I Receptor Gene Function in Mammary Gland Development: *In Vivo* and *In Vitro* Studies

by

Geetanjalee Modha

A thesis submitted to the Faculty of Graduate Studies in partial fulfillment of the requirements for the Degree of

Master of Science

Department of Pathology
Faculty of Medicine
University of Manitoba
Winnipeg, Manitoba

THE UNIVERSITY OF MANITOBA

FACULTY OF GRADUATE STUDIES

*****

COPYRIGHT PERMISSION PAGE

Insulin-like Growth Factor I Receptor Gene Function in Mammary Gland Development:

***In Vivo* and *In Vitro* Studies**

BY

Geetanjalee Modha

A Thesis/Practicum submitted to the Faculty of Graduate Studies of The University of Manitoba in partial fulfillment of the requirements of the degree of

MASTER OF SCIENCE

ABSTRACT

The insulin like growth factor I (IGF-I) and its receptor, IGF-IR, have been implicated to play an important role in normal and abnormal mammary gland growth and development. The mechanism by which the IGF-I/IGF-IR mediate their effect on growth and differentiation in the mammary gland is not well understood. To gain further insight into the role of the IGF-I/IGF-IR during mammary gland morphogenesis, the spatial and temporal pattern of IGF-IR gene expression during different stages of normal mouse mammary gland development was systematically examined. IGF-IR gene expression was analyzed using reverse transcription (RT) - real time PCR and *in situ* hybridization, and protein analysis was carried out using Western blot analysis. The levels of both gene and protein expression were significantly lower during late pregnancy and lactation but recovered during involution to the level of that observed in the virgin and early pregnant mammary gland. Through *in situ* hybridization techniques, it was further demonstrated that the IGF-IR mRNA was expressed at each stage of postnatal development. The transcripts were localized to the proliferating ductal epithelium of the mammary glands of virgin mice and in the ductal and alveolar epithelium of the mammary glands during pregnancy and lactation. In the involuting mammary gland, the transcripts were identified in the ductal epithelium. The differential pattern of IGF-IR gene expression suggests that is involved in mouse mammary gland morphogenesis and that IGF-I/IGF-IR may be important during some phases of development more than others.

The tetracycline regulatory system was used to further investigate whether it could be used to conditionally regulate the IGF-IR gene *in vitro*. Such a system would allow to more directly address IGF-IR function in mammary epithelial cells. MCF-7

human breast cancer cells were stably co-transfected with the tetracycline transactivator (rtTA) driven by the CMV promoter (CMV-rtTA) and a mutant dominant negative IGF-I receptor, IGF-IR-DN, fused to the tetracycline operator (tetOPh$_{CMV}$-IGF-IR-DN). The stable integration and expression of the rtTA plasmid was confirmed by Southern blot and RT-PCR analysis. IGF-IR-DN gene expression was observed in four independent clonal lines. The truncated β-subunit of the IGF-IR-DN was detected only in the stably transfected doxycycline-induced cells and was absent in both control cells and in uninduced cells. Furthermore, IGF-IR-DN protein expression was up-regulated (3-6 fold) in stably transfected doxycycline-induced cells compared to the uninduced cells. Autophosphorylation of the IGF-IR and phosphorylation of the downstream substrate, insulin receptor substrate-1 (IRS-1), was not inhibited in doxycycline and IGF-I treated cells. However, IGF-I induced cell proliferation was significantly reduced (1.4 fold) in doxycycline-induced cells compared to uninduced cells but no change in cell morphology was observed in these cells. These results demonstrated that the IGF-IR-DN gene expression was inducible in the stably transfected mammary epithelial cells and the mutant gene was efficiently translated. The data also suggest that activation of downstream substrates other than IRS-1 may be critical for optimal cell proliferation in this *in vitro* model system. These results suggest that the tetO-IGF-IR-DN model may be a useful system by which to further address IGF-I/IGF-IR signaling and function in normal mammary gland development, and ultimately breast cancer.

ACKNOWLEDGMENTS

First and foremost I would like to acknowledge my supervisor, Dr. Yvonne Myal, for her dedication, enthusiasm and strive to achieve the best in both research and in life. She has been there every step of the way and has helped me accomplish my goals in research. I will always be indebted to her for her role as mentor and her sincere support in my studies.

I thank my examining committee, Dr. Ian Adamson and Dr. Bob Shiu, for keeping their doors open for discussions. I am humbled to have two such knowledgeable and expert individuals as members of my committee. I especially thank Dr. Shiu for his insightful discussions regarding my project and helping me follow the right direction towards success of my experiments.

I am deeply grateful to Anne Blanchard for all her help in learning techniques, the many discussions and her friendship. Many thanks to Nicole DeCorby and Beverley Lee, my fellow students and friends, for providing shoulders to cry upon and hands to 'high-five' to celebrate the success of an experiment. No one knows better than a fellow student the excitement of seeing a black band on an X-ray film! I would also like to acknowledge Janine Sidorchuk for the stable transfection of the MCF-7 cells.

I would like to thank several members of the Departments of Pathology and Physiology for their help in learning experimental techniques, discussions, encouragement and their friendships. Thank you to Dr. Bill Orr, the department head, for all your help, encouragement and genuine interest in my career goals. Many thanks to Barbara Iwasiow (for teaching me techniques and for your valuable advice), Marcello Venditti and Alison Yarmill for their technical help and valuable advice. I would also like to thank Dr. Peter Watson, Molly Pind (there's no question that you cannot answer), Adewale Adeyinka, Sandra Troup, Ethan Emberley, Andrea Fristensky (your kind words and encouragement are deeply appreciated), Ladislav Tomes, Linda Snell, Yulian Niu, Charlton Cooper and Sylvia Santos for their support, friendships and aid in my research project.

Thank you to all my friends and family for their support and love and seeing me through the good and not-so-good times. Thanks for being there for me and also for sharing with me the road towards this final joyous achievement.

ABBREVIATIONS

α	Alpha
β	Beta
µg	Microgram
µl	Microlitre
µm	Micrometer
µM	Micromolar
Ab	Antibody
ANOVA	Analysis of Variance
bp	Base pairs
BBS	BES-buffered solution
BES	N, N-bis-(2-hydroxyethyl) aminoethanesulfonic Acid
BSA	Bovine Serum Albumin
°C	Degree Celsius
cDNA	Complimentary Deoxyribonucleic Acid
$CaCl_2$	Calcium Chloride
CCD	Charge-Coupled Device
CO_2	Carbon Dioxide
CM	Complete Medium
CMV	Cytomegalovirus
cpm	Counts Per Minute
dATP	Deoxyadenosine Triphosphate
dCTP	Deoxycytidine Triphosphate
dGTP	Deoxyguanosine Triphosphate
dNTP	Deoxynucleoside Triphosphate
dTTP	Deoxythymidine Triphosphate
ddH_2O	Deionized Distilled Water
DEPC H_2O	Diethyl Pyrocarbonate Water
DMEM	Dulbecco's Modified Eagle Medium
DMSO	Dimethylsulfoxide
DNA	Deoxyribonucleic Acid
DNase	Deoxyribonuclease
DTT	Dithiotreitol
Dox	Doxycycline
DN	Dominant Negative
EB	Elution Buffer
E. coli	*Escherichia coli*
EDTA	Ethylene Diamine Tetraacetic Acid
EGF	Epidermal Growth Factor
ELISA	Enzyme Linked Immunosorbent Assay
FBS	Fetal Bovine Serum
FGF	Fibroblast Growth Factor
g	Gram
GAPDH	Glyceraldehyde-3-Phosphate Dehydrogenase
GH	Growth Hormone

GRB	Gel Running Buffer
Grb2	Growth Factor Receptor Bound-2
HCl	Hydrochloric Acid
HSV	Herpes Simplex Virus
IGFBP	IGF Binding Protein
IGF-I	Insulin-like Growth Factor-I
IGF-II	Insulin-like Growth Factor-II
IGF-IR	Insulin-like Growth Factor-I Receptor
IGF-IIR	Insulin-like Growth Factor-II Receptor
IR	Insulin Receptor
IRS-1	Insulin Receptor Substrate-1
kb	Kilobase
KCl	Potassium Chloride
kDa	Kilodalton
kg	Kilogram
KH_2PO_4	Potassium Phosphate
K_2HPO_4	Potassium Phosphate Monobasic
LB	Luria-Bertani
M	Molar
M_r	Relative Molecular Weight
MAPK	Mitogen-Activated Protein Kinase
MCF-7	Michigan Cancer Foundation-7
MCID	MicroComputer Imaging Device
mg	Milligram
$MgCl_2$	Magnesium Chloride
$MgSO_4$	Magnesium Sulphate
ml	Milliliter
mm	Millimeter
mM	Millimolar
MMLV	Moloney Murine Leukemia Virus
MOPS	3N-Morpholino-Propane Sulfonic Acid
mRNA	Messenger Ribosomal Ribonucleic Acid
N_2	Nitrogen
NaCl	Sodium Chloride
Na_2HPO_4	Sodium Phosphate Dibasic Anhydrous
NaH_2PO_4	Sodium Phosphate Monobasic
NaOAc	Sodium Acetate
NaOH	Sodium Hydroxide
Na_3VO_4	Sodium Orthovanadate
neo	Neomycin
nM	Nanomolar
OD	Optical Density
PAGE	Polyacrylamide Gel Electrophoresis
PBS	Phosphate Buffered Saline
PCR	Polymerase Chain Reaction
Ph_{CMV}	Cytomegalovirus-derived Minimal Promoter

PI 3-kinase	Phosphatidylinositol 3-kinase
PMSF	Phenylmethylsulfonyl Fluoride
PTC	Programmable Thermal Controller
RIPA	Radioimmunoprecipitation Buffer
RNA	Ribonucleic Acid
RNase	Ribonuclease
RPM	Revolutions Per Minute
RT	Reverse Transcription
rtTA	Reverse Tetracycline Transcriptional Activator
SDS	Sodium Dodecyl Sulfate
SFM	Serum Free Medium
Shc	*src* Homology Domain-Containing
SSC	Sodium Chloride/Sodium Citrate
SSPE	Sodium Chloride/Sodium Phosphate EDTA
TAE	Tris/Acetate
Taq	Thermus Aquaticus
TBE	Tris/Borate Electrophoresis
TBS	Tris Buffered Saline
TBST	Tris Buffered Saline, Tween
TE	Tris/EDTA
TEB	Terminal End Bud
tetO	Tetracycline Operator
tetR	Tetracycline Repressor
TGF-α	Transforming Growth Factor alpha
Tris-Cl	Tris Hydrochloride
TEMED	N, N, N′, N′-tetramethylethylenediamine
tTA	Tetracycline Transcriptional Activator
U	Unit
UTP	Uridine Triphosphate
UTR	Untranslated Region
V	Volts
v/v	Volume per Volume
w/v	Weight per Volume
1X	One times
10X	Ten times
18S rRNA	18S Ribosomal Ribonucleic Acid
^{32}P	Phosphorous-Isotope 32
^{35}S	Sulphate-Isotope 35

LIST OF FIGURES

LIST OF TABLES

TABLE OF CONTENTS

1. INTRODUCTION

1.1. The Mammary Gland

The mammary gland is a specialized organ involved in the production of the milk, which is essential for the survival of the developing young of most mammals (Leeson *et al.,* 1985). The pattern of development of the gland is unique in that unlike most epithelial organs, its morphogenesis occurs postnatally in the juvenile and adult animal (Silberstein, 2001; Buhler *et al.,* 1993). Growth and development of the mammary gland can be divided into 4 stages: virgin, pregnancy, lactation and involution. It is only after lactation that differentiation is complete in mammals (Leeson *et al.,* 1985; Silberstein, 2001). There are many important influences in the mammary gland during growth and development – these include specific hormones and growth factors, as well as cell-cell contact, extracellular matrix and neural inputs (Dunbar and Wysolmerski, 2001).

1.1.1. Structure of the Mouse Mammary Gland

The mouse mammary gland consists of 15 to 20 lobes, each of which is an actual gland with a duct opening at the apex of the nipple (Leeson *et al.,* 1985; Silberstein, 2001). Each glandular lobe is surrounded by interlobar connective tissue that contains many fat cells. Intralobular ducts drain into interlobular ducts that join to form a single excretory duct from each lobe, called the lactiferous duct. The lactiferous duct progresses through the nipple and dilates into a lactiferous sinus at the apex of the nipple. The structural and functional development of the mammary gland can be divided into distinct stages: fetal development, growth of the gland at puberty, development and differentiation of the gland during pregnancy and lactation, and finally the involution of the gland.

1.1.2. Development of the Mouse Mammary Gland

At birth, the rudimentary mammary gland consists of a primary duct connected to the nipple with a few branching ducts (Figure 1) (Buhler *et al.,* 1993; Silberstein, 2001). During the first few weeks, growth of the mammary gland is minimal. At 4 weeks of age, at the onset of puberty, terminal end buds form at the distal ends of the immature mammary ducts (Buhler *et al.,* 1993) under the influence of ovarian and pituitary hormones (Silberstein, 2001). The immature ductal system differentiates and matures by enlarging, branching and extending through the terminal end buds. The resulting ductal tree structure is finally established by 8 weeks of age – at the end of puberty (Silberstein, 2001; Coleman-Krnacik and Rosen, 1994). Growth ceases until the onset of pregnancy.

Due to the alteration in circulating hormones during pregnancy, the gland undergoes extensive changes in preparation for lactation. Rapid epithelial (ductal cell) proliferation begins at the expense of the fatty connective tissue. The terminal end buds grow and branch out, forming tiny outpocketings or alveoli (Figure 1), which contain secretory cells. The alveolar structures develop in the spaces between the ductal tree network and act as the major functional units during lactation. The alveoli are generally empty early in pregnancy but become secretory in the second half of pregnancy (Silberstein, 2001; Leeson *et al.* 1985). By the end of pregnancy, the interlobular and intralobular fat and connective tissue is reduced and the 15-20 lobes become distinct entities. At this stage, the interlobular ducts, a lactiferous sinus with secretory product in its lumen is found in the interlobular connective tissue (di Fiore, 1987). Colostrum, a cloudy, watery fluid (the first milk) is secreted at the end of pregnancy (Leeson *et al.,* 1985).

Lactation is characterized by the active secretion of milk following parturition. Many alveoli become distended by milk and appear as saccules (Silberstein, 2001; Leeson *et al.,* 1985). In addition, there is further reduction in the interlobar connective tissue (Figure 1).

Involution of the mammary gland occurs following weaning. The gland undergoes apoptosis (programmed cell death) and major restructuring (Strange *et al.*, 1992). Apoptosis of secretory alveoli is widespread and the connective tissue and fat becomes abundant again, resulting in a duct system similar to that of the prepregnant or virgin mammary gland (Figure 1). Involution of the mammary gland can be divided into two distinct stages (Lund *et al.*, 1996). The first stage is reversible. Cell death is induced by local signals in the presence of survival factors, the systemic lactogenic hormones (Lund *et al.*, 1996; Marti *et al.*, 1999). The second stage involves a decrease in the level of the systemic lactogenic hormones and the activation of proteinase-dependent pathways (Lund *et al.*, 1996). Active tissue remodeling, destruction of alveolar structures and basement membranes, resulting in the irreversible loss of the differentiated function of the mammary gland is characteristic of this stage (Lund *et al.*, 1996).

1.1.3. The Influence of Hormones and Growth Factors on the Growth and Development of the Mammary Gland

Several hormones, as well as growth and differentiating factors, play an essential and critical role in the growth and development of the mammary gland (Rillema, 1994; Dunbar and Wysolmerski, 2001; Silberstein, 2001). Circulating hormones, estrogen and progesterone, influence growth and development of the mammary gland. At pregnancy, these circulating hormones stimulate duct cells to proliferate and promote the growth and

formation of the alveoli from the terminal end buds (Alberts *et al.,* 1989). Growth hormone (GH) has been shown to regulate end bud and ductal growth (Buhler *et al.,* 1993). Moreover, milk secretion following parturition is regulated by prolactin, a lactogenic hormone (Buhler *et al.,* 1993).

Developmental processes of the parenchymal (epithelial) and stromal elements of the mammary gland are facilitated by growth factors in an autocrine (the cell-induced signal affects itself and surrounding cells), paracrine (the cell-induced signal affects cells in the immediate vicinity) and/or endocrine fashion (long-range signaling) (Rillema, 1994; Dunbar and Wysolmerski, 2001). Thus, both systemic and locally produced signaling molecules, acting as positive and negative signaling agents, are involved in mammary gland development (Coleman-Krnacik and Rosen, 1994).

Gene expression of several growth factors during mammary gland development has been shown to be important in ductal and alveolar development. Their control and coordinated expression in precisely the correct temporal and spatial patterns are crucial for normal development (Coleman-Krnacik and Rosen, 1994). The expression patterns of the epidermal growth factor (EGF), fibroblast growth factor (FGF), and transforming growth factor α (TGF-α) are well documented (Dunbar and Wysolmerski, 2001; Silberstein, 2001; Coleman-Krnacik and Rosen, 1994). FGF is required for lobuloalveolar development of the mammary gland during pregnancy (Silberstein, 2001; Jackson *et al.,* 1997) and TGF-α has been shown to interact with other growth factors in mediating ductal growth during puberty (Snedeker *et al.*, 1991). The insulin-like growth factor (IGF) family is implicated to play an important role in normal mammary gland development (Silberstein, 2001; Kleinberg *et al.*, 2000; Hadsell and Bonnette, 2000) and

in breast transformation and breast cancer (Forsyth, 1989; Grimberg and Cohen, 2000; Werner and LeRoith, 2000; Surmacz, 2000).

1.2. The Insulin-like Growth Factor Family

The insulin-like growth factor (IGF) family is a complex system of cellular modulators that play an essential role in normal growth and development (Liu *et al.*, 1993; Baker *et al.*, 1993; Butler and LeRoith, 2001). The IGF family consists of two ligands, IGF-I and IGF-II, and their receptors, IGF-I receptor (IGF-IR) and the IGF-II receptor (IGF-IIR). Several groups have shown the essential role of IGFs in promoting growth both *in utero* and *ex utero* (Liu *et al.*, 1993; Baker *et al.*, 1993; Dechiara *et al.*, 1990). Intrauterine growth retardation was observed in mice lacking either IGF-I or IGF-II (Baker *et al.*, 1993). IGF-IR gene knockout mice were born with reduced birth weight and died soon after birth due to respiratory failure (Liu *et al.*, 1993). IGF-II knockout mice, though retarded in growth, were normal (Dechiara *et al.*, 1990). IGF-IIR knockout mice, in contrast, exhibited fetal overgrowth that was lethal (Ludwig *et al.*, 1996).

IGF effects are modulated by six IGF binding proteins (IGFBPs) (LeRoith *et al.*, 1995). The IGF binding proteins associate with free IGF-I peptides preventing their binding to the IGF-IR. In addition, IGFBPs bind to the IGF-II, thereby interfering with binding to the IGF-IR and thus reducing the competition between IGF-I and IGF-II.

1.2.1. The IGF-I Receptor

Both IGF-I and IGF-II bind to the IGF-IR, a tyrosine kinase membrane protein, with high affinity (Lorenzino, 1998). Upon activation, the IGF-I receptor undergoes

autophosphorylation, transferring the signal into the cell and eventually to the nucleus where regulatory gene products are activated. IGF-IIR lacks tyrosine activity and binds IGF-I with lower affinity. IGF-IIR acts in regulating the availability of the IGF-II by binding to it and also in modulating the interaction of the ligand with the IGF-I receptor (Ludwig *et al.*, 1996; Lorenzino, 1998).

1.2.1.1. Gene Structure

The human IGF-IR gene has been fully characterized (Abbott *et al.*, 1991). It is located on chromosome 15 and is encoded on 21 exons spanning 100 kilobases (kb) of genomic DNA (Lorenzino, 1998). The mouse IGF-IR gene has also been partially characterized (Wada *et al.*, 1993). The α-subunit of the mouse is very similar (91% homology) to the human IGF-IR α-subunit (Wada *et al.*, 1993).

The organization of the human IGF-I receptor into several different functional domains is reflected in the arrangement of the exons or coding regions of the gene (LeRoith *et al.*, 1995; Ward *et al.*, 2001; Adams *et al.*, 2000). Exons 1-3 encode the 5' untranslated region (UTR), the signal peptide, the non-cysteine-rich N terminal region and the cysteine rich domain of the α-subunit. The remaining sequence of the α-subunit is encoded by exons 4-10. Exon 11 encodes the peptide cleavage site (Arg-Lys-Arg-Arg) which results in the α- and β-subunits of the protein from the precursor protein. The β-subunit is encoded by exons 12-21; exon 14 encodes the transmembrane domain and the intracellular tyrosine kinase domain is coded by exons 16-20. The β-subunit can be differentiated into three major parts including the juxtamembrane domain, the tyrosine kinase domain and the C-terminal tail. The tyrosine kinase domain forms a fundamental portion of the β-subunit. Exon 21 contains the 3' UTR sequences.

An 11 kb mRNA transcript is transcribed from both the human (GenBank accession number XM133508) and mouse (GenBank accession number NM000875) IGF-IR genes and often a 7 kb band (only in humans) (LeRoith *et al.,* 1995). The coding region of IGF-IR mRNA spans about 5 kb. The coding region is flanked by a 1 kb 5' UTR and a 3' UTR that spans 5 kilobases.

The IGF-IR is a low abundance transcript but its expression is ubiquitous (LeRoith *et al.*, 1995); it is found in several types of mammalian tissues and cells (Bondy *et al.*, 1990; Werner *et al.*, 1989). In the rat, IGF-IR mRNA levels are most abundant during the embryonic stages and decrease to lower levels in adult animals (LeRoith *et al.*, 1995). Intermediate levels of mRNA are detected in the kidney, stomach, lung, testes and heart, while very low, almost undetectable, levels of mRNA are detected in the liver (Werner, 1999).

1.2.1.2. Protein Structure

The IGF-I receptor is a disulfide linked heterotetrameric ($\alpha_2\beta_2$) transmembrane protein (Figure 2). The α-subunit forms the extracellular domain while the β-subunit forms the transmembrane domain and the intracellular cytoplasmic domain. Both the α- and β-subunits are initially encoded and translated into a single αβ-precursor protein (Figure 3) which is 1367 amino acids in length. The precursor protein undergoes several co- and post-translational modifications such as glycosylation and removal of the signal peptide, to generate the mature α- and β-subunits (Ward *et al.*, 2001; Adams *et al.*, 2000). Separate α- and β-subunits are produced due to proteolytic cleavage at the cleavage site (Arg Lys Arg Arg; amino acid positions 707 to 710). The subunits are then linked by disulfide bonds (α-α and α-β disulfide bridges) forming the β-α-α-β receptors

(Lorenzino, 1998). The extracellular α-subunit contains the cysteine rich portion that is defined as the ligand binding site. The transmembrane domain of the β-subunit (amino acid positions 906 to 929) is composed of a unique 24 amino-acid hydrophobic sequence and the cytoplasmic portion of the β-subunit contains a tyrosine kinase catalytic domain (amino acid positions 973 to 1229). Sites for phosphorylation are clustered in a group of three tyrosines located at positions 1121, 1135 and 1136 (Figure 2, 3). The tyrosine residues are essential for signal transduction to occur (Ward *et al.*, 2001; Adams *et al.*, 2000).

1.2.1.3. Signal Transduction

The binding of the IGF-I to the membrane-bound α-subunit of the IGF-I receptor results in trans-phosphorylation of the two β-subunits and the subsequent activation of the signal transduction pathway (Lorenzino, 1998). Tyrosine kinase activity in the β-subunit is critical for receptor signaling. IGF function is abolished when the catalytic domain or the major autophosphorylation cluster (Tyr 1121, 1135, 1136) is mutated or not present (LeRoith *et al.*, 1995).

Upon activation of the receptor or autophosphorylation, the signal is propagated via several cytosolic and nuclear mediators (Figure 4) that ultimately lead to transcriptional activation of regulatory gene products (Samani and Brodt, 2001; Butler *et al.*, 1998). Early growth response genes such as c-fos and c-jun and cell cycle regulatory genes such as CDC2 and cyclin D1 are a few examples (Rubin and Baserga, 1995; Dupont and LeRoith, 2001). Furthermore, IGF-I induced signaling pathways leading to the activation of ras proteins and mitogen-activated protein kinases (MAP kinases) are required for optimal cell proliferation (Rubin and Baserga, 1995). The activation of ras

and other regulatory gene products is not direct but occurs via downstream substrates. Well-known substrates of the IGF-I receptor include the insulin receptor substrate-1 (IRS-1), the p85 regulatory subunit of phosphatidylinositol (PI) 3-kinase, the src homology domain-containing (Shc) protein, the growth factor receptor bound-2 (Grb2) protein and the CrkII and Crk-like (CrkL) proteins (Butler *et al.*, 1998; Adams *et al.*, 2000; Samani and Brodt, 2001).

The IRS-1, a tyrosine containing substrate, is a major substrate of the IGF-I receptor. It is well documented that the mitogenic actions of the IGF-IR are mediated through the IRS-1 (Samani and Brodt, 2001; White and Yenush, 1998; Blakesley *et al.*, 1996). Mice that do not express the IRS-1 are retarded in growth (Butler *et al.*, 1998). Additionally, the mitogenic response to IGF-I is reduced considerably in cultured cells derived from IRS-1 null mice (Butler *et al.*, 1998). The IGF-IR is known to influence multiple signaling pathways through the phosphorylation of IRS-1 (LeRoith *et al.*, 1995). The IRS-1 has over 20 potential tyrosine phosphorylation sites. Hence, it functions as a 'docking' protein, allowing the binding of proteins that act in further transmission of the signal. These signaling proteins include the p85 subunit of the PI 3-kinase and the adapter proteins, Grb2 protein and CrkII (Samani and Brodt, 2001).

The IGF-I receptor is linked to the phospholipid signal transduction pathway, via the IRS-1, which regulates PI 3-kinase activity (Butler *et al.*, 1998; Dupont and LeRoith, 2001). The PI 3-kinase is a heterodimer made up of an 85 kDa regulatory subunit and a 110 kDa catalytic subunit. The activation of the p110 catalytic subunit of phosphatidylinositol 3-kinase is mediated by the binding of the phosphorylated IRS-1 to the p85 subunit of the PI 3-kinase. Alternatively, the IGF-IR can activate PI 3-kinase by

binding directly to the p85 subunit. Using dominant negative PI-3 kinase mutants and other inhibitors of PI-3 kinase, evidence suggests that this pathway plays an important role in the anti-apoptotic effects of IGF-I (Butler *et al.*, 1998). Akt, a serine/threonine kinase, is activated through this pathway, which has been shown to have a role in the inhibition of apoptosis (Dudek *et al.*, 1997; Kulik *et al*, 1997). Indeed, anti-apoptotic effects of IGF-I are lost in cells expressing dominant-negative Akt mutants (Kulik *et al*, 1997).

Another phosphotyrosine substrate of the IGF-I receptor is the Shc (src homology domain-containing) protein (Butler *et al.*, 1998). The Shc family is made up of three proteins, p46, p53 and p66. Phosphorylated Shc associates with the adapter molecule, Grb2, which plays an essential role in regulation of the Ras-Raf-mitogen activated protein kinase (MAPK) pathway (required for optimal cell proliferation). Grb2 interacts with the guanine nucleotide exchange protein, mSos, which catalyzes the exchange of GDP for GTP on the GTP-binding protein Ras. This results in the activation of Ras and the successive activation of the MAPK pathway. IGF-I mitogenic response in Rat 1 fibroblasts has been shown to be inhibited by blocking the Shc pathway with anti-Shc antibodies (Sasaoka *et al.*, 1996).

Adapter proteins such as CrkII and Crk-like (CrkL), which mediate protein-protein interactions, have been suggested to play distinct roles in IGF-I receptor signal transduction (Butler *et al.*, 1998; Beitner-Johnson and LeRoith, 1995). Crk proteins are cellular homologs of the viral oncoprotein, v-Crk, and contain SH2 and SH3 domains (Matsuda, 1992; ten Hoeve *et al.*, 1992). The SH3 domains of the CrkII and CrkL bind to mSos, similar to the Grb2/mSos complex, and thus may play a role in the Ras pathway.

Phosphorylation of CrkII has been observed in IGF-I stimulated human embryonic kidney and NIH 3T3 mouse fibroblast cells (Beitner-Johnson and LeRoith, 1995). Furthermore, the overexpression of CrkII increases the mitogenic response of IGF-I (Beitner-Johnson *et al.*, 1996), indicating a distinct role for this adapter protein in IGF-I receptor signal transduction. Beitner-Johnson *et al.* (1996) further hypothesized that the CrkII, like the IRS-I, may be a direct substrate of the IGF-IR. However, the specific region of the IGF-I receptor that can indeed associate with and phosphorylate the CrkII is unknown.

1.2.1.4. Hybrid Receptors

The IGF-IR and the insulin receptor (IR) are similar in gene structure, with a 50-60% homology in overall sequence identity. The translated IR precursor protein is 1370 amino acids and the IGF-IR precursor is 1367 amino acids, with the highest degree of similarity (84%) in the tyrosine kinase domain (Ullrich, 1986). The end result of such close homology is the formation of hybrid insulin/IGF-I receptors. Experimental evidence indicates that when equal numbers of the IGF-I and insulin αβ-half-receptors are combined, 50% of each will form hybrid receptors (Frattali and Pessin, 1993). Several studies have shown the presence of these hybrid receptors in cell lines and tissues, including adipose tissue, skeletal muscle, heart, liver and placenta (Federici *et al.*, 1997; Bailyes *et al.*, 1997). These receptors are preferentially activated by IGF-I *in vivo,* as it is the IGF-I and not insulin that binds the hybrid receptor with high affinity. The physiological relevance of these atypical receptors is unknown.

1.2.1.5. Cell Cycle

It has been suggested that the IGF-I receptor may be responsible for maintaining the cell cycle at a normal rate (Figure 5; LeRoith *et al.*, 1995). The insulin-like growth factor influences cell proliferation by directly stimulating the passage through the cell cycle. IGF-I is required for progression through G1 into S phase, resulting in DNA synthesis and cell proliferation. The underexpression of the IGF-IR prevents this G1-S phase transition (Rubin and Baserga, 1995). IGF-I has been shown to induce expression of cyclin D1 early in G1, which is required to pass through the G1 phase. IGF-I mediated cyclin D1 gene expression may represent the importance of the role of IGF-I in cell cycle progression (LeRoith *et al.*, 1995; Dupont and LeRoith, 2001). Expression of other cell cycle modulators such as cyclin B1, cdc2 and cdk2 are increased later in the cell cycle (Furlanetto, 1994).

1.3. The Role of IGF-I/IGF-IR in Normal Development

IGF-I, which mediates its action through IGF-IR, plays an important role in regulation of the cell cycle, proliferation and apoptosis (LeRoith *et al.,* 1995; Adams *et al.*, 2001; Lorenzino, 1998). IGF-I has a dual function acting as a mitogen and a differentiation factor. It stimulates a mitogenic response in several cell types including mammary epithelial cells (Jones and Clemmons, 1995). Rubin and Baserga (1995) have demonstrated that the mitogenic effects of IGF-I are a result of specific interactions with the IGF-IR. Blockade of the IGF-I receptor such that IGF-I ligand binding is prevented results in the inhibition of mitogenesis. IGF-I also plays an important role in the regulation of the cell cycle as a progression factor (Rubin and Baserga, 1995). Regulation

of the cell cycle is critical in the normal processes of development and in the maintenance of tissues. The most convincing evidence that the IGF-I/IGF-IR play a critical role in growth and development has come from gene targeted mutagenesis (gene-knockout) studies. Knockout mice lacking the IGF-I (IGF-/-) were retarded in growth (60% of the normal birth weight) (Jones and Clemmons, 1995). Mice lacking the IGF-I receptor (IGF-IR-/-) were even smaller in size (45% of the normal birth weight) and were nonviable at birth (Liu *et al.*, 1993).

1.4. The Role of IGF-I/IGF-IR in Mammary Gland Development

In the normal mammary gland, IGF-I receptors have been localized to both stromal and epithelial cells (Campbell and Baumrucker, 1986; Dehoff *et al.*, 1998). Both *in vivo* and *in vitro* studies provide evidence that IGFs have a role in postnatal mammary gland development. *In vitro*, IGF-I and IGF-II elicit a mitogenic response in mammary epithelial cells (Rubini *et al.*, 1997; Coppola *et al.*, 1994; Jones and Clemmons, 1995). *In vivo*, IGF-I has been shown to stimulate ductal proliferation and the induction of terminal end bud and alveoli formation (Kleinberg, 2000; Hadsell and Bonnette, 2000). The interactions between growth hormone and IGF-I are also known to play a role in regulating the growth and development of the glandular structures in the breast (Pollak, 1998). It is known that growth hormone (GH) stimulates IGF-I mRNA synthesis in the mammary glands of rats (Kleinberg *et al.*, 1990) and that IGF-I can be substituted for pituitary or GH and produce the same effects on postnatal mammary gland development (Ruan *et al.*, 1992).

The overexpression of the IGF-I gene in the mammary glands of transgenic mice was shown to delay involution suggesting an important role for IGF-I/IGF-IR during this stage of development (Hadsell *et al.,* 1996; Neuenshwander *et al.*, 1996). Furthermore, using IGF-I null female mice, Ruan and Kleinberg (1999) demonstrated that mammary gland development, as measured by terminal end bud formation and branching of ducts, did not occur in the absence of IGF-I.

Richert and Wood (1999) have shown IGF-IR transcripts to be localized in the terminal end buds and ductal epithelium of the pubertal and post pubertal mammary gland. In the mammary glands of the pregnant mice, IGF-IR transcripts were found in the ductal and alveolar epithelium.

1.5. The Role of IGF-I/IGF-IR in Breast Cancer

Many breast cancer tumors overexpress the IGF-I receptor (Werner and LeRoith, 2000; Surmacz, 2000; Khandwala *et al.*, 2000). Overexpression is often associated with poor prognosis (Pollak, 1998; Khandwala *et al.*, 2000). The IGF-IR has been shown to be present in cultured breast cancer cell lines and in tumor biopsies (Surmacz, 2000; Khandwala *et al.*, 2000). IGF-IR binding has been demonstrated in breast cancer cells (Myal *et al.* 1984; Furlanetto and DiCarlo, 1984; Peyrat and Bonneterre, 1992) and IGF-I has been shown to stimulate growth of breast cancer cells in culture (Myal *et al.,* 1984; Karey and Sirbasku, 1988; Arteaga and Osborne, 1989; Dupont and LeRoith, 2001). Several studies indicate that IGF-IR was required for cellular transformation – an early event during progression to the cancerous state (Prager *et al.,* 1994; Rubin and Baserga, 1995; Valentinis and Baserga, 2001). Mouse embryo cells expressing a disrupted IGF-IR

gene failed to undergo transformation by the SV40 large T antigen and/or Ha-ras oncogene, while cells expressing the normal IGF-IR gene were easily transformed (Sell *et al.*, 1994). To demonstrate the obligatory role of IGF-IR in transformation, it was shown that the transfection of the wild type receptor cDNA into the IGF-IR-null cell lines restored the transforming ability of the SV40 large T antigen and/or Ha-ras oncogene. The resistance to transformation has also been observed in other systems in which IGF-I receptor levels have been reduced (Baserga, 2000; Kaleko *et al.*, 1990). Blocking of the IGF-IR with a monoclonal antibody, αIR-3, in human breast cancer cells inhibited the mitogenic effects of IGF-I and IGF-II (Arteaga and Osborne, 1989; Cullen *et al.*, 1990). In addition, the growth was inhibited in tumor cell lines engineered to express antisense RNA to the IGF-I receptor (Baserga, 2000). *In vivo* tumorigenesis was also inhibited in mice injected with tumor cells expressing antisense IGF-IR mRNA. Prager *et al.* (1992) have further demonstrated the requirement of IGF-IR in the establishment of transformation by using a mutant IGF-IR, which has a dominant negative effect on normal IGF-IR function. The mutant IGF-I receptor was shown to inhibit transformation/tumorigenesis both *in vitro* (Prager *et al.*, 1992) and *in vivo* (Prager *et al.*, 1994). Conversely, the overexpression of wild-type IGF-IR was shown to induce ligand-dependent transformation (Kaleko *et al.*, 1990).

To date, the mechanism by which the IGF-IR facilitates cellular transformation is not known, a mutant form of IGF-IR that induces transformation has not been isolated. Identification of mutant forms of the IGF-I receptor and the mechanisms by which the IGF-I/IGF-IR facilitate transformation may help in further understanding its role in tumorigenesis.

The balance between cell death and growth is an important determinant of tumor growth (Baserga, 1985). The extent of apoptosis, in part, determines the aggressiveness of a tumor (Fisher, 1994; Baserga, 1994). In addition to playing a critical role in tumorigenesis, the IGF-I receptor is implicated to play a protective role in programmed cell death (Jones and Clemmons, 1995). The IGF-IR inhibits apoptosis both *in vitro* (Tamm and Kikuchi, 1990) and *in vivo* (Resnicoff *et al.*, 1995). In the presence of IGF-I, cells overexpressing IGF-IR were partially resistant to etoposide-induced apoptosis, while the death of the IGF-IR negative cells was not prevented. In addition, IGF-I prevented the death of breast cancer cells by cycloheximide (an inhibitor of protein synthesis) (Geier *et al.*, 1992).

The anti-apoptotic role of IGF-IR was examined *in vivo* using a bio-diffusion chamber placed in the subcutaneous tissue of mice (Resnicoff *et al.*, 1995). Cells expressing either sense or antisense RNA to IGF-IR were placed in the bio-diffusion chambers, later removed and examined for growth, viability and evidence of apoptosis. The cells expressing IGF-IR antisense mRNA (express few IGF-I receptors) underwent apoptosis whereas control cells survived. These studies indicate that a decrease in the number of IGF-I receptors causes tumor cells to undergo apoptosis *in vivo* and *in vitro*, abrogating the protective effect of IGF-IR against cell death.

The mechanism by which IGF-IR protects cells from apoptosis is poorly understood. Some studies suggest that the anti-apoptotic effect of IGF-I/IGF-IR is likely produced via the phosphorylation of cytosolic mediators. A study by Kulik *et al.* (1997) indicates that the activation of Akt is an important step in the inhibition of apoptosis. Apoptosis was not prevented by IGF-I in cells expressing dominant negative Akt

mutants. It has been shown that upon Akt activation, BAD, a pro-apoptotic protein, is phosphorylated, thus preventing its pro-apoptotic actions (Kulik *et al.*, 1997).

1.6. Cell Culture and Animal Models

Cultured mammalian cells and transgenic mice have been extensively used to examine the role of the IGF-IR in normal development and in breast cancer (Hadsell and Bonnette, 2000; Werner and LeRoith, 2000). Gene overexpression and gene knockouts are some of the techniques used to study gene function. However, these methods are limited as a genetic change can result in embryonic lethality, undermining studies on adult animals. Furthermore, some knockout strategies affect every cell in the animal, thus it is problematical to observe the changes due to the gene of study in a complex phenotype. Such approaches make it difficult to answer specific questions about gene function. Recent strategies have been developed that allow tight, regulated control of gene expression (Gossen *et al.*, 1995; Ryding *et al.*, 2001). The gene expression can be turned 'on' or 'off' using a specific stimulus, at any point during embryonic or postnatal development. The cre-lox recombinant system and the tetracycline regulated system are powerful tools for regulated transgene expression (Ryding *et al.*, 2001). These strategies can be used to by-pass neonatal lethality by delaying expression to later time points. In addition, tissue specific promoters can be used to restrict expression of the gene to a particular tissue or cell type (Ryding *et al.*, 2001). Therefore, these methods allow temporal and spatial control of gene expression. The tetracycline regulated system offers an advantage over the cre-lox recombinant system in that transgene expression can be turned on and off rapidly and reversibly, allowing more flexibility for gene regulation (Ryding *et al.*, 2001).

1.6.1 The Tetracycline-Controlled Gene Expression System

The ability to regulate gene expression in cultured mammalian cells and in transgenic mice has become an essential tool to study gene function. The tetracycline-controlled gene expression system designed by Gossen and Bujard (1992) allows stringent control, temporal and spatial, of the expression of an individual gene.

The tetracycline-controlled gene expression system (Tet system) exploits pathways that control the tetracycline resistance gene in *Escherichia coli*. This gene is negatively regulated by the tetracycline repressor (tetR) protein, which binds to tetracycline operator (tetO) sequences in the promoter. Transcriptional repression is relieved by tetracycline, which binds to tetR with a high affinity. Thus, tetracycline resistance is regulated by tetracycline itself in an on/off manner.

The Tet system, used to conditionally regulate gene expression, has two components: i) a tetracycline transcriptional activator (tTA) and ii) a cytomegalovirus (Ph_{CMV})-derived minimal promoter fused with the tetO sequences (Ryding *et al.*, 2001). The tTa is a hybrid molecule generated by the fusion of the tetR with the activation domain of the herpes simplex virus VP16 protein. The VP16 is a virally encoded factor that recruits cellular transcription factors and activates viral transcription. The CMV-derived minimal promoter, fused with the tetO sequences controls transgene expression. In the absence of tetracycline, tTa binds to the tetO sequences and activates transcription of the downstream target gene. In the presence of tetracycline, tTA does not bind to tetO and the target gene is not activated. This system is referred to as the 'tet-off' system as tetracycline turns off gene expression. The 'tet-on' system is a variant of the tTa system, developed by mutating the tTA to generate a reverse tTA (rtTA) that binds tetO in the

presence of doxycycline, an analog of tetracycline (Freundlieb *et al.*, 1997). In this system, gene induction occurs rapidly because low to moderate amounts of doxycycline are sufficient for transcriptional activation. Gene induction by the tTa is slower, since doxycycline clearance can take a few days. The tet-on system is more desirable since transgene expression can be turned on by an activator, rather than by removing a repressor as in the tet-off system.

1.6.2. Generation of Stably Transfected Mammary Cell Lines with an Inducible Dominant Negative IGF-IR

Several mutant IGF-I receptor constructs have been developed. One of these is the truncated β-subunit, 952 STOP mutant (human) IGF-I receptor (Figure 6; Prager *et al.*, 1994). The mutant receptor has been used to demonstrate the dominant-negative (DN) inhibition/suppression of the function of endogenous IGF-IR (Prager *et al.*, 1992). This effect is produced by the formation of a hybrid receptor (endogenous/mutant receptor). The mutant IGF-I half receptor suppresses the response of the wild-type IGF-I half receptor. When overexpressed in cells, it is 'dominant' to the normal receptor, as there are more copies of the mutant IGF-I half-receptor, and also induces a 'negative' effect as it inhibits the function of the wild type receptor (Herskowitz, 1987). The truncated IGF-I receptor or IGF-IR-DN lacks the critical tyrosine kinase domain and thus cannot undergo autophosphorylation and is unable to transmit the signal induced by the IGF-I ligand. In effect, the inhibition of the signal transduction pathway blocks the activation of transcription factors, subsequent gene expression, thus undermining the function of the IGF-I receptor.

The perturbation of receptor function is a technique commonly used to study the role of growth factors (Campochiaro *et al.,* 1996, Prager *et al.,* 1994, Xie *et al.,* 1997). The tetracycline regulatory system is a useful tool to study IGF-IR function in mammary epithelial cells, where expression of the gene can be conditionally regulated (Gunther *et al.*, 2002). Inhibition of normal IGF-IR function using the dominant negative receptor can be used to show the effects of blocking IGF-IR signal transduction in mammary epithelial cells. This model can provide an effective strategy to study the changes in cell proliferation, cell morphology and in the activation/inhibition of downstream substrates due to the inhibition of the IGF-IR signaling pathway.

In our laboratory, MCF-7 human breast cancer cell lines have been previously stably cotransfected with the reverse tetracycline transcriptional transactivator (rtTA; see Section 1.6.1) driven by the CMV promoter (CMV-rtTA) and the dominant negative IGF-IR fused to the tetracycline operator (tetOPh$_{CMV}$-IGF-IRDN) (Figure 7). These stably transfected cell lines have been generated to evaluate the functionality of these constructs.

2. Rationale and Hypothesis

The IGF-I/IGF-I receptor have been implicated to play an important role in growth and development of both the normal and abnormal mammary gland. In normal mammary gland development, IGF-I/IGF-IR have been shown to stimulate ductal proliferation and the induction of terminal end bud and alveoli formation (Kleinberg, 2000; Hadsell and Bonnette, 2000). The IGF-IR is overexpressed in most breast cancer tumors (Werner and LeRoith, 2000; Khandwala *et al.*, 2000). IGF-IR binding has been demonstrated in breast cancer cells and IGF-I has been shown to stimulate growth of breast cancer cells in culture (Myal *et al.*, 1984; Furlanetto and DiCarlo, 1984; Karey and Sirbasku, 1988).

However, to date the spatial and temporal pattern of IGF-IR gene expression during normal postnatal development has not been fully elucidated. We have hypothesized **that the gene will be expressed throughout mammary gland development and will show a differential pattern of gene expression.**

The development of a system that will allow the regulation of gene expression would be a useful tool to assess IGF-IR gene function in mammary epithelial cells, both *in vitro* and *in vivo*. We have also hypothesized **that *in vitro*, the tetracycline regulatory system can be used to demonstrate the conditional regulation of IGF-IR gene expression in mammary epithelial cells.**

Ultimately, the generation of a transgenic mouse model in which the inducible IGF-IR-DN can abrogate normal IGF-IR function can be used to study more precisely the stage(s) of mammary gland development at which IGF-IR function is most critical.

3. Research Objectives

There are two objectives:

1) **To systematically examine IGF-I receptor gene expression during different stages of normal mouse mammary gland development.**

Specific aims:

a) *To determine the temporal and spatial pattern of IGF-IR gene expression in the mouse mammary gland.* IGF-IR gene expression will be analyzed by real time quantitative RT-PCR and *in situ* hybridization.

b) *To examine whether IGF-IR protein expression in the mouse mammary gland correlates with gene expression.* IGF-IR protein expression will be analyzed by Western blot analysis and quantified by densitometry.

2) **To examine the conditional gene regulation of IGF-I/IGF-IR in mammary epithelial cells using a novel tetO-IGF-IR-DN *in vitro* model system.**

Specific aims:

a) *To determine whether the mutant IGF-IR-DN gene expression is inducible by doxycycline (an analog of tetracycline) in the stably transfected breast cancer cell line.* Doxycycline-induced cells will be analyzed for IGF-IR-DN gene expression by Northern blot analysis and RT-PCR.

b) *To identify the mutant IGF-I receptor protein in the stably transfected breast cancer cell line.* Western blot analysis will be used to detect the IGF-IR-DN protein and the ratio of the wild type receptor and the mutant receptor will be quantified by densitometry.

c) *To determine whether the IGF-IR-DN inhibits the IGF-I signaling pathway.* The mutant IGF-IR lacks the critical tyrosine kinase activity necessary for IGF-IR signal transduction. IGF-IR autophosphorylation and phosphorylation of the downstream substrate, insulin receptor substrate 1 (IRS-1), will be examined using Western blot analysis.

d) *To study the biological effects of inhibiting IGF-IR function in vitro.* The mitogenic effects of IGF-I are a result of specific interactions with the IGF-I receptor. IGF-I stimulation and its effect on cell growth in both doxycycline-induced and uninduced cells will be investigated. Cell proliferation will be measured using the crystal violet assay. Morphological changes will be examined by light microscopy.

4. Significance of the Study

The establishment of the pattern of IGF-IR gene and protein expression is a first step in addressing the functional role of the IGF-IR in normal postnatal mammary gland development. A differential pattern of gene expression would suggest that the IGF-IR is involved in mammary gland morphogenesis and that it may be critically important during some phases more than others. The results may be useful in not only providing a better understanding of IGF-IR function in normal human mammary gland development but also provide further understanding of the function of the IGF-IR in breast tumorigenesis.

The demonstration that the expression of IGF-IR-DN can be conditionally regulated *in vitro* and that the IGF-IR-DN can effectively inhibit the IGF-I signaling pathway will suggest that the novel tetO-IGF-IR-DN *in vitro* model is an effective system and that it can be used to fully address the role of IGF-I/IGF-IR in mammary epithelial cells. Additionally, these studies will establish whether these constructs can be used to generate a transgenic mouse model in which IGF-IR function can be conditionally regulated. The regulation of the gene expression of the IGF-I receptor in a mouse model should allow us to study the *in vivo* role of IGF-I/IGF-IR in the mammary gland. We would be able to address further whether there are critical stages of mammary gland development that may be sensitive to normal and abnormal IGF-I stimulation.

Altogether these studies will contribute to a better understanding of the *in vivo* role of IGF-I/IGF-IR in normal mammary gland development, and ultimately breast cancer.

5. MATERIALS AND METHODS

Part A - IGF-IR gene and protein expression during normal mammary gland development.

5.1. Animals and Tissue Collection

Wild type CD1 male and female mice (6-8 weeks old) were purchased from the Central Animal Care Services (CACS), Faculty of Medicine, University of Manitoba (Winnipeg, Manitoba, Canada). Mice were housed in plastic cages and fed Agway PROLAB rodent chow (RMH 3200; Agway Inc., Syracuse, NY, USA) and tap water *ad libitum*. They were maintained by the CACS staff and were handled according to the ethical guidelines set by the University of Manitoba. Female mice were mated, then sacrificed at various stages of mammary gland development and the mammary glands dissected and immediately frozen at -70°C. Mammary glands were collected from virgin (8 weeks), pregnant (days 2, 10, 15 and 19) and lactating (days 3 and 10) female mice. The involuting (days 3 and 10) glands were collected from dams following weaning. Pups were removed only after full lactation was established (21 days of nursing). Each time point was represented by three tissue samples dissected from three different animals. Each sample was evenly divided, one half set-aside for RNA extraction and the other for protein extraction. The tissues were immediately frozen on dry ice and stored at -70°C until needed. Portions of the tissues were also set aside for *in situ* hybridization studies.

5.2. Isolation of Total RNA

Total RNA was extracted from mammary glands using the TRIzol Reagent

(Invitrogen Corporation, Carlsbad, CA, USA) according to the manufacturer's instructions. Briefly, 1 ml of TRIzol Reagent was added to 50-100 mg of tissue and homogenized in 2 ml polypropylene microcentrifuge tubes (Fisher Scientific, Whitby, ON, Canada) using a Brinkmann Polytron Homogenizer (Brinkmann Instruments, Westbury, NY, USA). The homogenized samples were then incubated at room temperature for 5 minutes and 0.2 ml of chloroform was added for every 1 ml of TRIzol Reagent. The samples were shaken for 15 seconds and left at room temperature for 2-3 minutes. The homogenate was centrifuged at 12,000 RPM in an IEC Micro-MB centrifuge (International Equipment Company; IEC, Needham Heights, MA, USA) for 15 minutes at 4°C. The clear upper aqueous phase was removed and placed on ice. To precipitate the RNA, 0.5 ml of isopropanol (for every 1 ml of TRIzol Reagent) was added to the samples, shaken for 15 seconds, and incubated for 10 minutes at room temperature. The samples were then centrifuged at 12,000 RPM for 10 minutes at 4°C. The supernate was carefully pipetted off and the RNA pellet washed with 1 ml cold 75% ethanol and spun for 5 minutes at 9500 RPM. The ethanol was again carefully removed and the tube centrifuged for an additional 5 minutes to separate out any residual ethanol, which was then removed. The pellet was air-dried and dissolved in 50-100 µl diethylpyrocarbonate (DEPC; Sigma Chemical Company, St. Louis, MO, USA) treated water. The purity and yield of the RNA were determined by spectrophotometric absorbance readings at 260 nm with a Spectronic 1001 Plus Spectrophotometer (Milton Roy, Rochester, NY, USA). The concentration of RNA was determined using the following equation:

Equation 1:

[Optical Density X 40 X Dilution Factor] / 1000= RNA (μg/μl)

Purity of the extracted RNA was measured by absorbance readings of 260 nm and 280 nm. Only RNA samples that gave a 260/280 ratio between 1.7 and 2.0 were used. The total RNA isolated was stored at –70°C for reverse transcription-polymerase chain reaction studies.

For each time point, total RNA was collected from three animals and pooled.

5.3. Mini-Gel Electrophoresis of RNA

The quality of the extracted RNA was also analyzed by gel electrophoresis. A 1.5% (w/v) agarose (Invitrogen Corporation) gel was prepared using 1X Gel Running Buffer (GRB; 1X GRB = 0.04 M morpholinopropanesulfonic acid (MOPS) pH 7.0, 10 mM sodium acetate, 1 mM ethylenedinitroltetraacetic acid (EDTA) pH 8.0). Total RNA (1 μg) was denatured at 65°C for 10 minutes in 10 μl of a master mix solution containing 10 μl formamide (Fisher Scientific), 3.5 μl of 37% formaldehyde (Fisher Scientific) and 2 μl 5X GRB (0.2 M MOPS pH 7.0, 50 mM sodium acetate, 5 mM EDTA pH 8.0) (as outlined by Maniatis *et al.*, 1982) and 0.25 mg/ml ethidium bromide. The samples were immediately placed on ice following incubation and then briefly centrifuged at room temperature. Sample loading buffer (50% glycerol, 0.5 mM EDTA pH 8.0, 0.25% Bromophenol Blue, 0.25% Xylene Cyanol FF) was added to the RNA samples and electrophoresed using a RunOne Electrophoresis System (EmbiTec, San Diego, CA, USA) at 100 V for 30 minutes in a running buffer of 1X GRB. The gel was illuminated

with long wave ultraviolet light and photographed using a CCD camera and the Microcomputer Imaging Device (MCID) M4 software version 2.0 (Imaging Research Inc., St. Catherine's, ON, Canada).

5.4. Deoxyribonuclease (DNase) I Treatment

RNA samples were treated with DNase I Amplification Grade (Invitrogen Corporation) to eliminate any residual contaminating genomic DNA. Each RNA sample was DNase I treated in duplicate. A mixture of 1 µl total RNA (1 µg), 1 µl DNase I Amplification Grade (1.0 U/µl), 1 µl 10X DNase I reaction buffer (1X DNase I buffer = 20 mM Tris-HCl pH 8.4, 2 mM $MgCl_2$, 50 mM KCl), and 7 µl DEPC-treated water was prepared in 0.5 µl microcentrifuge tubes on ice. The tubes were incubated for 15 minutes at 22°C. The DNase I was heat inactivated at 65°C for 10 minutes in the presence of 2.5 mM EDTA pH 8.0. The EDTA solution was added to chelate magnesium that catalyzes non-specific cleavages in RNA at high temperatures.

5.5. Reverse Transcription (RT)

Following the DNase I treatment, 11 µl of the DNase I treated RNA sample was reverse transcribed into single stranded cDNA. The reaction was carried out using 1 µg of total pooled RNA in the presence of 5X RT buffer (Invitrogen Corporation; 1X RT buffer = 50 mM Tris-HCl (pH 8.3), 75 mM KCl, and 3 mM $MgCl_2$) containing 0.5 mM each of dATP, dCTP, dGTP, dTTP (Amersham Pharmacia Biotech, Baie d'Urfe, PQ, Canada), 10 mM DTT (Invitrogen Corporation), 37.8 units RNA guard (Amersham Pharmacia Biotech), 5 µg/µl BSA (New England Biolabs; NEB, Mississauga, ON, Canada), 0.25 µM random

hexadeoxynucleotide primers (Amersham Pharmacia Biotech) and 100 units Moloney Murine Leukemia Virus (MMLV) reverse transcriptase (Amersham Pharmacia Biotech) in a final volume of 50 µl. A RT minus (RT-) control, in which no MMLV reverse transcriptase was added, was performed for each sample to rule out genomic DNA contamination. A second negative control (RT blank) containing all reagents minus the RNA template was also included. Reverse transcription was conducted in a PTC-100 Programmable Thermal Controller (MJ Research, Inc., Watertown, MA, USA) for 1 hour at 37°C. Following RT, the samples were heated for 5 minutes at 70°C, cooled to 4°C and either used directly for PCR or stored at -20°C and utilized later.

RNA samples that were not treated with DNase I Amplification Grade were also reverse transcribed into single stranded cDNA using a modification of the procedure of Myal *et al.* (1984). The reaction was carried out using 1 µg of total pooled RNA in the presence of 5X RT buffer (Invitrogen Corporation; 1X RT buffer = 50 mM Tris-HCl (pH 8.3), 75 mM KCl, and 3 mM $MgCl_2$) containing 200 nM each of dATP, dCTP, dGTP, dTTP (Amersham Pharmacia Biotech), 1 µg BSA (NEB) 10 mM DTT (Invitrogen Corporation), 19 units RNA guard (Amersham Pharmacia Biotech), 0.25 µM random hexadeoxynucleotide primers (Amersham Pharmacia Biotech) and 200 units MMLV Reverse Transcriptase (Amersham Pharmacia Biotech) in a final volume of 20 µl. RT- and RT blank controls were included. The RNA samples were reverse transcribed in triplicate.

5.6. Real Time, Quantitative Polymerase Chain Reaction (PCR)

Quantitative real time PCR was carried out using the iCycler iQ Multi Colour Real Time PCR Detection System (Bio-Rad Laboratories, Hercules, CA, USA) to

measure IGF-IR gene expression. A standard curve was derived using the amplified fragment of the target sequence subcloned in a pGEM-T Easy vector.

5.6.1. Generation of IGF-IR cDNA and 18S cDNA pGEM-T Easy Constructs

The PCR amplification of the IGF-IR gene was carried out using a modified procedure of Gebauer *et al.* (1998). The primers (Table 1) were purchased from the University of Calgary DNA Services (Calgary, Alberta, Canada). The reverse transcribed RNA samples were amplified using the optimized reaction conditions described in Table 2. A master mix (10X PCR buffer (Amersham Pharmacia Biotech; 1X PCR buffer = 10 mM Tris-HCl pH 9.0, 1.5 mM $MgCl_2$, 50 mM KCl), 2.5 U Taq DNA Polymerase (Amersham Pharmacia Biotech), 0.2 mM each of the 4 deoxynucleoside triphosphates and 200 nM each of the IGF-IR forward and reverse primers) was prepared on ice. The mix was aliquoted into 0.5 ml microcentrifuge tubes and PCR amplifications were carried out on 5 µl of the DNase I treated reverse transcribed RNA in a final volume of 50 µl in a PTC-100 Programmable Thermal Controller. The negative control was prepared by using 5 µl ddH_20 as the template instead of cDNA.

The mouse 18S ribosomal ribonucleic acid (18S rRNA) gene (constitutively expressed in all cell types) was used as an internal control (Thellin *et al.*, 1999). The PCR amplification of the 18S rRNA gene was carried out using the optimized reactions conditions (Table 2) for the primers (Table 1), which were purchased from Invitrogen Corporation.

The RT-PCR products were analyzed using gel electrophoresis to confirm that the products were of the expected size. The expected size of the PCR products obtained were 502 bp and 151 bp for the IGF-IR and the 18S rRNA, respectively. The PCR products

were separated on a 1.5% (w/v) agarose gel containing 1X TBE (0.089 M Tris-borate, 0.089 M boric acid, 0.002 M EDTA) in 1X TBE running buffer at 130 V for 45 minutes. The Ready Load (Invitrogen Corporation) 100 bp DNA ladder was used to indicate the size of the PCR products. The gel was illuminated with long wave ultraviolet light and photographed using a CCD camera and the MCID M4 software version 2.0.

The IGF-IR cDNA was inserted into the pGEM-T Easy (Promega Corporation, Madison, WI, USA) vector according to the manufacturer's instructions. The 18S cDNA, which was used as a control gene, was also subcloned into the pGEM-T Easy vector. Briefly, a reaction containing approximately 50 ng PCR product, 50 ng pGEM-T Easy vector, 2X Rapid Ligation buffer (60 mM Tris-HCl pH 7.4, 50 mM KCl, 1 mM DTT, 2 mM ATP 10% PEG) and 3 U T4 DNA ligase was prepared on ice and incubated overnight at 4°C in the PTC-100 Programmable Thermal Controller. The following day, 2 µl of the pGEM-T Easy vector ligation reaction was added to a microcentrifuge tube containing 33 µl *Escherichia coli* (*E. coli*) DH5α bacteria and incubated on ice for 30 minutes. The cells were heat-shocked at 42°C for 45 seconds and immediately placed on ice for 2 minutes. One-hundred µl Luria-Bertani (LB) (1% Tryptone, 0.5% Bacto Yeast Extract, 1% NaCl; Difco Laboratories, Detroit, MI, USA) broth was then gently added to the cells and the tubes placed in a shaking incubator (225 RPM) at 37°C for 1 hour. The transformation culture (50 and 100 µl) was plated on duplicate LB agar plates containing 100 µg/ml ampicillin (Roche Molecular Biochemicals, Laval, QC, Canada) and incubated overnight at 37°C. Bacterial colonies (white colonies) were picked and glycerol stocks were prepared and stored at –70°C.

E. coli transformants were amplified by adding one loopful of the glycerol stock

to 5 ml of LB broth containing 100 μg/ml ampicillin and growing overnight in a shaking incubator at 37°C. The next day, 3 ml of each overnight culture was pelleted by centrifuging at 13,000 RPM for 1 minute at room temperature. Plasmids were isolated using the GenElute Plasmid Miniprep kit (Sigma Chemical Company) according to the manufacturer's instructions. The plasmid DNA was eluted with 50 μl sterile ddH_20. The concentration of the plasmid was determined by spectrophotometric analysis using an ultraviolet wavelength of 260 nm. The following equations were used to determine the copy number of the plasmid DNA:

Equation 2:

(# bases of vector) + (# bases of insert) X 660 = A (g/mol)

Equation 3:

$6.02X10^{23}$ molecules/mol X A = B (molecules/g)

Equation 4:

Optical Density X 50 X Dilution Factor / 1000= DNA (μg/μl)

Equation 5:

DNA (μg/μl) X B (molecules/g) = C (molecules/μl)

The standards were diluted to generate a standard curve for real time PCR. A 10-fold dilution series was prepared starting from a stock of 10^8 molecules/μl to 10^3 molecules/μl.

The purified plasmids were analyzed by PCR to verify the insertion of the cDNA in the pGEM-T Easy vectors. The plasmids were amplified (see Table 2 for reaction

conditions) using the appropriate primers (Table 1) and analyzed by gel electrophoresis as described above. Empty pGEM-T Easy vector was used as a negative control for the subcloning reaction. Reverse transcribed normal mouse mammary gland RNA was used as a positive control.

5.6.2. Quantification of IGF-IR Gene Expression during Mammary Gland Development using Real Time PCR

The reverse transcribed RNA samples (RT+ and RT-) were amplified using IGF-IR and 18S rRNA primers (Table 1), separately, using optimized reaction conditions (Table 3). The reaction conditions were previously optimized for the iCycler Thermal Cycler by using a range of annealing temperatures (58.0-67.0°C) and magnesium concentrations (2.0-4.0 mM).

To minimize sample-to-sample and/or tube-to-tube variation, a master mix (10X PCR buffer (Invitrogen Corporation; 1X PCR buffer = 20 mM Tris-HCl pH 8.4, 50 mM KCl), 2.5 mM $MgCl_2$ (Invitrogen Corporation), 1.25 U Platinum Taq DNA Polymerase (Invitrogen Corporation), 1% dimethylsulfoxide (DMSO), 1:2000 dilution of the 10,000X stock solution SYBR Green I (Sigma Chemical Company), 0.5 μM Fluorescein Calibration Dye (Bio-Rad Laboratories), 0.2 mM each of dCTP, dGTP, dATP and dTTP and 200 nM each of the forward and reverse primers outlined in Table 1) was prepared on ice for each experiment. The mix was aliquoted into a 96 well thin-wall PCR plate and PCR amplifications were carried out on 5 μl of the DNase I treated reverse transcribed RNA in a final volume of 50 μl. Only 1 μl of the reverse transcribed RNA, which was not treated with DNase I, was used in a final volume of 50 μl. The negative control was prepared by using 5 μl (or 1 μl) ddH_20 as the template instead of cDNA. Two replicates

of each sample were included in the 96 well thin-wall PCR plate. Since RT reactions were carried out in triplicate there were a total of 6 reactions for each sample.

To generate the standard curve, 10-fold dilution series of the pGEM-T Easy plasmid containing the IGF-IR (or 18S rRNA) cDNA were prepared using 10^8-10^3 plasmid copies. Three replicates of each dilution were included in the 96 well thin-wall PCR plate. The PCR products were stored at –4°C and/or visualized immediately on 1.5% agarose gels as described in Section 5.6.1.

5.6.2.1. Data Analysis

Data analysis was carried out using the iCycler iQ Real Time Detection System version 2.3 software (Bio-Rad Laboratories). The IGF-IR gene expression was standardized/normalized to the 18S rRNA gene expression (Equation 6).

Equation 6:

IGF-IR copy number/18S rRNA copy number = IGF-IR/18S rRNA Ratio

Normalization of the data yielded a corrected relative value to provide an estimate of the relative changes in gene expression between samples (Ambion's QuantumRNA, 1999).

5.6.2.2. Statistical Analysis

One way analysis of variance (ANOVA) and Tukey tests were used to assess the statistical significance of the data using the GraphPad Prism version 3.02 (GraphPad Software, Inc., San Diego, CA, USA). ANOVA was used to compare the IGF-IR/18S rRNA ratio measurements between each time point of mammary gland development

followed by a Tukey test. The time points were then grouped together as 6 distinct intervals to further assess the differences observed in gene expression during mammary gland development. The 6 distinct intervals were: virgin (8 weeks), early-to-mid pregnancy (day 2, 10, 15), late pregnancy (day 19), lactation (day 3 and 10) and early (day 3) and late involution (day 10). Comparisons between the 6 different intervals were made using ANOVA and the Tukey tests. A probability of $P<0.05$ was considered to be statistically significant.

5.7. *In Situ* Hybridization

For *in situ* hybridization, tissue sections (5 μm) from mammary glands were fixed in formalin for 24 hours, washed in 70% ethanol and paraffin embedded. Sense and antisense RNA riboprobes for IGF-IR were prepared using a 502 bp IGF-IR PCR product subcloned into the pGEM-T vector (Promega Corporation). 20 μg DNA was linearized with the restriction enzymes, Nco I (5 μl) and Sal I (5 μl) for 2 hours at 37°C. The DNA was electrophoresed in a 0.8% agarose gel for an hour using 1X TBE buffer (as outlined in Section 5.6.1.), excised and further purified using the QIAquick Gel Extraction kit (Qiagen, Inc., Mississauga, ON, Canada). The concentration of the samples (See Equation 4) was determined by spectrophotometric absorbance at 260 nm with a Milton Roy Spectronic 1001 Plus Spectrophotometer and stored at –20°C until further use.

The linearized IGF-IR plasmid cDNA was used to generate the ^{35}S UTP labeled riboprobes using the Riboprobe^{R} Gemini II Core System kit (Promega Corporation) according to the manufacturer's instructions and purified using a Quick spin G50 sephadex column (Roche Molecular Biochemicals). The sense and antisense riboprobes

(1×10^6 cpm/μl) were applied to paraffin sections pretreated with triethanolamine/acetic anhydride and proteinase K. Coverslips were placed on each section, sealed with rubber cement and incubated at 42°C overnight. The coverslips were removed the following day and the sections incubated with posthybridization solution (20 mM Tris, 1 mM EDTA, 0.3 M NaCl, 10 mM DTT and 50% deionized formamide) for 10 minutes at 55°C. The slides were then placed in buffered RNase A (0.5 M NaCl, 10 mM Tris and 1 mM EDTA and 20 μg/ml RNase A; Roche Molecular Biochemicals) for 30 minutes at 37°C. To wash off bound nonspecific label probe, sodium chloride/sodium citrate (SSC) buffer was used in the following descending dilutions: 2X SSC, twice each for 5 minutes, 1X SSC once for 15 minutes and 0.1 X SSC three times each for 15 minutes. Slides were then dehydrated with graded concentrations of ethanol starting with 50% ethanol, 70%, 95% and twice with 100% containing 300 mM ammonium acetate and finally dried overnight under the fumehood. For autoradiographic detection, the slides were dipped in Kodak NTB-2 emulsion (Interscience, Markham, ON, Canada) at 40°C, dried for 1 hour in a humidified chamber and placed in black, light tight slide boxes at 4°C for 4 weeks. Slides were then counterstained with Lee's methylene blue and basic fuchsin, and photographed (Leica, Wetzlar, Germany).

5.8. Protein Extraction

Frozen tissue samples (50-100 mg) were homogenized in 50 mM Tris-HCl (pH 6.8), 20 mM EDTA, 5% SDS, 5 mM β-glycerophosphate in the presence of Protease Inhibitor Cocktail (Roche Molecular Biochemicals) containing serine, cysteine, metalloproteases and calpains (1 Complete Mini tablet/10 ml of extraction solution). The homogenized tissues

were sonicated three times for 30 seconds using the Vibra Cell (Sonics and Materials, Inc., Danbury, CT, USA) and boiled for 5 minutes. Following centrifugation at 21,000 g for 15 minutes at 22°C, the supernatants were collected and stored at -20°C.

5.8.1. Determination of Protein Concentration

For each time point, total protein was collected from three animals and pooled together. The concentrations of the pooled protein were determined by the Bradford's method using the Bio-Rad protein assay (Bio-Rad Laboratories). Briefly, protein samples in SDS-isolation buffer were diluted 1:5 in ddH_2O. To 0.8 ml Phosphate Buffered Saline (1X PBS; 137 mM NaCl, 2.7 mM KCl, 4.3 mM $Na_2HPO_4 \cdot 7H_2O$, 1.8 mM KH_2PO_4), 1 µl of each diluted sample was added, while 1 µl of the 1:5 dilution of SDS-isolation buffer was added to each BSA standard and blank. To each sample, 0.2 ml of the Bio-Rad's Protein Assay Dye Reagent Concentrate (Bio-Rad Laboratories) was added. The tubes were gently vortexed and incubated at room temperature for 15 minutes. The BSA standard concentrations used for optical density measurement were 1.25 µg/ml, 2.5 µg/ml, 5.0 µg/ml, 7.5 µg/ml, 10 µg/ml. 15 µg/ml, 20 µg/ml and 25 µg/ml. The absorbance was measured at a wavelength of 595 nm and a BSA standard curve was plotted using the GraphPad Prism version 3.02 software. The slope (m) and y-intercept (b) was obtained and used to calculate the unknown concentrations of the protein samples according to the following equation with a dilution factor of 5.

Equation 7:

$$[\text{Optical Density} - b)/m] \times \text{Dilution Factor} = \text{Protein } (\mu g/ml)$$

5.9. SDS-PAGE, Western Blot Analysis

Broad range Kaleidoscope and Precision prestained standards (Bio-Rad Laboratories) were used as molecular weight markers. Equal amounts (350 μg) of protein samples were boiled for 5 minutes in the presence of 4X SDS buffer (1X SDS = 1.25 mM Tris pH 6.8, 10% glycerol, 2% SDS, 0.01% w/v bromophenol blue, and 0.05 M DTT). Protein extract from mouse kidney was used as a positive control, and mouse liver extract as a negative control. SDS-PAGE was performed using the Bio-Rad Protean II (Bio-Rad Laboratories) and samples were separated in a 4% polyacrylamide stacking gel and 10% polyacrylamide separating gel. Protein electrophoresis was performed with the Tris-Glycine buffer system (5X Running Buffer = 125 mM Tris, 960 mM Glycine, 0.5% SDS pH 8.3). The gel was transferred for 2 hours onto a 0.45 μm nitrocellulose membrane (Osmonics, Westborough, MA, USA) using Bio-Rad's Transblot Electrophoretic transfer cell. Coomassie Brilliant Blue (Bio-Rad Laboratories) staining of the gel was used to visualize the fractionated proteins.

Following transfer, Ponceau S Staining Solution (Sigma Chemical Company) was used to visualize proteins on the nitrocellulose membranes. The membranes were immersed in the Ponceau S Staining Solution (0.1% Ponceau S (w/v) and 5.0% acetic acid (w/v)) for 5 minutes. The membranes with visible protein bands were scanned using an Epson Perfection 1650 Series scanner (Epson America, Inc., Long Beach, CA, USA). The nitrocellulose membranes were then rinsed with distilled water, immersed in a solution of 0.1 M NaOH to remove the red Ponceau S stain, and rinsed again under running water for 2-3 minutes. The membranes were then used for immunoblotting.

Blocking procedure was carried out for 2 hours at room temperature in 1X Tris-

buffered saline containing Tween 20 (1X TBST = 20 mM Tris, 137 mM NaCl pH 7.6 and 0.05% Tween 20, (Fisher Scientific) and 5% skim milk powder. The blots were then incubated overnight at 4°C in a 1:200 dilution of rabbit polyclonal antibody (C-20) raised against the IGF-IR β-subunit (Santa Cruz Biotechnology, Inc., Santa Cruz, CA, USA) on a Vari-mix aliquot Mixer (Barnstead/Thermolyne, Dubuque, IA, USA). The membranes were washed in 1X TBST (5X for 5 minutes, 2X for 15 minutes) and incubated for 1 hour in a 1:2500 dilution of goat anti-rabbit horseradish peroxidase conjugated IgG (Bio-Rad Laboratories). Following a second washing in 1X TBST (5X for 5 minutes, 2X for 15 minutes), colour development was performed using the Supersignal West Pico Chemiluminescent Substrate kit (Pierce, Rockford, IL, USA) according to the manufacturer's instructions. The Fluor-S MAX MultiImager (Bio-Rad Laboratories) was used to acquire images of the membranes at 10, 20, 30 and 60 seconds. Membranes were also exposed to Kodak BioMax MR film (Interscience) for different time periods. Four independent Western blots were performed on each sample.

5.9.1. Densitometric Analysis

The protein bands captured by the FluorS-MAX MultiImager were analysed using the quantitation software program, Quantity One version 4.2 (Bio-Rad Laboratories), which measured band density. The density was measured as the total intensity of all the pixels in the volume divided by the area of the volume. The volume was defined as the intensity data inside a defined boundary around the band. The density of each protein band was determined from the membrane images acquired at 10, 30 and 60 second intervals (See Section 5.9.). The band density determined from the membrane image acquired at 30 seconds was compared to the density of the same band determined at 60 seconds. A ratio of

two was calculated. This value was indicative of a linear relationship, since the band intensity of the signal at 60 seconds should be twice as that of the signal at 30 seconds. This comparison verified the reliability of the detection system.

In order to compare the values obtained from different blots, the density of the IGF-IR protein band was standardized to the density of the positive control band. Loading differences between samples were evaluated by comparing density measurements on an evenly distributed non-specific protein band visible in the Ponceau S stained membranes (See Section 5.9. SDS-PAGE, Western Blot Analysis). IGF-IR protein level was standardized against the level of this control by using the ratio of the density of IGF-IR/density of the non-specific protein signals. Statistical analysis was performed using ANOVA followed by a Tukey tests (see Section 5.6.2.2. Statistical Analysis). Densitometric values obtained from four separate blots were used for the statistical analysis.

Part B – Doxycycline inducible expression of the dominant negative IGF-I receptor in stably transfected MCF-7 cells.

5.10. Tissue Culture

5.10.1. Cell Lines

The MCF-7 cell line is a human breast cancer cell line originally isolated from an adenocarcinoma obtained from a 69-year-old female patient (Soule *et al.*, 1973). A clonal cell line (Clone #89) stably transfected with the CMV-rtTA and a neomycin resistance gene, used for this study, was a kind gift from Dr. R.P.C. Shiu (Department of Physiology, University of Manitoba, Winnipeg, Canada).

5.10.2. Culture Conditions

MCF-7 cells were grown and maintained as a monolayer culture in complete media (CM) containing Dulbecco's Modified Eagle Medium (DMEM; Sigma Chemical Company) supplemented with 5% (v/v) dialyzed fetal bovine serum (Invitrogen Corporation), 10 units/ml penicillin (Invitrogen Corporation), 10 units/ml streptomycin, 30% (w/v) glucose and 2 mM L-glutamine (Invitrogen Corporation). The cells were maintained at 37°C in a humidified atmosphere of 95% air and 5% CO_2 in 75 cm^2 polystyrene culture flasks (Corning Inc., Corning, NY, USA).

5.10.3. Propagation of Cell Lines

For routine cell passage, the media was aspirated and the cells rinsed with 3 ml trypsin/EDTA (Invitrogen Corporation) solution containing 0.05% trypsin and 0.02% EDTA pH 7.4. The trypsin/EDTA was carefully removed, 2 ml of fresh trypsin/EDTA added, and the flask incubated at 37°C, 5% CO_2 for 5 minutes. Eight ml of CM was added and the cell suspension was pipetted 8 times to completely disperse cells. One ml

of cell suspension was added to 10 ml of fresh CM in a new flask to continue growth of the culture.

The remaining cell suspension was poured into a 15 ml sterile polypropylene centrifuge tube (Fisher Scientific) and centrifuged at 1000 RPM (IEC Centra-8R; International Equipment Company, Needham Heights, MA, USA) for 8 minutes at room temperature. The supernatant was poured out and the cell pellet was resuspended in 2 ml freezing solution (10% DMSO, 20% fetal bovine serum in CM) and transferred into cryogenic vials (Nalge Company, Rochester, NY, USA). Cells were stored at –70°C for 2-3 days and then transferred to liquid nitrogen and/or stored at –150°C.

5.10.4. Cell Count

The cells were removed from the culture flasks (as described in Section 5.10.3.) and passaged through a 21-gauge needle six times to prevent clumping. Half a ml of this suspension was diluted in 9.5 ml of Isoton-II Coulter Balance Electrolyte solution (Coulter Corporation, Miami, FL, USA), mixed well and counted with a Coulter Counter (Coulter Electronics Inc., Hialeah, FL, USA). Cell number was determined using a known dilution factor. The desired number of cells was prepared by diluting an aliquot of the cell suspension in CM in a 50 ml sterile polypropylene centrifuge tube (Fisher Scientific).

5.11. Plasmid Constructs

5.11.1. pTet-On/pUHD172-1neo

The regulator plasmid, pTet-On/pUHD172-1neo vector, (Figure 8A; Clontech Laboratories, Inc., Palo Alto, CA, USA) contains the reverse tetracycline transactivator

(rtTA) downstream of the cytomegalovirus (P_{CMV}) promoter and a neomycin-resistance cassette. This CMV-rtTA vector has been successfully used to stably transfect MCF-7 human breast cancer cells.

5.11.2. pBSK+/IGF-IR-DN

The truncated human IGF-I receptor (IGF-IR-DN) cDNA cloned into the expression vector, pBSK+, was provided by Dr. Shlomo Melmed (Cedars Sinai Medical Centre-UCLA School of Medicine, Los Angeles, California). To generate this construct, the wild-type human IGF-IR was truncated by creating an in-frame stop codon at position 952 by inserting an Xba linker 5′ TGC TCT AGA GCA 3′ into the Sca I site present in the IGF-IR cDNA (Figure 6).

5.11.3. pTRE/pUHD10-3zeo

The response plasmid, pTRE/pUHD10-3zeo, (Figure 8B; Clontech Laboratories, Inc.) contains seven copies of tetracycline operator sequences ($tetO_7$) upstream of a minimal human cytomegalovirus promoter (Ph_{CMV}). The pUHD10-3 vector that was modified to contain a zeocin-resistance cassette was a gift from Dr. Robert Shiu (Department of Physiology, Winnipeg, Manitoba). The EcoRI/BamHI IGF-IR-DN cDNA fragment was removed from the pBSK+ plasmid (See Section 5.11.2) and subcloned into the multiple cloning site (EcoRI/BamHI) downstream of the Ph_{CMV} promoter in the pUHD10-3 vector.

5.12. Amplification of Plasmid DNA

The IGF-IR-DN cDNA inserted into the pUHD10-3 vector containing the zeocin selection marker was transfected into *E. coli* DH5α bacteria. Glycerol stocks of the *E.*

coli transformants were prepared and stored at –70°C. The bacteria were grown overnight in 5 ml of LB Broth (Difco Laboratories) containing 100 ug/ml ampicillin (Roche Molecular Biochemicals). The cultures were placed overnight in a shaking incubator at 37°C.

Plasmids were isolated using a modified Alkaline Lysis Miniprep DNA method (Maniatis *et al.*, 1982). The tubes with the 5 ml overnight culture were gently shaken and 1.5 to 1.8 ml was transferred into a 2 ml eppendorf tube and centrifuged at 13,000 RPM for 45-60 seconds. The supernatant was aspirated and the bacterial pellet resuspended in 100 µl of Miniprep 1 solution (50 mM glucose, 10 mM EDTA pH 8.0, 25 mM Tris-HCl pH 8.0) supplemented with 5 mg/ml lysozyme (Roche Molecular Biochemicals) and incubated on ice for 5 minutes. Maintaining the sample on ice, 200 µl of Miniprep 2 solution (0.2 N NaOH, 1% SDS) was added, mixed and incubated for 5 minutes. Following the incubation, 150 µl of Miniprep 3 solution (5M glacial acetic acid, 3M potassium acetate) was added to the sample, vortexed briefly and incubated further for 5 minutes. The sample was centrifuged at 13,000 RPM for 5 minutes at room temperature, the supernatant transferred to a fresh tube and an equal volume of phenol/chloroform/isoamyl alcohol 25:24:1 solution pH 6.7 (Fisher Scientific) was used to extract plasmid DNA. The tube was vortexed and centrifuged at 13,000 RPM for 5 minutes at room temperature. The top aqueous layer was carefully collected and transferred into a new 1.5 ml polypropylene tube. To precipitate the plasmid, two volumes of 95% ethanol and 24 µl sodium acetate (3M NaOAc pH 5.2) were added, the mixture inverted several times, placed at –70°C for 1 hour and centrifuged at 13,000 RPM for 30 minutes at 4°C. The supernatant was poured out and washed with 70%

ethanol. The ethanol was then poured out and the pellet was air dried at room temperature for 5 to 10 minutes. The pellet was redissolved in Tris/EDTA (TE) pH 8.0 buffer containing 1 mg/ml RNase A. The concentration of the isolated plasmid (See Equation 4) was determined by spectrophotometric analysis using an ultraviolet wavelength of 260 nm.

The restriction enzymes, Xba I and Xho I (Amersham Pharmacia Biotech) were used to perform a diagnostic cut of the extracted plasmid. Digestion was performed overnight at 37°C in a 10 µl reaction volume containing 1 µl of each enzyme, 1 µl REACT 2 (50 mM Tris-HCl pH 8.0, 10 mM $MgCl_2$, 50 mM NaCl; Invitrogen Corporation) buffer and the IGF-IR-DN plasmid. The sample was loaded into a 0.8 % (w/v) agarose gel containing 1X TBE and run in 1X TBE buffer. The products were electrophoresed at 130 V for 45 minutes until the bands were well separated.

5.13. Generation of Stable Cell Lines

Stable transfectants were produced by a modified calcium phosphate transfection method using the Mammalian Transfection Kit (Stratagene, La Jolla, CA, USA) according to the manufacturer's instructions. Briefly, the MCF-7 rtTA cells (clonal cell line 89) were counted (See Section 5.10.4.) and $5X10^5$ cells were seeded on 100 mm culture dishes (100 X 20 mm; Nalge Nunc International Corporation, Naperville, IL, USA) in 10 ml media and grown to approximately 10-20% confluency. The calcium phosphate transfection was performed using 0, 15 and 25 µg of the tetOPh$_{CMV}$-IGF-IR-DN plasmid linearized by Sal I. The DNA was diluted in 450 µl ddH_2O and mixed with 50 µl of 2.5 M calcium chloride (2.5 M $CaCl_2$; Sigma Chemical Company) solution and

500 µl of 2X BES-buffered solution (BBS), 50 mM N, N-bis (2-hydroxethyl)-2-aminoethanesulfonic acid in buffered saline (BES; Calbiochem-NovaBiochem Corporation, San Diego, CA, USA), 280 mM NaCl, 1.5 mM Na_2HPO_4 pH 6.95) and incubated at room temperature for 10-20 minutes. The suspension was added drop-wise to the plates and gently mixed. The cells were incubated at 37°C and in 3% CO_2 for 24 hours. The cells were then rinsed with 1X phosphate buffered saline (1X PBS; 136 mM NaCl, 2.7 mM KCl, 10 mM Na_2HPO_4, 1.8 mM KH_2PO_4) and fresh media was added to the cells and incubated at 37°C, 5% CO_2 for 24 hours. The following day the cells were detached from the plates. A 1 to 10 dilution of the cell suspension was plated in fresh complete medium before adding selection media containing 250 µg/ml zeocin (Invitrogen Corporation). Zeocin was added daily to the transfectants for 14 days until the control, untransfected cells died. The media was changed every other day until resistant colonies appeared on the selection plates.

5.13.1. Isolation and Expansion of Stable Clonal Cell Lines

Resistant colonies growing in the selection media were isolated using Whatman (Fisher Scientific) filter-paper discs saturated with trypsin/EDTA solution. One disc was placed on top of each colony for 2-3 minutes and gently removed with sterile forceps, and transferred to 96-well plates for expansion. Resistant clones were passaged and grown in 800 µg/ml geneticin (G-418 sulfate; Invitrogen Corporation) and 250 µg/ml zeocin to select for double transfectants. Cell stocks were stored in liquid nitrogen for further analysis (See Section 5.10.3.).

5.14. Genomic DNA Extraction

Genomic DNA was extracted from the stably transfected MCF-7 cells and analyzed by Southern blot for IGF-IR-DN gene integration as follows. Confluent cells (80-90%) grown in large tissue culture dishes (140 X 20 mm; Nalge Nunc International Corporation) were washed with 1X PBS after aspirating the medium. Cells were scraped off the plates, pelleted by centrifugation at 800 RPM for 7 minutes and either stored at –70°C or used immediately. To extract DNA, 500 µl of Proteinase K extraction solution (100 mM Tris-HCl pH 8, 100 mM NaCl, 5 mM EDTA pH 8.0, 1% SDS, 100 ug/ml Proteinase K (Roche Molecular Biochemicals) was added to the pellet and incubated overnight in a shaking water bath at 37°C. Following incubation, 200 µg/ml RNase A was added to the solution and incubated at 65°C for 15 minutes. Buffer saturated phenol (Fisher Scientific) was added to the tube and inverted 100 times and then centrifuged at 12,500 RPM for 5 minutes at room temperature. This process was repeated after transferring the aqueous layer to a new tube. This process was repeated twice more using 1:1 phenol:chloroform:isoamyl alcohol (25:24:1) instead of phenol and then once with 24:1 chloroform:isoamyl alcohol. After transferring the aqueous phase to a new tube, the DNA was precipitated by adding 0.04X volumes of 5 M NaCl and 2.2 volumes of 95% ethanol. The DNA pellet was air dried and resuspended in TE buffer. The concentration of the DNA was determined by reading optical densities at 260 nm (See Equation 4) and stored at -4°C until further use.

5.15. Southern Blot Analysis

Genomic DNA (10 µg) extracted from the cells was digested overnight at 37°C

using EcoR V (100 U/μl; NEB), 1X NEBuffer 3 (100 mM NaCl, 50 mM Tris-HCl, 10 mM $MgCl_2$, 1 mM DTT pH 7.9) and 100 μg/ml BSA. A 0.8% (w/v) agarose (Invitrogen Corporation) gel was prepared and the digested DNA samples were electrophoresed at 25 V overnight in a running buffer of 1X TBE. The IGF-IR-DN plasmid was run along with the samples to serve as a positive control. DNA extracted from untransfected MCF-7 cells was included as a negative control. The ethidium bromide stained gel was photographed under ultraviolet light. To denature the DNA, the gel was placed in 1 M NaCl, 0.5 M NaOH for one hour on a shaking water bath at room temperature, followed by one hour in neutralizing solution (1 M ammonium acetate, 0.02 M NaOH) under the same conditions. The agarose gel was transferred overnight to nitrocellulose membrane (Micron Separations, Westborough, MA, USA) in neutralizing solution. The following day, the membranes were baked at 80°C for 2 hours in a dry oven (Lab-Line Instruments, Melrose Park, IL, USA).

Nitrocellulose membranes were then prehybridized in 10 ml prehybridization solution (50% (v/v) formamide, 20X SCP (2M NaCl, 0.6 M Na_2HPO_4, 0.02M Na_2HEDTA pH 6.2), 20% N-lauryl sarcosine (sarkosyl), 200 μg/ml sheared salmon sperm DNA, 5X Denhardt's solution (1X Denhardt's = 0.02% (w/v) each of Ficoll, Polyvinylpyrrolidone and BSA) for 2 hours in 35 X 300 mm glass tubes (Robbins Scientific, Sunnyvale, CA, USA) in a rotating hybridization incubator at 42°C (Robbins Scientific). The cDNA (30-50 ng) probe was prepared with ^{32}P-labeled dCTP isotope and the RadPrime DNA Labeling System (Invitrogen Corporation). The probe was purified with NICK columns (Amersham Pharmacia Biotech) containing Sephadex G-50 DNA grade. The labeled probe was denatured by boiling for 5 minutes, immediately cooled and

added to 10 ml of fresh hybridization solution containing 10% dextran sulfate. The hybridization solution containing the labeled probe was added to the membranes in the glass tubes and allowed to hybridize overnight at 42°C in the rotating incubator.

The blots were then washed once with 6.6X SCP/1% sarkosyl at room temperature for 15 minutes on a shaker and followed by washing in 1X SCP/1% sarkosyl at 65°C for an additional 15 minutes. The blots were then placed on Whatman chromatography paper (3mm; Whatman International, Maldston, England) to remove excess liquid and placed into a heat-sealable polyethyelene bag (Fisher Scientific). The membranes were exposed to Kodak X-OMAT AR film (Interscience) using an intensifying screen for 1-4 days at –70°C.

5.16. Doxycycline Treatment

A stock solution (1 mg/ml) of doxycycline HCl (a water-soluble analog of tetracycline; Sigma Chemical Company) was prepared in filter sterilized distilled water, aliquoted and stored in the dark at -20°C. The stably transfected MCF-7 clones, positive for the IGF-IR-DN by Southern blot analysis, were treated with doxycycline HCl.

5.16.1. Dosage Analysis

To determine the amount of doxycycline needed to induce maximal transgene expression, a dose dependent assay was performed. Clone #35 was grown to 70-80% confluency in 140 mm culture dishes (See Section 5.10.2.) in CM containing doxycycline at concentrations of 0, 0.5, 1.0, 1.5, 2.0 μg/ml. The cells were incubated at 37°C, 5% CO_2 for 24 hours. The media was aspirated, the cells washed twice with 1X PBS and collected for RNA analysis.

5.16.2. Time Course Analysis

To determine the optimal time required to induce gene expression in the stably transfected cells, a time course analysis was performed. Clone #35 was grown (See Section 5.10.2.) and treated with CM containing doxycycline (1 μg/ml) for 0, 12, 24 and 48 hours to induce IGF-IR-DN gene expression. The cells were collected for RNA analysis.

5.17. Induction of IGF-IR-DN Gene Expression

Upon determining the optimal dose of doxycycline (1 μg/ml) and time (24 hours), cells were grown to 70-80% confluency in 140 mm culture dishes in CM. The media was aspirated and replaced with CM containing doxycycline (1 μg/ml) and incubated at 37°C, 5% CO_2 for 24 hours. The cells were washed twice with 1X PBS after aspiration of the medium and either collected for RNA or protein analysis.

5.17.1. RNA Isolation

Confluent cells (80-90%) grown in 140 mm dishes were washed twice with 1X PBS after aspiration of the medium. Total RNA was extracted from the cells using the TRIzol Reagent (as outlined in Section 5.2. Isolation of Total RNA) with the following modifications. TRIzol Reagent (3 ml) was added directly onto the 140 mm dishes containing the MCF-7 cells, scraped with a plastic cell scraper and transferred to a 15 ml tube. The cell lysate was homogenized by syringing the lysate several times through an 18-gauge needle, followed by a 21-gauge needle. The homogenized samples were then incubated at room temperature for 5 minutes. The appropriate amounts of reagents were then added to each of the samples for every 3 ml of TRIzol Reagent used as described in

Section 5.2. Centrifugation of samples was performed in a Beckman JA-21 centrifuge (Beckman Instruments, Palo Alto, CA, USA) with the JA-20 rotor at 4°C.

5.17.2. RT-PCR Analysis for rtTA Gene Expression

rtTA gene expression was confirmed by RT-PCR. Initially, total RNA was pretreated with DNase I (see Section 5.4.), reverse transcribed into single stranded cDNA (see Section 5.5.). The reverse transcribed RNA samples (RT+ and RT-) were amplified (see Section 5.5.) using the rtTA gene specific primers (Table 1) and cycle profile (Table 2). Reverse transcribed RNA from untransfected MCF-7 cells was used as a negative control. Reverse transcribed RNA from Clone #89 cells was used as a positive control. In addition, the 18S rRNA primers (Table 1, 2) were used to amplify the 18S rRNA internal control gene. The PCR products were electrophoresed in a 1% (w/v) agarose gel, illuminated with long wave ultraviolet light and photographed using a CCD camera and the MCID M4 software version 2.0 (Imaging Research, Inc.).

5.17.3. Northern Blot Analysis

Doxycycline-induced IGF-IR-DN gene expression in the stably transfected cell lines was analyzed by Northern blot analysis. A 0.8% (w/v) agarose gel was prepared containing 1X GRB and 2.2 M formaldehyde. Total RNA (30 μg) isolated from the MCF-7 cells, was prepared in denaturing solution (See Section 5.3.) and placed in a water bath at 65°C for 15 minutes. The samples were immediately placed on ice following the incubation time to prevent reannealing and briefly centrifuged. The RNA samples were loaded in the gel and electrophoresed overnight at 25 V in a running buffer of 1X GRB. The gel was exposed to ultraviolet light and photographed using a CCD camera and the MCID M4 software (Imaging Research, Inc.). The agarose gel was transferred overnight

to nitrocellulose membrane in 20X SSC buffer (1X SSC = 0.15M NaCl, 0.015 M sodium citrate). The nitrocellulose membranes were baked at 80°C for 2 hours in a dry oven (Lab-Line Instruments).

Membranes were prehybridized in 10 ml prehybridization solution (50% (v/v) formamide, 5X SSPE (1X SSPE = 0.15M NaCl, 0.01 NaH_2PO_4, 1 mM EDTA, ph 7.7), 5X Denhardt's Solution, 0.1% sodium dodecyl sulfate (SDS) and 250 μg/ml salmon sperm DNA) for 2 hours at 42°C. The cDNA (30-50 ng) probe was prepared and the membranes hybridized as outlined in Section 5.15. The blots were washed once with 2X SSC/0.1% SDS at room temperature for 5 minutes and then washed in 0.1X SSC/0.1% SDS at 65°C for 5 minutes. The membranes were exposed to Kodak BioMax MS film (Interscience) using an intensifying screen for 1-4 days at –70°C. Bands on the exposed film were analyzed using an image analyzer (MCID-M4 Imaging Research, Inc.) and quantified by densitometry (Quantity One Version 4.2 software; Bio-Rad Laboratories).

5.17.4. RT-PCR Analysis for IGF-IR-DN Gene Expression

A combination of RT-PCR analysis and a restriction digestion strategy were used to confirm IGF-IR-DN gene expression in the stably transfected MCF-7 cells.

5.17.4.1. PCR

The DNase I treated reverse transcribed RNA samples (See Section 5.17.2.) were used for PCR amplification of IGF-IR using the IGF-IR/IGF-IR-R2 primers (Table 1). The original forward primer (Table 1) was used and a new reverse primer (IGF-IR-R2; Table 1) was designed incorporating a sequence downstream from the 952 stop site (i.e., the Xba I linker site at position 2981) in the mutant transgene. The resulting PCR product contained the Xba I linker site. This strategy allowed us to differentiate between the

expression of the endogenous IGF-IR gene and the mutant IGF-IR gene upon digestion with the Xba I restriction enzyme. A 931 bp fragment was expected upon amplifying cDNA prepared from both the doxycycline-induced and uninduced cells. The identity of the amplified fragments, whether mutant or normal, was determined using restriction analysis.

The PCR amplification was performed using the IGF-IR/IGF-IR-R2 primers under the reaction conditions outlined in Table 2. To amplify large amounts of the desired IGF-IR-DN fragment, the PCR was done in quintuplet, More specifically, 5 identical reactions were performed on each RT product.

5.17.4.2. Extraction and Purification of the PCR Product

A modification of the QIAquick Gel Extraction Kit protocol (Qiagen, Inc.) was used to purify the PCR products. Each of the 5 identical PCR tubes were pooled together, mixed and centrifuged briefly. About 50 µl of the PCR product was set aside while 200 µl of the product was purified. The PCR product for each sample (200 µl) and 400 µl of Buffer QG (Solubilization and Binding Buffer was applied to a QIAquick column (with a silica-gel membrane) and centrifuged for 1 minute to bind the DNA and the flow-through discarded. To wash the DNA, 0.75 ml of the Buffer PE (Wash Buffer with added ethanol) was added to the column and centrifuged for 1 minute after letting the column stand for 5 minutes. The flow through was discarded and the column was spun once more to remove any residual ethanol. The QIAquick column was then placed into a clean 1.5 ml microfuge tube. The DNA was eluted out by adding 30 µl of the Buffer EB (10 mM Tris-HCl pH 8.5). The sample was allowed to stand for 1 minute before centrifuging for 1 minute. The tubes containing the purified PCR products were placed on ice and prepared

for restriction digest.

5.17.4.3. Restriction Digestion Strategy

Approximately 26 µl of the purified PCR products was recovered. A reaction mixture containing 9 µl ddH_20, 4 µl of REACT 2 buffer and 1 µl of the Xba I (Invitrogen Corporation) enzyme was prepared on ice. RT-PCR products from wild type MCF-7 cell RNA and Clone #89 were used as negative controls. Mouse RNA from a transgenic mouse expressing IGF-IR-DN was used as a positive control. The IGF-IR-DN plasmid (See Section 5.11.2) served as a control for the restriction digest. The samples were incubated in a total volume of 40 µl at 37°C for 2 hours and immediately analyzed.

All samples were loaded into a 1% (w/v) EtBr agarose gel (See Section 5.6.1.) and run at 130 volts for 40 minutes. The gel was then illuminated with ultraviolet light and photographed. The IGF-IR-DN gene was easily identified from the endogenous gene by the presence of 417 and 514 base pair bands - the Xba I cleaves the 931 base pair PCR product at the unique site (Xba linker).

5.18. Analysis of IGF-IR-DN Protein Expression

5.18.1. Protein Preparation

The stably transfected MCF-7 cells were treated with doxycycline using the protocol described in Section 5.16. Confluent cells (80-90%) grown in 140 mm dishes were washed twice with 1X PBS after aspiration of the medium. Cells were lysed in 1 ml of SDS-lysis buffer (50 mM Tris-HCl pH 6.8, 20 mM EDTA, 5% SDS, 5 mM β-glycerophosphate) in the presence of Protease Inhibitor Cocktail (Roche Molecular Biochemicals) containing serine, cysteine, metalloproteases and calpains (1 Complete Mini

tablet/10 ml of extraction solution) and scraped with a plastic scraper and transferred to 1.5 ml eppendorf tubes. Following centrifugation at 21,000 g for 15 minutes at 22°C, the supernatants were collected and stored at -20°C. Total protein concentrations were determined by the Bradford method (See Section 5.8.1) using the Bio-Rad protein assay (Bio-Rad Laboratories).

5.18.2. IGF-IR-DN Protein Analysis

Western blot analysis was carried out as described in Section 5.9. with a few modifications. Cell lysates collected using the SDS-lysis buffer were boiled in the presence of 4% SDS and 0.4 M DTT, separated on a 7.5% SDS-PAGE gel and transferred on nitrocellulose membranes. The blots were blocked for 2 hours in 1X TBST containing 5% skim milk powder, followed by incubation with primary antibody (diluted in the buffers outlined in Table 4) overnight on a Vari-mix Aliquot Mixer (Barnstead/Thermolyne) at 4°C. The rabbit polyclonal antibody (N-20) raised against the IGF-IR α-subunit (Santa Cruz Biotechnology, Inc.) was used to detect the ratio of endogenous and mutant receptor in the doxycycline-induced cells. The blots were also immunoblotted with a rabbit polyclonal antibody raised against the IGF-IR β-subunit (H-60; Santa Cruz Biotechnology, Inc.). The H-60 was chosen to distinguish the truncated β-subunit of the IGF-IR-DN from the wild-type or endogenous IGF-IR. The H-60 recognizes the amino acids 741-800 of the β-subunit of the IGF-IR, above the truncation site (amino acid 950). Thus, both the endogenous and mutant IGF-I receptors were easily identified based on size.

The membranes were stripped and immunoblotted with an antibody raised against actin (I-19; Santa Cruz Biotechnology, Inc.) (diluted in the buffers outlined in Table 4)

which was used to reflect sample loading. In similar studies, actin, which is a constitutively expressed protein, is the protein of choice to evaluate sample loading (Dupont *et al.*, 2000).

To reprobe the nitrocellulose membranes with a different antibody, the membranes were first immersed in 100 ml of stripping solution (2% SDS, 62.5 mM Tris pH 6.8, 0.05 M DTT), shaken gently in a waterbath at 55°C for 20 minutes. The blots were then washed twice with 1X TBST for 10 minutes each. To verify the complete removal of the antibody from the target protein, the membrane was incubated with Supersignal West Pico Chemiluminescent Substrate (Pierce) for 5 minutes and exposed to Kodak BioMax MR film (Interscience) for a minimum of 1 hour. The absence of protein bands verified that the antibody was removed. The stripped membrane was washed twice with 1X TBST for 10 minutes each, before blocking and reincubating with a primary antibody.

5.19. Protein Phosphorylation Studies

5.19.1. IGF-I Treatment

A stock solution of recombinant human IGF-I (Sigma Chemical Company) was prepared by making a 0.5 mg/ml solution in 10 mM HCl. The stock solution was aliquoted and stored at –70°C. For experiments, a working solution was prepared by diluting the IGF-I stock solution with filter sterilized 1X PBS supplemented with 1% BSA.

Cells were grown in phenol-red free CM to 70% confluency. The media was replaced with phenol-red free, serum-free medium (SFM), supplemented with 200 μg/ml bovine serum albumin (BSA) and 10 μg/ml iron-poor human apo-transferrin (Sigma

Chemical Company) for 24 hours. The next day, fresh media was added to the cells and treated with doxycycline (1 μg/ml) for 24 hours at 37°C. The cells were then incubated with the supplemented serum-free media containing doxycycline (1 μg/ml) and IGF-I (5 nM) for 10 minutes at 37°C.

The four experimental groups were:

a) Supplemented SFM + doxycycline + IGF-I (5 nM)

b) Supplemented SFM + doxycycline - IGF-I

c) Supplemented SFM - doxycycline + IGF-I (5 nM)

d) Supplemented SFM - doxycycline - IGF-I

5.19.2. Cell Lysis

Cells were washed twice in ice cold 1X PBS and lysed with modified radioimmunoprecipitation (RIPA) buffer (50 mM Tris-HCl pH 7.4, 1% NP-40, 150 mM NaCl, 1 mM EDTA, 1mM phenylmethyl sulfonyl fluoride (PMSF; Sigma Chemical Company), Protease Inhibitor Cocktail, 1mM sodium orthovanadate (Na_3VO_4; Sigma Chemical Company). As recommended, in order to prepare cell lysates for kinase assays, sodium deoxycholate was not added to the RIPA buffer as the ionic detergent can denature enzymes, causing them to lose activity. The lysates were gently rocked on a Vari-mix aliquot Mixer (Barnstead/Thermolyne) for 15 minutes at 4°C, centrifuged at 15,000 RPM for 15 minutes at 4°C and the supernatants collected and frozen at –20°C until further use. Protein concentrations were determined using the Bio-Rad protein assay kit (See Section 5.8.1.).

5.19.3. Detection of Phosphorylated Proteins

Cell lysates, collected using the modified RIPA buffer, were boiled in the presence

of 4% SDS and 0.4 M DTT and separated on a 6.5% SDS-PAGE gel. Western blot analysis was carried out as described (see Section 5.9.) with a few modifications. To detect tyrosine phosphorylated proteins, the nitrocellulose blots were blocked for 2 hours at room temperature in 1X Tris-buffered saline and 0.1% Tween 20 (TBST) pH 7.4, containing 3% BSA (Fisher Scientific). The blots were then incubated with the mouse monoclonal antiphosphotyrosine antibody (PY-20; BD Biosciences, Mississauga, ON, Canada) (diluted in the buffers outlined in Table 4) at room temperature. The blots were washed in 1X TBST and incubated with goat anti-mouse horseradish peroxidase conjugated IgG (Bio-Rad Laboratories) for 1 hour. Following a second washing in 1X TBST, colour development was performed using the Super Signal substrate kit (Pierce). The blots were stripped and incubated with the rabbit phospho-insulin receptor substrate-1 (Ab-1; Oncogene Research Products, Boston, MA, USA) as well as a rabbit polyclonal antibody (Upstate Biotechnology, Lake Placid, NY, USA) raised against the insulin receptor substrate - 1 (IRS-1) (See Table 4 for dilutions).

To verify expression of the IGF-IR-DN protein in the IGF-I treated cells, the same nitrocellulose blots were immunoblotted with the N-20 and H-60 primary antibodies (diluted in the buffers outlined in Table 4). An antibody raised against actin (I-19) (diluted in the buffers outlined in Table 4) was used to account for possible variation in protein loading. Nitrocellulose membranes were reused using the protocol described in Section 5.18.2.

5.20. Cell Proliferation Studies

The cells were counted (See Section 5.10.4) and plated in 96-well microtiter plates (Invitrogen Corporation) at 3000 cells per well and allowed to attach overnight. The culture medium was then changed to the supplemented serum-free medium for 24 hours to establish a state of quiescence prior to cell stimulation (designated as day –1). The following day, the medium was changed to a) supplemented SFM + doxycycline (1 μg/ml) and b) supplemented SFM – doxycycline for 24 hours (designated as day 0). The cells were then treated with IGF-I (5 nM) for 24, 48 and 72 hours, replacing the media every other day.

The four experimental groups were:

a) Supplemented SFM + doxycycline + IGF-I (5 nM)

b) Supplemented SFM + doxycycline - IGF-I

c) Supplemented SFM - doxycycline + IGF-I (5 nM)

d) Supplemented SFM - doxycycline - IGF-I

The crystal violet staining assay based on the binding of the crystal violet dye (Fisher Scientific) to total cellular proteins was used to determine cell density at Day –1, 0, 2, 4 and 6. Briefly, the medium was removed from the 96-well microtiter plate and 100 μl of crystal violet stain (20 mM Tris-HCl pH 7.5, 0.25% (w/v) crystal violet, 0.9% (w/v) NaCl, 20% (w/v) methanol) was added (Alfa and Jay, 1988). Following a gentle washing of plates in distilled water, the cell bound dye was extracted with 100 μl of methanol and the absorbance at 590 nm was determined using an enzyme-linked immunosorbent assay (ELISA) SpectraMAX plus Microplate reader (Molecular Devices Corporation, Sunnyvale, CA, USA) and the SOFTmax PRO version 3.0 (Molecular Devices

Corporation).

5.20.1. Statistical Analysis

The ANOVA and Tukey's test was used to assess the statistical significance of the data using the GraphPad Prism version 3.02 (GraphPad Software, Inc.). Cell growth measurements in each of the four experimental groups were compared. A probability of $P<0.05$ was considered to be statistically significant.

5.21. Morphological Studies

Cells were directly examined under the light microscope (Nikon Inverted Microscope Model MS; Nippon Kogaku, K.K., Tokyo, Japan). Cells were photographed using a Nikon FE camera and Nikon inverted microscope DiaPhot-Tmd (Nippon Kogaku K.K.) before and after doxycycline treatment and following IGF-I stimulation. Cells were photographed on Days 0, 2, 4 and 6 of the treatment period. Cells in the centre of the 100 mm culture dishes were photographed.

6. RESULTS

Part A - IGF-IR gene and protein expression during normal mammary gland development.

6.1. Quantitative Analysis of IGF-IR Gene Expression during Normal Mouse Mammary Gland Development using Real Time PCR

Real time PCR was used to quantitate IGF-IR gene expression throughout mammary gland development (Figure 9). The 18S rRNA was used as an internal control for these studies (See Section 5.6. in Materials and Methods). Since the 18S rRNA gene sequence does not contain introns, all total RNA extracted from mouse mammary gland tissues (Figure 10) was treated with DNase I to remove any contaminating residual genomic DNA, which could be amplified. However, the initial results showed that DNase I treatment created a new problem as it significantly reduced (by 10 fold) the copy number of both the IGF-IR and 18S rRNA amplicons (Table 5). In addition, the variability among triplicate samples was more pronounced for IGF-IR (Table 5). Therefore, since earlier precautions were taken to design IGF-IR primers that crossed an intron-exon boundary, the presence of genomic DNA was not a concern for RT-PCR amplification of IGF-IR. In addition, it was also determined by both semi-quantitative and quantitative PCR, that with or without DNase I treatment, the 18S rRNA gene expression was consistent from sample to sample. Therefore, to circumvent the problems brought about by DNase I, untreated RNA was used for all future studies. The amplification reaction was not affected by primer dimer formation or any non-specific products as indicated by the single peak melt curves, which corresponded to the IGF-IR (Figure 11) and 18S rRNA (Figure 12).

The IGF-IR gene was expressed at each stage of mammary gland development analyzed (Figure 9, 13). Using ANOVA statistical analysis, IGF-IR gene expression levels were significantly different between stages (R^2 = 98.16%, P<0.0001; Figure 13A). IGF-IR gene expression was detected in mammary glands collected from virgin (8 weeks), early (days 2 and 10) and mid pregnant (day 15) glands. However, there was no significant difference in gene expression levels between these time points. The level of gene expression decreased significantly (3.9 fold, P<0.001) during day 19 of pregnancy compared to that observed during day 15 of pregnancy. Gene expression levels continued to decrease (6.7 fold, P<0.001; 10 fold, P<0.001) during early and late lactation compared to expression levels during day 15 of pregnancy. Following late lactation, IGF-IR gene expression levels increased (8.2 fold, P<0.01; 20.4 fold, P<0.01) during early involution and late involution. The level of gene expression during late involution was significantly higher (2.5 fold, P<0.001) than that during early involution.

Samples were then grouped according to broader developmental phases: virgin (8 weeks), early pregnancy (day 2, 10 and 15), late pregnancy (day 19), lactation (day 3 and 10), early involution (day 3), late involution (day 10) (Figure 13B). Within each group, levels of IGF-IR gene expression between sub-categories were not significantly different. IGF-IR gene expression levels in mammary glands of virgin mice were not significantly different than that observed in glands of early pregnant mice. Gene expression decreased significantly (5 fold, P<0.001) during late pregnancy and appeared to decrease (2 fold, P>0.05) during lactation. However, IGF-IR gene expression levels at lactation were not statistically significant from that observed during late pregnancy. The decrease (10 fold) in gene expression from early pregnancy to lactation, however, was significant

(P<0.001). The level of gene expression increased (6.8 fold, P<0.001; 16.9 fold, P<0.001) at early and late involution compared to that during lactation. Overall, the highest level of IGF-IR gene expression was detected during late involution and the lowest at lactation.

6.2. Localization of IGF-IR Transcripts in the Mammary Gland

In parallel to the RT-PCR analysis of gene expression, *in situ* hybridization studies were carried out to investigate the temporal and spatial pattern of IGF-IR gene expression in the developing mammary gland. IGF-IR transcripts were detected in the epithelium at each stage of postnatal gland development (Figure 14). The antisense IGF-IR probe hybridized to the ductal epithelial cells and to the epithelial cells of the terminal duct unit in mammary gland tissues derived from virgin (Figure 14A) and early pregnant mice (Figure 14C). At late pregnancy (Figure 14E) and early involution (Figure 14I), IGF-IR mRNAs were localized in both ductal and alveolar epithelium. During lactation (Figure 14G), the IGF-IR transcripts were detected in the alveolar epithelium and at late involution (Figure 14K), transcripts were localized to the ductal epithelium. Much low signals reflecting non-specific binding were observed in the tissue sections labeled with the radioactive sense strand (Figure 14B, D, F, H, J).

6.3. IGF-IR Protein Expression during Normal Mouse Mammary Gland Development

Results from Western blot analysis showed that the anti-IGF-IR antibody (C-20) recognized a protein of approximately 90 kDa, which corresponds to the size of the β-subunit of the IGF-IR (Figure 15A). The protein densities were measured from four

independent blots. The IGF-IR protein density values were standardized to the density of the positive control band (Figure 15A). Although in other previous reports, β-actin has been used to normalize protein and gene expression levels in the rat mammary gland (Thellin *et al.*, 1999; Saji *et al.*, 2001), we however observed temporal regulation of the β-actin gene expression in the mouse mammary gland. Therefore, we used Ponceau S staining of a non-specific protein band on the nitrocellulose membrane to evaluate sample loading on the gel (Figure 15B). In addition, we also compared IGF-IR protein levels with a non-specific protein on the Coomassie blue stained gel (Figure 15C).

The pattern of protein expression was similar to that previously observed for gene expression. Using ANOVA statistical analysis, we established that IGF-IR protein levels were significantly different between stages (R^2 = 82%, P <0.0001; Figure 16A). Through further analysis, we determined that there was no significant difference in IGF-IR protein expression in virgin (8 weeks), early (days 2 and 10) and mid pregnant (day 15) mammary glands. A significant decrease (1.9 fold, P<0.05) in protein expression levels was observed at day 19 of pregnancy compared to day 15 of pregnancy. A downward trend in protein expression was observed throughout lactation (day 3 and 10) but was not significant. However, the decrease (4.1 fold) in protein levels during late lactation compared to day 15 of pregnancy was significant (P<0.001). A further increase (2.0 fold, P>0.05; 3.9 fold, P<0.001) was observed during early and late involution compared to late lactation. Protein expression at late involution was significantly higher (2.0 fold, P<0.05) than that observed during early involution.

Results obtained from the analysis of IGF-IR protein at individual time points were then grouped, as previously done for gene expression, according to broader stages

of gland development (Figure 16B; See Section 6.1.). Values between virgin and early pregnant glands were not significant, but the decrease (2.2 fold) observed during late pregnancy was significant ($P<0.001$). Expression appeared to decrease (1.3 fold) further during lactation but was not statistically significant ($P>0.05$), although the increase (2.4 fold) observed during late involution was significant ($P<0.001$). In addition, the increased level (1.8 fold) of IGF-IR protein expression during late involution was significantly higher ($P<0.001$) than that during early involution.

Part B – Doxycycline inducible expression of the dominant negative IGF-I receptor in stably transfected MCF-7 cells.

6.4. Identification of IGF-IR-DN Stably Transfected Cells

CMV-rtTA carrying MCF-7 cells (Clone #89) cotransfected with the tetOPh$_{CMV}$-IGF-IR-DN plasmid were screened with the neomycin and zeocin selection agents. Thirty-eight positive clones were identified.

To confirm that the IGF-IR-DN transgene was successfully integrated into the genome, DNA was extracted from all 38 clonal cell lines and analyzed using Southern blotting. Using a ^{32}P-labeled IGF-IR-DN probe (See Section 5.15 in Materials and Methods), a total of 10 positive clonal cell lines were identified (Figure 17; all data not shown). The presence of a 1.071 kb band confirmed that the transgene was stably integrated. Clone #89 was used as a negative control. Five out of the 10 lines (#10, 11, 35, 39 and 41) were selected for further characterization.

6.5. rtTA Gene Expression in Positive Clonal Lines

Following the stable cotransfection of the tetOPh$_{CMV}$-IGF-IR-DN response plasmid, we verified whether the CMV-rtTA expression was intact in the positive clonal cell lines. RNA extracted from clonal cell lines was DNase I treated prior to reverse transcription to get rid of any contaminating genomic DNA. The success of this treatment was verified by the fact that the RT- (no RTase) lanes were blank, indicating the absence of genomic DNA contamination (Figure 18). rtTA gene expression was detected in five clonal cell lines; Clones 10, 11, 35, 39 and 41. Wild type MCF-7 cells, which lacked the

rtTA gene, were used as a negative control. Clone #89, an rtTA expressing clone, was used as the positive control.

6.6. Analysis of IGF-IR-DN Gene Expression in the Stably Transfected Mammary Epithelial Cells

6.6.1. Dosage Analysis

Further experiments were carried out using the clonal cell line, Clone #35, which was shown to express high levels of doxycycline-induced IGF-IR-DN. To determine the optimal concentration of doxycycline required to achieve the highest level of gene expression, a dosage analysis was carried out. Following doxycycline induction (at concentrations of 0, 0.5, 1.0, 1.5 and 2.0 μg/ml) for 24 hours, the highest level of gene expression was achieved at 1 μg/ml (Figure 19).

6.6.2. Time Course Analysis

To determine the optimal time required to achieve maximal expression of the IGF-IR-DN gene, a time course analysis for doxycycline was carried out. Results show that the maximal level of IGF-IR-DN expression was observed with 1 μg/ml doxycycline after 24 hours; the lowest level after 12 hours (Figure 20). At 48 hours, the level of IGF-IR-DN gene expression fell to the same level observed after 12 hours.

6.6.3. Analysis of IGF-IR-DN Gene Expression in Five Positive Clonal Cell Lines

IGF-IR-DN gene expression was found to be induced by doxycycline in 4 out of 5 clonal cell lines (Figure 21; Clones 10, 11, 35 and 41). Different levels of induction of gene expression were observed in each cell line. The highest level (3.3 fold) of induction was observed in Clone #35 relative to the other 3 clones. IGF-IR-DN gene expression was not induced by doxycycline in Clone #39 (Figure 21A) although the transgene was

positive, by Southern blot analysis, for integration in the genome. We therefore used this cell line as a negative control for IGF-IR-DN gene expression in all other experiments. By this technique, a low but persistent level of gene expression appeared to be present in the uninduced clonal lines (Figure 21A). The band densities were quantitatively measured by densitometry (Figure 21B).

6.6.4. RT-PCR Analysis of Gene Expression

IGF-IR-DN gene expression was also examined by RT-PCR. As outlined in Materials and Methods (see Section 5.17.4.), an Xba I strategy was used to discriminate between the presence of the transgene and the endogenous IGF-IR. A 931 bp PCR product was evidence of the presence of both the endogenous IGF-IR gene and the IGF-IR-DN transgene (Figure 22). The results show that 4 clonal cell lines, 10, 11, 35 and 41, expressed the IGF-IR-DN transgene (Figure 22A) as indicated by the presence of the two smaller bands, 514 bp and 417 bp, following Xba I digestion (Figure 22B). Also, the 514 bp and 417 bp bands were observed only in the doxycycline-induced cells but not in the uninduced cells nor in Clones 39 and 89.

6.7. IGF-IR-DN Protein Expression in the Stably Transfected Cells

Western blot analysis was used to examine whether the expressed IGF-IR-DN gene was translated into the protein. Using antibodies specific to the α-subunit (N-20) of the IGF-I receptor, the 135 kDa α-subunit was detected in both the doxycycline-induced and uninduced cells (Figure 23A). An increase in IGF-IR protein (135 kDa) expression was observed in the clonal cell lines treated with doxycycline. Different levels of protein expression were observed in the different cell lines. Two cell lines (Clones 11 and 35)

that were previously demonstrated to express high levels of IGF-IR-DN gene expression (Figure 21) also displayed high levels of protein expression (Figure 23).

The results also show that the 90 kDa endogenous IGF-IR β-subunit, detected with the antibody against the β-subunit of the IGF-I receptor (H-60), was present in both induced and uninduced cells (Figure 23B). The mutant receptor (50 kDa), also detected with the same H-60 antibody, was present only in the stably transfected cells treated with doxycycline (Figure 23C). The mutant receptor was absent in uninduced cells and in Clone #39.

6.8. Detection of Phosphorylated Proteins

To determine whether the IGF-IR-DN protein was functional, its ability to inhibit the autophosphorylation of the IGF-I receptor and phosphorylation of the downstream substrate, insulin receptor substrate 1 (IRS-1), were used as criteria. Autophosphorylation of the IGF-IR β-subunit (90 kDa) and phosphorylation of the IRS-1 (185 kDa) was observed in all clones (Figure 24A-D) including Clones 39 and 89, which were negative controls (Figure 24C, D). Doxycycline did not alter the phosphorylation status of the IRS-1 in Clones 39 and 89. Autophosphorylation of the IGF-IR and phosphorylation of the IRS-I was detected in both the doxycycline-induced and uninduced cells treated with IGF-I (Clones 11 and 35) (Figure 24A, B). This was unexpected since overexpression of the mutant IGF-I receptor gene (Figure 21) and protein (Figure 23) had been previously confirmed in these two clonal cell lines.

We further investigated whether increasing the concentration of doxycycline (2 μg/ml) could inhibit protein phosphorylation. Following IGF-I (2.5, 5 and 10 nM)

stimulation, it was observed that the 185 kDa and 90 kDa bands were once again detected in the IGF-I stimulated cells, regardless of doxycycline treatment (Figure 25). Phosphorylation of the receptor was detected in cells treated for 10 minutes with 2.5 nm IGF-I and increased linearly with 5 and 10 nm IGF-I. The levels of phosphorylation in the doxycycline-induced cells compared to the uninduced cells were undistinguishable.

To confirm that the 185 kDa band (Figure 24) was indeed the IRS-1 phosphoprotein, blots were stripped and immunoblotted with an antibody against the phosphorylated IRS-1 (Ab-1). The antibody recognized a 185 kDa band (Figure 26), which corresponded to the size of the phosphorylated protein in the lanes containing protein isolated from IGF-I treated MCF-7 cells. In addition, the same blots were stripped and immunoblotted with an antibody against the IRS-1 protein. The IRS-1 protein (185 kDa) was expressed in all the samples.

6.8.1. IGF-IR-DN Protein Expression in the IGF-I Stimulated Clonal Lines

Follow-up studies were carried out to further examine why the doxycycline failed to inhibit autophosphorylation of the IGF-IR and phosphorylation of the IRS-1 in the stably transfected cells (Figure 24, 25, 26). We first wanted to confirm the presence of the dominant negative IGF-I receptor. To do this, the nitrocellulose blots (used to detect for tyrosine phosphorylation) were stripped and reprobed with the antibodies specific to the α-subunit (N-20) and β-subunit (H-60) of the IGF-I receptor. The 135 kDa IGF-IR α-subunit was detected in both the doxycycline-induced and uninduced cells (Figure 27A-D). The intensity of the 135 kDa band was higher in the doxycycline induced cells (Clone $^{\#}$11; 2.7 fold; Clone $^{\#}$35; 5.6 fold) than the uninduced cells, indicating increased expression of the IGF-I receptor in the doxycycline-induced cells. In addition, the mutant

receptor (50 kDa band) was only present in the doxycycline-induced cells (Figure 27A, B). Equal levels of the endogenous IGF-IR protein (α and β-subunit) were observed in the doxycycline-induced (Figure 27A, B) and uninduced negative control cell clones (Figure 27C, D). As expected, the mutant protein was absent in the control cell lines.

6.9. Cell Proliferation Assays

Growth of the clonal cell lines was evaluated under different conditions (See Section 5.20. in Materials and Methods). Data (Figure 28) are presented from two independent experiments (with six measurements per experiment for each condition; n=12) as means ± standard deviation (S.D.) Serum-free media (SFM) was used in order to synchronize the cells in the G_0 phase. No change (Table 6) in growth rate was observed at days –1 and 0 of treatment (prior to addition of IGF-I). No difference (Table 6) in growth rates was observed among the parental cell line (Clone #89) and Clone #39 grown with or without doxycycline following IGF-I stimulation (Day 2 and 4). In contrast, growth rate was significantly reduced (Table 6) in doxycycline treated cells (Clones 11 and 35) compared to untreated cells, following IGF-I stimulation (Day 2, 4 and 6). In comparison to control cells, no cell growth was observed in either doxycycline-induced or uninduced cells (Clones 11, 35 and 39) in the absence of IGF-I (Figure 28). Interestingly, the parental cell line, Clone #89, continued to grow slowly even in the absence of IGF-I (Figure 28).

Changes in the rate of cell growth rate (as a measure of fold difference) under the different conditions are illustrated in Figure 29. IGF-I-stimulated growth was significantly increased (6.2 fold; $P<0.001$) in uninduced cells (Clone #11) at day 4

compared to cells grown without IGF-I (Figure 29A). An increase (2.5 fold; $P<0.001$) in cell growth was also observed in Clone #35 in the presence of IGF-I, compared to untreated cells (Figure 29A). IGF-I stimulated cell growth was lower in doxycycline-induced cells compared to uninduced cells; Clone #11 cell growth was significantly decreased (1.3 fold; $P<0.01$) and Clone #35 cell growth was also significantly decreased (1.4 fold; $P<0.001$). An increase in growth (above basal levels) was not observed in either doxycycline-induced or uninduced cells in the absence of IGF-I (Clones 11, 35, 39). Doxycycline treatment, however, did not reduce ($P>0.05$) growth of IGF-I stimulated clonal cell lines 39 and 89 (Figure 29B). Overall, IGF-I stimulated cell growth was significantly decreased in doxycycline-induced cells compared to uninduced cells (Clones 11 and 35; Figure 29A).

6.10. Morphological Studies

Cell morphology was evaluated following doxycycline treatment and following IGF-I stimulation in the stably transfected MCF-7 cells. Observations were carried out at days 0, 2, 4, and 6 of treatment (Figure 30). Throughout the treatment period, the MCF-7 cells were flat and polygonal, exhibiting typical epithelial-like features. In addition, debris and a higher number of rounded-up, floating cells were observed in both the doxycycline-induced and uninduced conditions while few cells exhibiting these characteristics were observed in the control cell line, Clone #89, in both the induced and uninduced cells.

Though a change in morphology was not observed, the IGF-I stimulated cells grown in the absence of doxycycline appeared denser than those grown in the presence of

doxycycline (Figure 30, 31). We examined clonal cell lines 11, 35 and 39 in more detail. Clone #35 (Figure 30), #11 and #39 (Figure 31) grown for 6 days with IGF-I in the absence of doxycycline visually appeared denser than those grown with doxycycline and IGF-I. Under doxycycline-free conditions, the cells (clonal cell lines 11, 35 and 39) had completely covered the bottom of culture dish (Figure 30, 31). In contrast, cell density was low in both the doxycycline-induced and uninduced cells (Clones 11 and 35; Figure 30, 31) grown in the absence of IGF-I. No notable difference in cell density was observed in IGF-I stimulated Clone #39 cells grown with or without doxycycline (Figure 31). The visually apparent differences in cell density corresponded with the results obtained from the cell growth assays (See Section 6.9; Figure 28-31 and Table 6).

7. DISCUSSION

Part A - IGF-IR gene and protein expression during normal mammary gland development.

Previous studies have shown that IGF-IR is important for ductal proliferation and that the overexpression of the IGF-I results in delayed involution of the mammary gland (Hadsell *et al.*, 1996; Kleinberg, 1998; LeRoith *et al.*, 1995). Whether IGF-IR function is critical at specific stages of mammary development is not known. As a first step in understanding the role of IGF-IR function during mammary gland development, the postnatal pattern of gene and protein expression was systematically examined in the mouse.

It has been well documented that the steady state mRNA levels of the IGF-IR in many tissues decrease dramatically during postnatal development resulting in very low levels of gene expression (Werner, 1999). Thus, in anticipation that the level of IGF-IR gene expression in the mammary gland might also be low, expression was assessed by both Northern blot analysis and quantitative RT-PCR analysis. Indeed, gene expression by Northern blot analysis was undetectable and measurable results were only obtained with the more sensitive quantitative RT-PCR technique.

By quantitative real time PCR, the IGF-IR gene was found to be expressed at all stages of mammary gland development. The levels of IGF-IR gene expression between mammary glands from 8 week virgin and early pregnant (day 2, 10 and 15) mice were not significantly different. However, gene expression decreased significantly (5 fold) from early to late (day 19) pregnancy. Although gene expression appeared to decrease (2

fold) throughout lactation (day 3 and 10), this change was not significant. Gene expression levels once again significantly increased (6.8 fold) at early and late involution (16.9 fold). Overall, it was highest during late involution (day 10) and lowest during lactation.

There are several plausible explanations for the pattern of IGF-IR gene expression observed during mammary gland development. First, the IGF-I ligand, a known 'survival factor' important for cell proliferation (Jones and Clemmons, 1995), may be required for the promotion of alveolar cell survival during early pregnancy and thus is more highly expressed at this stage of development (Hadsell and Bonnette, 2000). The latter is well documented to be a period of rapid proliferation and alveolar development (Hadsell and Bonnette, 2000; Kleinberg *et al.*, 2000). In response to high IGF-I levels, IGF-IR, which mediates the mitogenic action of IGF-I, is up-regulated (Clarke, 1997; Ruan *et al.*, 1995). In fact, Richert and Wood (1999) recently demonstrated by *in situ* hybridization that both the IGF-I and IGF-IR transcripts were highly expressed during this phase of development.

In addition, the observation that IGF-IR gene expression is elevated during early pregnancy provides further evidence that the IGF-IR gene expression is required for terminal end bud proliferation (Kleinberg *et al.*, 2000). The down-regulation of IGF-IR gene expression during the period of late pregnancy and early lactation suggests that its role may not be critical at these stages. It is also possible that other growth factors and hormones may be involved during these stages of mammary gland development. In the lactating mammary gland, the epithelium undergoes terminal differentiation and is replaced by actively milk-secreting alveoli (Daniel and Silberstein, 1987; Silberstein,

2001). The process of lactation involves the synthesis and secretion of several milk proteins (Forsyth, 1989; Rilemma, 1994; Dunbar and Wysolmerski, 2001). Thus, the decrease in IGF-IR mRNA levels during lactation could also reflect the increase in expression of milk protein genes during lactation, which may dilute out or mask the expression of the IGF-IR gene. When IGF-IR gene expression was normalized against 18S rRNA gene expression, the level of IGF-IR gene expression was indeed lower during lactation compared to early pregnancy.

A second plausible explanation for the observed increase in IGF-I receptor levels during early pregnancy followed by a decrease during lactation may be attributed to IGF-I receptor regulation by the IGF-I itself. It is well known that the IGF-I ligand can modulate receptor levels (Werner, 1999; Eshet *et al.*, 1993). For instance, an increase in IGF-I binding can decrease the number of IGF-I receptors (Werner, 1999). Indeed, others have recently demonstrated that IGF-I is up-regulated during early pregnancy (Richert and Wood, 1999). Therefore, a decrease in IGF-IR gene expression during lactation may be a direct response to increased IGF-I levels during early pregnancy.

Thirdly, the observed changes in gene expression may be attributed to apoptotic events. The level of gene expression during early involution was not significantly different from the levels observed in the pre-pregnant or virgin mammary gland. To date, mammary gland involution is not well understood, but it is well documented histologically that the involuting mammary gland undergoes dramatic tissue regression and epithelial cell death (Walker *et al.*, 1989; Strange *et al.*, 1992). Also, mammary gland involution is thought to be associated with a loss of survival factors, such as IGF-I (Neuenshwander *et al.*, 1996), epidermal growth factor (EGF; Baik *et al.,* 1998) and other glucocorticoid and systemic

lactogenic hormones (Lund *et al.*, 1996). Therefore, apoptotic events may attribute to the observed reduction in IGF-I/IGF-IR during early involution. Hadsell *et al.* (1996) showed that overexpression of IGF-I in the mammary glands of transgenic mice delayed involution.

Fourthly, the complex hormonal milieu of the developing mammary gland cannot be disregarded in explaining the differential pattern of IGF-IR gene expression. The IGF-IR gene is tightly controlled by the local and circulating levels of a number of hormones and growth factors found during mammary gland morphogenesis (Rilemma, 1994). For example, estrogen level increases gradually during pregnancy and is highest at parturition (Topper and Freeman, 1980; McCormack and Greenwald, 1974). In addition, estrogens can sensitize cells to the mitogenic activity of IGF-I by increasing receptor number (Ruan *et al.*, 1995; Kleinman *et al.*, 1995; Clarke *et al.*, 1997). In addition to estrogen, progesterone, prolactin, growth hormone, epidermal growth factor, fibroblast growth factor and transforming growth factor-α, have all been shown to influence mammary gland morphogenesis (Silberstein 2001; Dunbar and Wysolmerski, 2001). It is plausible that hormones and growth factors that may act as inhibitors or activators regulate IGF-IR gene expression during mammary gland development, particularly during pregnancy and lactation.

Through *in situ* hybridization analysis, IGF-IR transcripts were detected in virgin (20 weeks), pregnant (day 8 and 19), lactating (day 3 and 10) and involuting (day 3 and 10) mouse mammary glands. In direct agreement with the real time PCR results, the levels of IGF-IR transcripts were more abundant during pregnancy. In the mammary glands of pregnant and lactating mice, IGF-IR transcripts were observed in the ductal and alveolar epithelium, respectively. While this study was in progress, Richert and Wood

(1999) demonstrated that IGF-IR transcripts were localized in the terminal end buds and ductal epithelium of the pubertal (5-6 weeks) and post-pubertal (15 week) mammary gland and in the ductal and alveolar epithelium of the mammary glands from pregnant mice (days 12, 13 and 18). Our studies therefore confirm these observations. We additionally demonstrated that IGF-IR transcripts were expressed in the alveolar epithelium in the lactating and in the ductal epithelium in the involuting mammary glands.

Protein expression studies showed measurable levels of IGF-IR protein at each stage of postnatal mammary gland development. There was no observed difference in levels between virgin (8 weeks) and early pregnant (days 2, 10 and 15) mammary glands. As with gene expression, protein levels decreased significantly during late (day 19) pregnancy (2.2 fold) and appeared to decrease during lactation (day 3 and 10; 1.3 fold); however this downward trend in protein expression was not statistically significant. Increased levels of the IGF-IR protein were observed at early (1.2 fold) and late involution (2.4 fold) following lactation. In addition, when IGF-IR protein levels during late involution (day 10) were compared to the protein levels during late pregnancy (day 19), there was a significant (1.8 fold) difference.

Overall, our studies indicate that for the most part, the pattern of IGF-IR protein expression was similar to the pattern of IGF-IR gene expression, suggesting that protein expression may be correlated with gene expression. But, some observed differences do exist. Although higher levels of the IGF-IR protein were observed in the virgin mammary glands as compared to involuting mammary glands, this was not significant (Figure 16). On the other hand, a significantly lower level of gene expression was observed in the

virgin mammary gland compared to the involuting mammary gland (Figure 13). We cannot explain for certain why this is the case, but one explanation may be due to differences in the sensitivity of the two techniques used to quantify gene and protein expression. Alternatively, post-translational modification, changes in efficiency of translation and/or rapid protein turn-over occurring during the synthesis of proteins may attribute to the observed differences in gene and protein levels.

In summary, our gene expression studies demonstrate that the IGF-IR gene was expressed throughout mammary gland development and that a differential pattern of gene expression exists. To our knowledge, this is the first study to systematically examine IGF-IR gene and protein expression at each stage of postnatal mammary gland development. More importantly, we have shown that the pattern of IGF-IR protein expression reflected the pattern of IGF-IR gene expression. The present study provides evidence that IGF-IR is involved in the development of the mammary gland and that it may be important during some phases more than others.

Problems encountered

Housekeeping genes such as glyceraldehyde-3-phosphate dehydrogenase (GAPDH), actins, 28S and 18S rRNAs and cyclophilins are widely used as internal standards for quantitative assays in many tissues, including the mammary gland (Thellin *et al.*, 1999; Bustin, 2000). However, the GAPDH and β-actin genes were found to be differentially expressed when examined during the different stages of mammary gland development, thus making them inappropriate internal controls for the present study. In addition, these genes are known to be present as pseudogenes, which can interfere with the interpretation of RT-PCR results (Bustin, 2000). Therefore, the 18S rRNA gene was selected as an internal standard because several studies have also employed the use of the rRNA gene expression as an internal control (de Leeuw *et al.*, 1989, Schmittgen and Zakrajsek, 2000; Thellin *et al.*, 1999). In fact, Barbu and Dautry (1989) have carried out studies to specifically address the question and have demonstrated that rRNA levels are less likely to vary under conditions that affect mRNA expression, making the 18S rRNA gene a favourable internal standard for mRNA quantification. However, one disadvantage of using 18S rRNA for RT-PCR studies is that the 18S rRNA gene does not contain introns. Thus, with the primers selected it was difficult to discriminate between PCR products derived from genomic DNA and the cDNA template following amplification, a factor that may interfere with the interpretation of results. To circumvent this problem, DNase I was used to degrade any contaminating genomic DNA. Although the DNase I treatment was effective in this regard, a new problem arose, the inability to completely remove all residual DNase I. As a result, this residual DNase I interfered with the RT-PCR reaction.

In particular, DNase I consistently reduced the copy number of IGF-IR transcripts when compared to non-DNase I treated samples (Table 5). This low copy number further led to vast variability among triplicate values for each time point, during quantitative real time PCR analysis (Table 5). On the other hand, DNase I did not have such an effect on the 18S rRNA transcripts. It is plausible that because in general, the levels of IGF-IR transcripts are low in many tissues, including mammary glands (Werner, 1999), and the levels of 18S rRNA transcript in the mammary gland are high, the effect of DNase I on the latter was minimal. In addition, when the 18S rRNA PCR products were visualized following semi-quantitative and quantitative RT-PCR amplification, the 18S rRNA appeared to be consistently expressed throughout all stages of mammary gland development. Consequently, a decision was made to omit DNase I treatment of all RNA samples used in these studies.

Part B - Doxycycline inducible expression of the dominant negative IGF-I receptor in stably transfected MCF-7 cells.

The tetracycline regulatory system was chosen to allow conditional regulation of the expression of a dominant negative (DN) mutant IGF-I receptor (IGF-IR-DN) *in vitro*. The latter has been previously shown to effectively inhibit the function of the endogenous receptor, both *in vivo* (Prager *et al.,* 1994) and *in vitro* (Prager *et al.,* 1992), by a dominant negative mode of action. The development of this *in vitro* model was to in part, address the role of the IGF-I/IGF-IR gene in mammary epithelial cells.

The MCF-7 breast cancer cell line was chosen for this study because it is an established mammary epithelial cell line that which overexpresses IGF-IR (Khandwala *et al.*, 2000; Surmacz, 2000). In this cell line, IGF-I/IGF-IR is also known to enhance growth and inhibit apoptosis (Werner and LeRoith, 2000; Guvakova and Surmacz, 1997). Therefore, this is an ideal cell line to examine inhibition of IGF-I/IGF-IR function.

In the *in vitro* model system (Figure 7), generated in our laboratory, induction of gene expression of the dominant negative IGF-IR fused to the tetracycline operator (tetO) sequence and the cytomegalovirus-derived minimal promoter (tetOPh$_{CMV}$-IGF-IR-DN), was placed under the regulation of the doxycycline-sensitive reverse tetracycline transactivator (rtTA). The objective was to examine the ability of the IGF-IR-DN to inhibit IGF-I receptor function. This would be accomplished by demonstrating that the inhibition of receptor function affected cell growth and the phosphorylation of downstream substrates. These studies involved providing evidence that the mutant receptor was present in the cells and that its expression was inducible.

First, doxycycline ability to induce IGF-IR-DN gene expression was examined by Northern blot analysis. Doxycycline was added to the cells at 1 μg/ml for 24 hours, as these parameters appeared to be optimal (Figure 19, 20). The induction of IGF-IR-DN gene expression was demonstrated in four out of five clonal cell lines analyzed; the highest level (3.3 fold) of expression in Clone #35. One clone, Clone #39, was negative for IGF-IR-DN gene expression and was therefore selected as a negative control for these experiments. The parental rtTA expressing cell line, Clone #89, which did not contain the IGF-IR-DN transgene, was also used as another negative control. However, in uninduced cells, a low level of gene expression (Figure 21) was detected suggesting the possibility of some low level of leakiness in the tetracycline system. On the other hand, these bands were merely non-specific. Because leaky expression in the uninduced cells would make it difficult to interpret the results, the same RNA was analyzed by RT-PCR and a unique Xba I restriction digest strategy (See Section 5.17.4. in Materials and Methods).

RT-PCR being a much more sensitive technique than Northern blot analysis, was used to confirm the induction of the IGF-IR-DN transgene in the four clonal cell lines and further examine if there was a problem with leakiness in the system. Xba I digestion of the PCR product, amplified from clones that were positive for inducible transgene expression, resulted in the appearance of two smaller bands, 514 and 417 bp in size. The same four positive clones previously identified by Northern blot analysis (Figure 21), were also positive by this method (Figure 22). In addition, when clones were not induced by doxycycline, these bands were absent confirming that indeed the tetracycline system was not leaky, and that the ambiguous bands visible in uninduced clones were merely

non-specific (Figure 21, 22). Also, the mutant protein was not detected in the uninduced cells (Figure 27).

For protein studies, the IGF-IR β-subunit antibody (H-60; Santa Cruz Biotechnology, Inc.) was selected as it recognises the β-subunits of the both the mutant and endogenous receptor. The results from Western blot analysis showed that the mutant receptor protein was present only in the doxycycline-induced cells and not in the uninduced cells nor in the negative controls (Clones #39 and #89). On the other hand, the endogenous receptor (β-subunit), as evidenced by the presence of the 90 kDa band, was detected in both the doxycycline-induced and uninduced cells.

To determine the level at which the mutant receptor was expressed, an indirect method of comparing the levels of the IGF-IR α-subunit in the doxycycline-induced and the uninduced cells was used. The reason being that increased levels of the IGF-I receptor α-subunit in the doxycycline-induced cells would suggest that the mutant IGF-I receptor is overexpressed and therefore available to produce a dominant-negative effect on the endogenous receptor. Indeed, the IGF-IR α-subunit was more abundant in the doxycycline-induced cells (Figure 23). As previously observed with gene expression, varying levels of protein were detected in the four clonal cell lines, the highest level detected in Clone #35. These results provided evidence that the mutant receptor gene expression of the mutant receptor was inducible, the IGF-IR-DN protein was effectively translated and was also overexpressed.

To investigate whether the signalling pathway was indeed inhibited by the mutant receptor, the autophosphorylation of the IGF-IR and the phosphorylation of the downstream substrate, insulin receptor substrate – 1 (IRS-1) was examined. In one out of

three experiments, increased phosphorylation of the IRS-1 protein in the uninduced cells compared to doxycycline-induced cells was demonstrated in one clone, Clone #35 (Figure 26B). However, this was not observed in the other clonal cell line #11 (Figure 26A), nor was it observed in two other experiments. This suggests that the results from the first experiment were likely due to differences in sample loading (Figure 26). Furthermore, addition of IGF-I (2.5 to 10 nm) failed to inhibit autophosphorylation of the IGF-I receptor and phosphorylation of the IRS-1 in both the doxycycline-induced and uninduced cells (Figure 25). The results showed that in this system, doxycycline induction did not inhibit IGF-I stimulated phosphorylation of the IRS-1 and autophosphorylation of the IGF-IR. These results were surprising since the dominant negative IGF-IR-DN has been previously shown to effectively inhibit endogenous IGF-IR function in GC rat pituitary cells (Prager *et al.*, 1992). In addition, IRS-1 phosphorylation was blocked in IGF-I stimulated pituitary cells that constitutively expressed the dominant negative receptor.

There are a number of plausible explanations why the mutant receptor failed to inhibit autophosphorylation of the IGF-I receptor and phosphorylation of the downstream substrate, IRS-1. First, the inability of the doxycycline-induced mutant receptor to inhibit IGF-I signalling may be merely due to the presence of an insufficient number of the mutant receptors which may be unable to block the endogenous receptor. If more endogenous than mutant receptors are present, then the probability of the mutant receptor forming hybrids with the endogenous receptor and inhibiting receptor activity is diminished. Indeed, the IGF-I receptor is overexpressed in estrogen-responsive breast cancer cells (Mauro *et al.*, 2001) such as the MCF-7 cells and ligand-independent

tyrosine kinase activity is up-regulated in breast cancer cells (Mauro *et al.*, 2001). Therefore, it is likely that since this cell line already expresses high levels of the IGF-I receptor, the level of IGF-IR-DN gene expression achieved following doxycycline treatment was not adequate to completely inhibit IGF-I signalling.

Second, the half-life of the mutant receptor may be short, which may explain the lack of available mutant receptors to block endogenous receptor activity. However, in Rat 1 fibroblast cells, the biosynthetic half-life of the mutant receptors and the mutant receptor degredation rate, measured by Prager *et al.*, (1992), was much slower that that of the wild type receptor. But this may be unique to fibroblasts and different for mammary epithelial cells. Therefore, it is still possible that the quick degredation of the mutant receptor may account for the failure of the IGF-IR-DN to inhibit autophosphorylation of the IGF-I receptor and phosphorylation the IRS-1.

Third, it is possible that the doxycycline following administration readily became inactive. However, this was highly unlikely because as a precautionary step, fresh doxycycline was added each time the media was changed (every 2 days).

Fourth, the experimental conditions used for phosphorylation studies were not the same as those used for gene and protein expression studies. Therefore, it is possible that autophosphorylation of the IGF-I receptor and phosphorylation the IRS-1 was not inhibited because of experimental variation. To rule this out, the same nitrocellulose membranes previously utilized for the phosphorylation studies, were used to demonstrate IGF-IR-DN gene expression induction. The membranes were immunoblotted with the IGF-IR specific antibodies. Indeed, higher levels (3 to 6 fold; Figure 27A, B) of the IGF-I

receptor α-subunit were detected in the doxycycline-induced cells compared to the uninduced cells.

It is well established that the IGF-I receptor and the insulin receptor (IR) are similar in structure and also share common signalling pathways, via the major substrate, IRS-1 (Lorenzino *et al.*, 1998; White and Yenush, 1998; Roth *et al.*, 1991). Phosphorylation of the IRS-1 and activation of the downstream pathways, such as the P13/Akt pathway, is common to the IR and the IGF-IR (Myers *et al.*, 1993). It is therefore possible that the endogenous half-receptor may have a higher binding affinity to the insulin half-receptor than to the mutant receptor. Thus, even in the presence of the overexpression of the mutant receptor, the mutant receptors may not be able to form disulphide links with the endogenous receptor and subsequently inhibit IGF-I induced phosphorylation.

It is also possible that the observed phosphorylation of the IRS-1 substrate in these experiments may have resulted from the activation of the insulin receptor by the IGF-I. Several groups have shown that IGF-IR/IR hybrids are capable of not only binding the IGF-I ligand but also of activating the hybrid receptor (Siddle *et al.*, 1994; Soos *et al.*, 1993; Frattali *et al.*, 1993). Also, previous studies have suggested that the Crk proteins are preferentially or specifically activated by the IGF-IR (Butler *et al.*, 1998; Beitner-Johnson *et al.*, 1996). Therefore, it may be that phosphorylation of the Crk substrate is an appropriate end point to measure. However, these studies were not done.

In hormone-responsive breast cancer cells, such as MCF-7 cells, it has been shown that the stimulation by IGF-I is increased by estrogen (Stewart *et al.*, 1990; Van Der Berg *et al.*, 1988; Varma and Conrad, 2002). However, it is unlikely that estrogen

presented a problem in these studies since all experiments were conducted in phenol-red free media (Karey and Sirbasku, 1988).

Whether the mutant receptor had an effect on cell growth was also examined (Figure 28). In both the doxycycline-induced and uninduced cells, cells failed to proliferate in the absence of IGF-I. Cells did, however, grow in response to IGF-I, with and without doxycycline. However, cell density was significantly lower (Table 6) in the cells grown in the presence of doxycycline. No significant change in cell density was seen in control cells (Clone 39 and 89) treated with or without doxycycline in the presence of IGF-I, providing evidence that doxycycline was not toxic to the cells. In addition, the concentration of doxycycline used was comparable to that used in several other studies (Venditti *et al.*, 2002; Fife and Sledge, 1998). Overall, the present study indicated that the mutant receptor only partially but not completely inhibited cell proliferation. Indeed, some of the previous reasons listed to explain why the mutant receptor did not inhibit the phosphorylation of a downstream substrate protein may also apply here.

The proliferative response to IGF-I/IGF-IR in MCF-7 cells is known to be mediated by the PI 3-kinase and MAP kinase pathways, following insulin receptor substrate - I phosphorylation (Dufourny *et al.*, 1997; Lee and Yee, 1995). IGF-I stimulated proliferation was observed in both the doxycycline-induced and uninduced cells while no cell growth was observed in the absence of IGF-I. In spite of IGF-I stimulated phosphorylation of the IRS-1, cell growth was reduced in the doxycycline-induced cells. These findings suggest that the IRS-1 phosphorylation may not be critical for cell growth in this *in vitro* model system. One possible explanation is that other

downstream signals may be involved for optimal cell proliferation of MCF-7 cells. Activation of downstream substrates such as the MAP kinases and/or the binding of the p85 subunit of the phosphotidylinositol 3-kinase to the p110 catalytic subunit may not occur as a result of the inhibition of the endogenous IGF-I receptor by the mutant receptor. In addition, there is some evidence that Crk proteins are preferentially or specifically activated by the IGF-IR (Butler *et al.*, 1998). CrkII phosphorylation has been observed in IGF-I stimulated human embryonic kidney and NIH 3T3 fibroblast cells (Beitner-Johnson and LeRoith, 1995). Furthermore, Crk proteins have been suggested to play a role in the Ras pathway, which plays an important role in IGF-IR induced cell proliferation (Butler *et al.*, 1998; Matsuda, 1992; ten Hoeve *et al.*, 1992). The overexpression of CrkII was also shown to increase the mitogenic response to IGF-I in mouse fibroblasts (Beitner-Johnson *et al.*, 1996). To date, the role of the Crk proteins in IGF-I receptor signal transduction in MCF-7 cells has not been elucidated. Based on the evidence from other cell types, it is plausible that optimal proliferation of the MCF-7 cells is induced upon activation of the Crk proteins. The possibility that the IGF-I induced growth of the cells, which was significantly reduced in the presence of the dominant negative IGF-I receptor, does not involve IRS-1 needs to be addressed further to fully understand IGF-I/IGF-IR signalling in the MCF-7 breast cancer cells.

To further assess the effect of the mutant receptor in the stably transfected MCF-7 cells, the effect on cell morphology was examined (Figure 30). No obvious phenotypic differences were observed upon doxycycline treatment. The cells remained attached to culture dishes and retained normal epithelial-like features. Consistent with these findings, Prager *et al.* (1994) showed that Rat 1 fibroblasts transfected with the truncated IGF-I β-

subunit receptor cDNA had a normal phenotypic appearance and cell morphology did not change in the presence of IGF-I ligand. In addition, a higher number of floating, rounded-up cells were observed in both the doxycycline-induced and uninduced conditions while few cells exhibiting these characteristics were observed in the control cell line, Clone #89, in both doxycycline-induced and uninduced cells. Although these characteristics are typical of dying cells (Resnicoff *et al.,* 1995; Peruzzi *et al.,* 1999), further tests needs to be carried out to determine whether these cells were indeed dying and whether cell death was induced by apoptosis and/or necrosis.

Summary

- This is the first study to systematically examine IGF-IR gene expression at each stage of postnatal mouse mammary gland development. We demonstrated that IGF-IR gene was expressed throughout all stages of postnatal mammary gland development and that a differential pattern of gene expression exists. More importantly, we have shown that the pattern of IGF-IR protein expression correlated with the pattern of IGF-IR gene expression. Furthermore, we showed that IGF-IR transcripts were most abundant in regions of the mammary gland associated with proliferation and secretion.
- We have developed a novel *in vitro* model system in which expression of the IGF-IR-DN was conditionally regulated. IGF-I stimulated cell growth was significantly reduced in mammary epithelial cells expressing the inducible mutant IGF-I receptor. Our data suggest that the phosphorylation of IRS-1 may not be critical for cell growth in this *in vitro* model system.

Future Studies

Part A - IGF-IR gene and protein expression during normal mammary gland development.

It is known that estrogen induces IGF-IR expression in breast tumor epithelial cell lines (Zhang and Yee, 2000; Stewart *et al.*, 1990) and high levels of both the estrogen receptors and the IGF-IR are correlated with susceptibility to breast cancer in humans (Surmacz, 2000; Lee and Yee, 1995). A parallel study to examine estrogen receptor gene expression will allow us to compare and understand the interplay between estrogen and IGF-IR in normal mammary gland development. Also, since growth hormone (GH) is known to regulate IGF-I gene expression during mammary gland development (and in bone growth; Nilsson *et al.*, 1986), an analysis of the relationship between GH and IGF-I levels, would also provide further insight in the role of IGF-IR in mammary gland development (Kleinberg *et al.*, 2000).

Part B - Doxycycline inducible expression of the dominant negative IGF-I receptor in stably transfected MCF-7 cells.

Additional steps can be taken to more fully characterize the tetO-IGF-IR-DN inducible model system that we have developed. As a first step, the type of IGF-I receptors formed after doxycycline treatment can be examined. The presence of insulin/IGF-I hybrid receptors, for example, may explain the inability of the IGF-IR-DN to inhibit IGF-I induced phosphorylation and proliferation. An analysis of downstream substrates, other than the IRS-1, would also provide clues in understanding why IGF-I stimulated cell growth was reduced in doxycycline-induced cells. Since IRS-1 phosphorylation was not inhibited in these cells, it is possible that other downstream substrates may play a role in cell growth in this system. These studies will contribute additional information about IGF-I/IGF-IR signalling and may allow us to determine why the IGF-I signalling pathway was not inhibited in the presence of the mutant receptor, in the MCF-7 cell line.

FIGURES

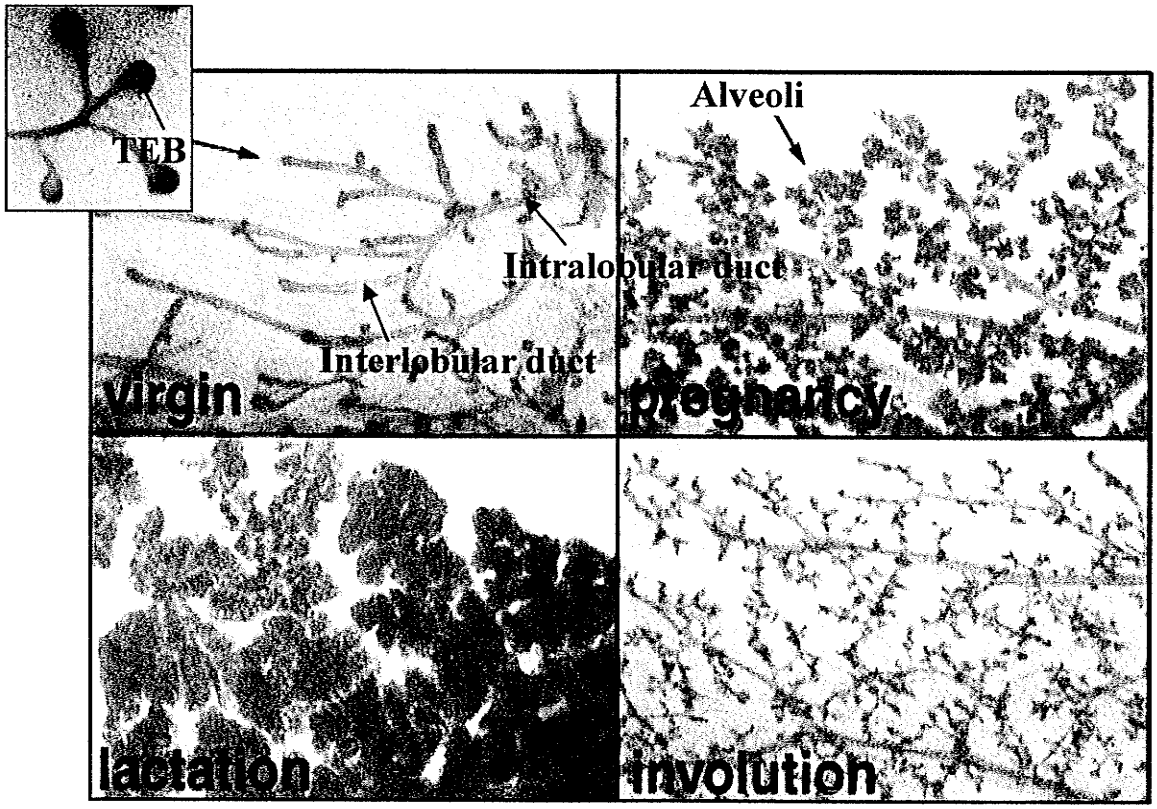

Figure 1. Stages of mammary gland development. The 4 major stages of mammary gland development are depicted: virgin, pregnancy, lactation and involution. The interlobular and intralobular ducts can be seen during the virgin state. Terminal end buds (TEB) are shown in the virgin mouse (inset). Proliferation of the ductal epithelium at pregnancy results in the formation of alveoli from the terminal end buds. At lactation, secretory material is collected in the alveoli, which become dilated and appear as saccules. The mammary gland undergoes retrogressive changes during involution. (Figures adapted from http://mamm.dev.ipg)

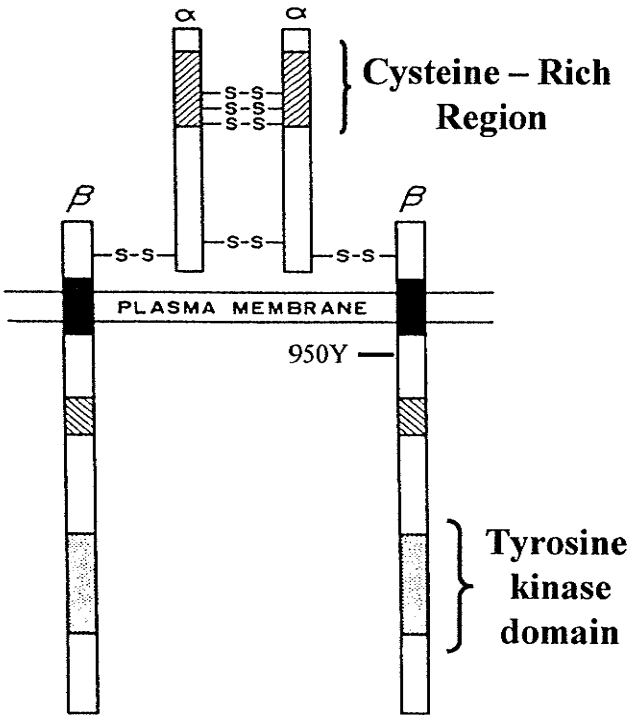

Figure 2. The structure of the IGF-I receptor protein. The IGF-I receptor exists as a heterodimer consisting of two α-subunits and two β-subunits. The subunits are linked by disulfide bonds (α-α and β-β disulfide bridges) forming the β-α-α-β receptor. The extracellular α-subunit contains the cysteine rich portion that is defined as the ligand binding site. The β-subunit contains the transmembrane domain, the critical tyrosine kinase domain and the C-terminal tail. (Figure adapted from Rubin and Baserga, 1995)

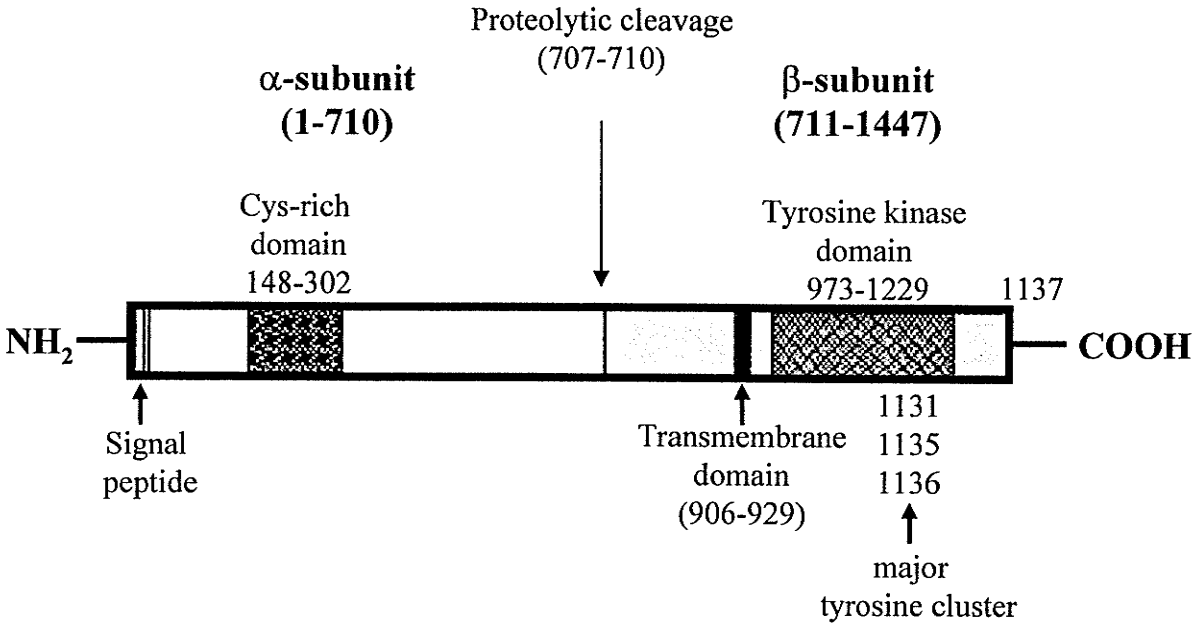

Figure 3. The structure of the IGF-IR precursor protein. The 1367 amino acid polypeptide contains a signal peptide, and the cysteine non-rich and cysteine-rich domain in the α-subunit. The β-subunit contains the transmembrane domain, the critical tyrosine kinase domain and the C-terminal tail. Proteolytic cleavage at residues 707-710 releases the α and β subunits. The subunits are linked by disulfide bonds giving rise to the mature heterotetrameric receptor. (Figure adapted from Lorenzino, 1998)

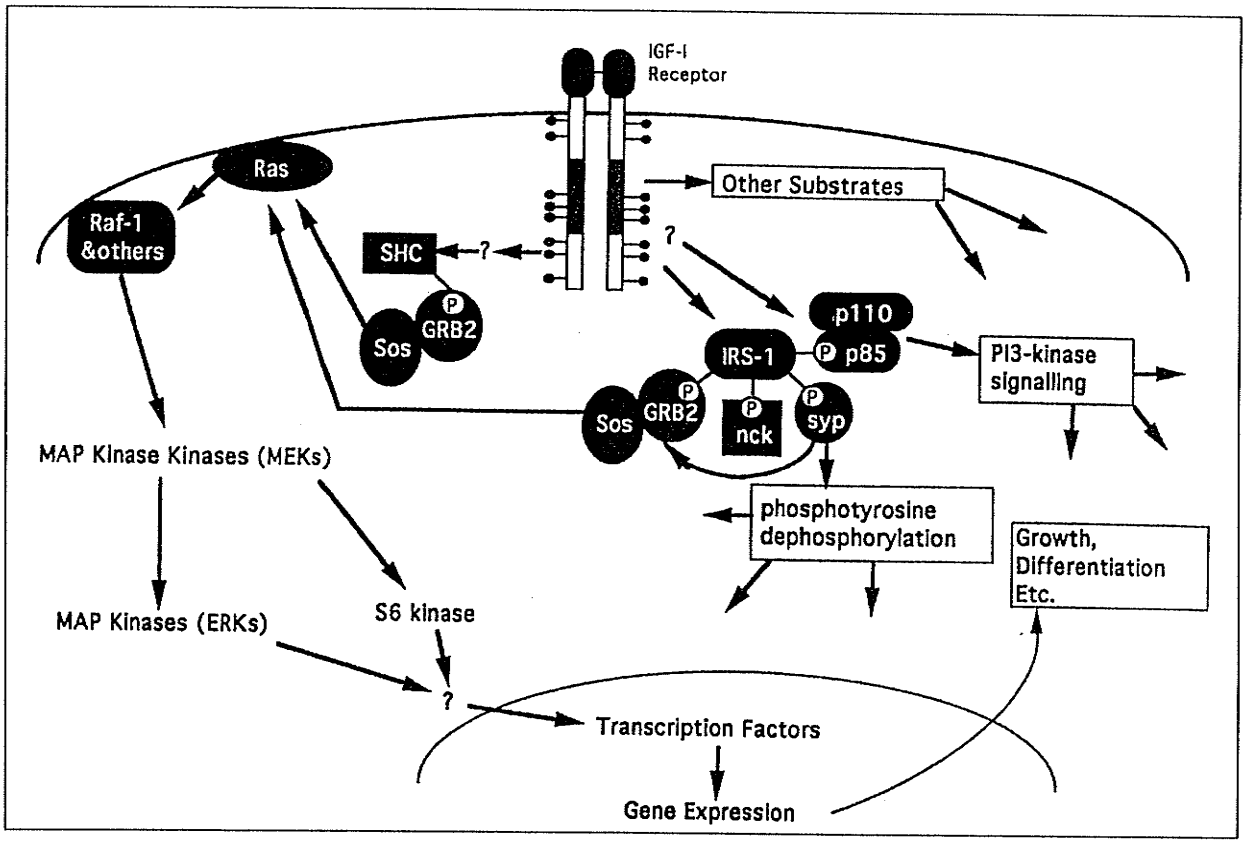

Figure 4. The intracellular signaling pathways of the IGF-I receptor. The IGF-IR undergoes autophosphorylation upon binding of the IGF-I. The intrinsic tyrosine kinase activity of the receptor phosphorylates IRS-1 to which several SH-containing proteins bind (PI-3, Grb2, Nck and Syp) activating multiple signaling pathways. The activated IGF-IR can also phosphorylate Shc, which forms a complex with Grb2. This complex eventually leads to the activation of Ras and the subsequent activation of a series of MAP kinases. These multiple cascades of activated protein kinases activate several nuclear transcription factors and is followed by subsequent gene expression. The longer term effects of the alterations in expression of IGF-I responsive genes include growth and differentiation. (Figure from LeRoith *et al.,* 1995)

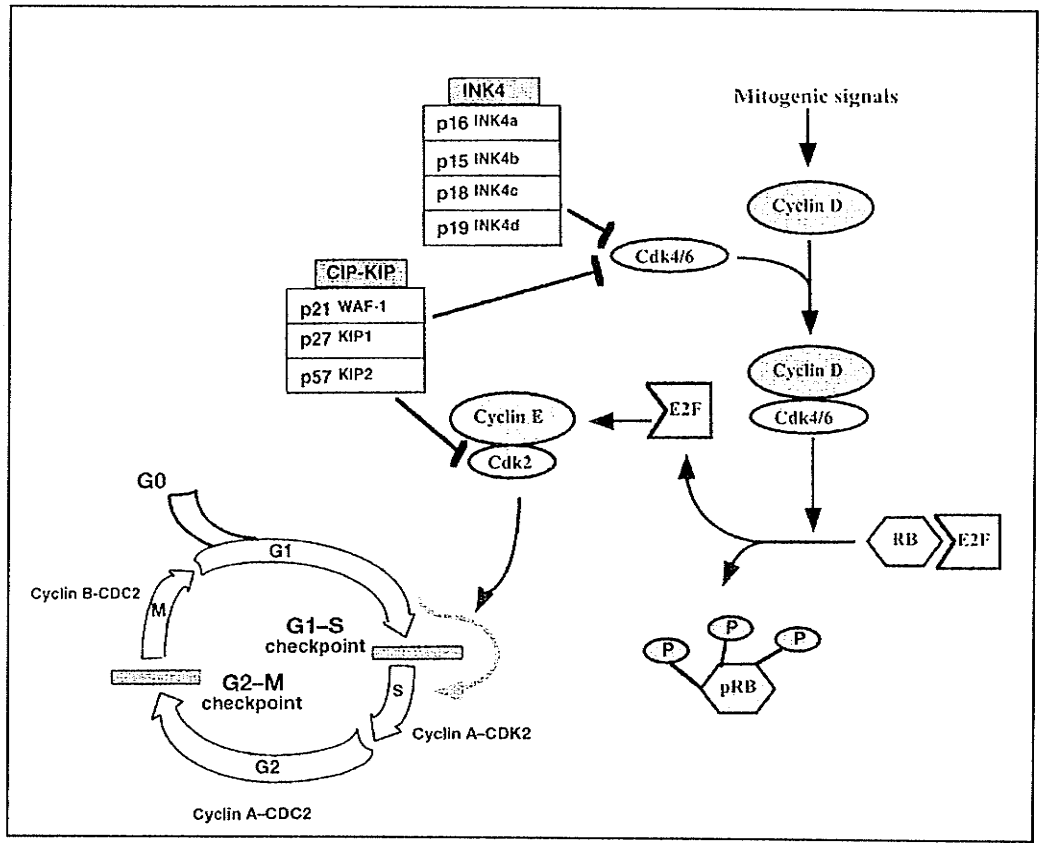

Figure 5. The IGF-I/IGF-I receptor and the cell cycle. The different phases of the cell cycle are shown: quiescent (G0), mitosis (M), first gap (G1), DNA synthesis (S) and second gap (G2). Replication occurs after the cell has passed the G1-S checkpoint or the restriction point. The progression up to and through this point is driven by mitogenic growth factors, which drive the cell to proliferate. IGF-I is required for cell cycle progression through G1-S phase transition and underexpression of IGF-IR prevents passage through the G1-S checkpoint. The unphosphorylated (RB) and hyperphosphorylated (pRB) forms of the retinoblastoma protein are shown. (Figure adapted from Dupont and LeRoith, 2001)

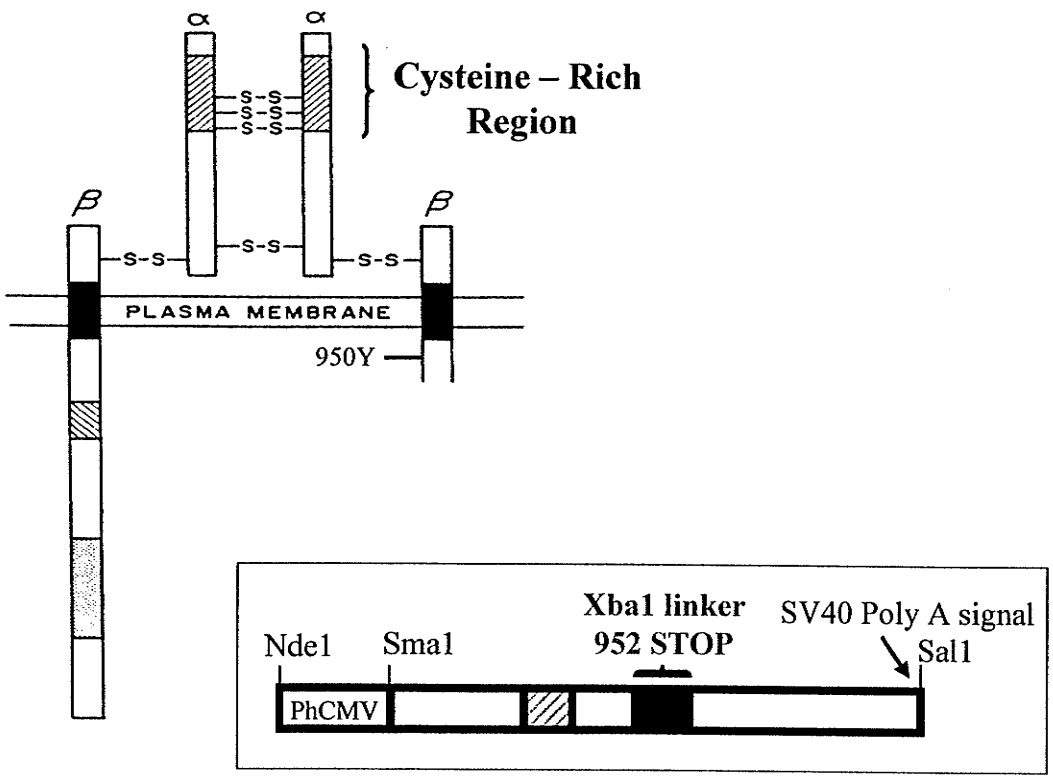

Figure 6. The dominant-negative IGF-I receptor. The mutant IGF-I receptor is a truncated protein that forms a hybrid receptor with the wild-type receptor. The mutant IGF-IR cDNA (inset, a gift from S. Melmed, University of California) was constructed by inserting a synthetic codon loop by use of an Xba linker at position 952 (952 STOP) in the intracellular membrane domain of the human IGF-IR β-subunit. The resultant IGF-IR protein product lacks the critical tyrosine kinase domain (located downstream of the synthetic stop codon) and inhibits the function of the normal IGF-I receptor through a dominant-negative mode of action (Prager *et al.*, 1992).

Figure 7. Schematic representation of the tetracycline regulated IGF-IR-DN gene expression system. The tetracycline-regulated gene expression system (Gossen and Bujard, 1992) was used to conditionally regulate IGF-IR-DN gene expression in the MCF-7 human breast cancer cell line. The reverse tetracycline transcriptional activator - a fusion of the tetracycline repressor and the VP16 activation domain of the herpes simplex virus - driven by the cytomegalovirus (CMV) promoter is constitutively expressed in the stably co-transfected mammary epithelial cells. Upon induction by doxycycline (a tetracycline analog), the reverse tetracycline transcriptional activator binds to the tet operator sequences and activates the cytomegalovirus-derived minimal (Ph_{CMV}) promoter to transcribe the gene of interest, IGF-IR-DN. In the absence of doxycycline, the reverse tetracycline transcriptional activator cannot bind to the tet operator sequences. Thus, IGF-IR-DN gene transcription will not be induced.

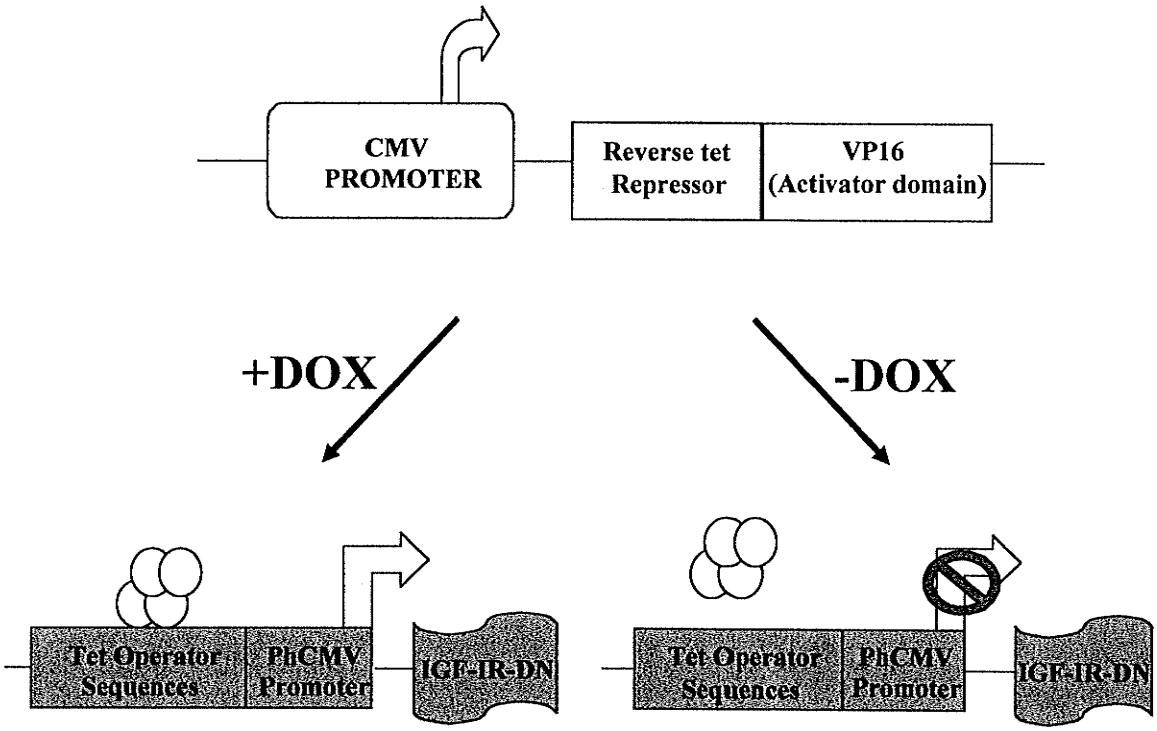
CMV
PROMOTER
Reverse tet
Repressor
VP16
(Activator domain)
+DOX
-DOX
Tet Operator
Sequences
PhCMV
Promoter
IGF-IR-DN
Tet Operator
Sequences
PhCMV
Promoter
IGF-IR-DN

Figure 8. The pTet-On/pUHD172-1neo and pTRE/pUHD10-3zeo vectors used to generate the stably transfected MCF-7 human breast epithelial cell lines. (A) The regulator plasmid, pTet-On/pUHD172-1neo vector, (Clontech Laboratories, Inc.) contains the reverse tetracycline transactivator (rtTA) downstream of the cytomegalovirus promoter (P_{CMV}). This CMV-rtTA vector has been successfully used to stably transfect MCF-7 human breast cancer cells. Clone $^{\#}89$ is a positive cell line, which expresses the rtTA gene fused to the CMV promoter and a neomycin-resistance cassette. (B) The response plasmid, pTRE/pUHD10-3zeo (Clontech Laboratories, Inc.), contains seven copies of tetracycline operator sequences ($tetO_7$) upstream of a minimal human cytomegalovirus promoter (Ph_{CMV}). The pUHD10-3zeo vector was modified to contain a zeocin-resistance cassette. The EcoRI/BamHI IGF-IR-DN cDNA fragment (See Figure 6) was subcloned into the multiple cloning site (EcoRI/BamHI) downstream of the Ph_{CMV} promoter in the pUHD10-3zeo vector. (Figures adapted from http://www.clontech.com/tet/index.shtml)

A

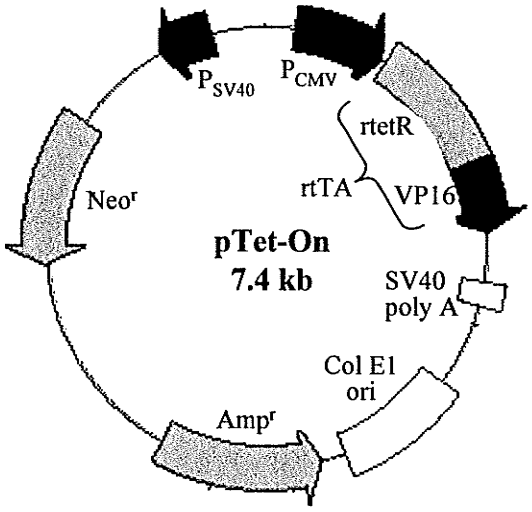
P_{SV40}
P_{CMV}
rtetR
rtTA
VP16
Neo^r
pTet-On
7.4 kb
SV40
poly A
Col E1
ori
Amp^r

B

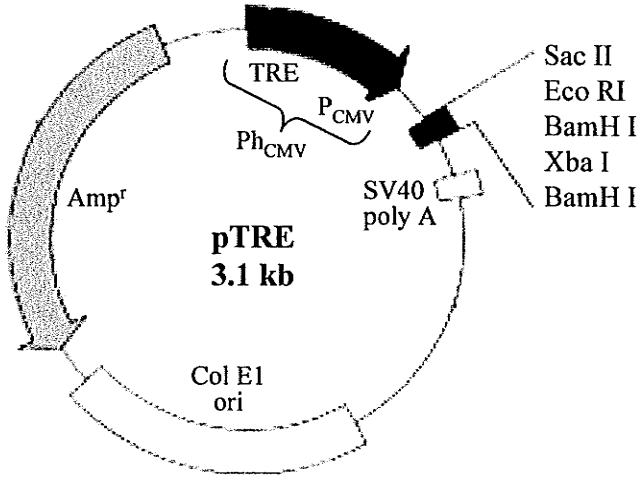
TRE
P_{CMV}
Ph_{CMV}
Sac II
Eco RI
BamH I
Xba I
BamH I
Amp^r
SV40
poly A
pTRE
3.1 kb
Col E1
ori

Figure 9. RT-PCR analysis of IGF-IR gene expression during mouse mammary gland development. Total RNA was extracted from mouse mammary glands (n=3), pooled, and quantitative real time RT-PCR was performed to amplify the (A) IGF-IR and (B) 18S rRNA cDNAs. The 18S rRNA was used to confirm integrity, equal loading and normalizing of samples. IGF-IR gene expression was up-regulated in mammary glands during early-to-mid pregnancy (day 2, 10 and 15) compared to levels observed in virgin mice (8 week). Gene expression was highest during involution (days 3 and 10) and lowest at lactation (days 3 and 10). The PCR products were visualized on a 1.5% agarose gel with ethidium bromide. Duplicate PCR products from two independent experiments are shown. RT- controls were used to indicate the efficient removal of any residual DNA in the RNA. Abbreviations: d = day, wk = weeks.

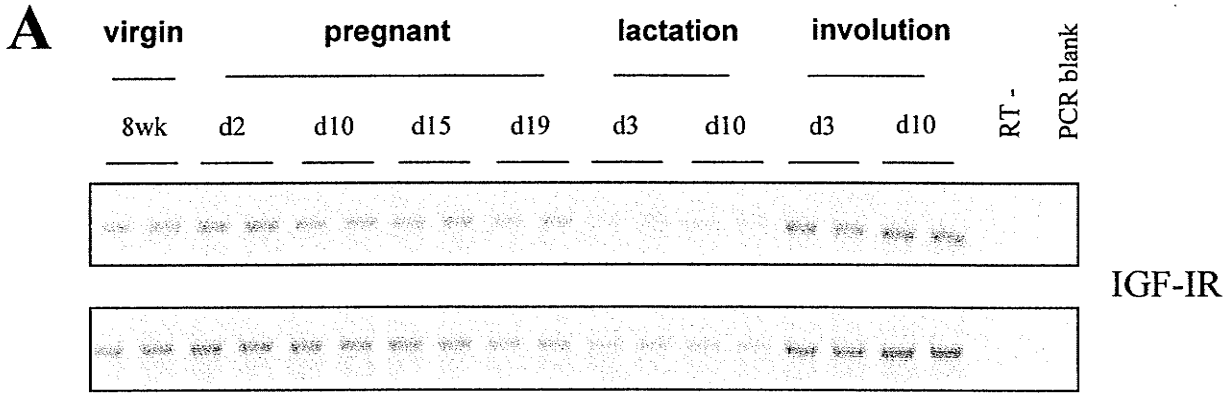
A
virgin
pregnant
lactation
involution
8wk
d2
d10
d15
d19
d3
d10
d3
d10
RT -
PCR blank
IGF-IR

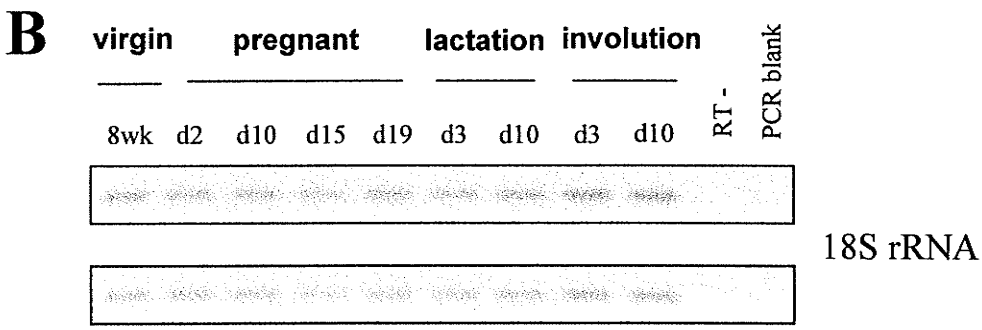
B
virgin
pregnant
lactation
involution
8wk
d2
d10
d15
d19
d3
d10
d3
d10
RT -
PCR blank
18S rRNA

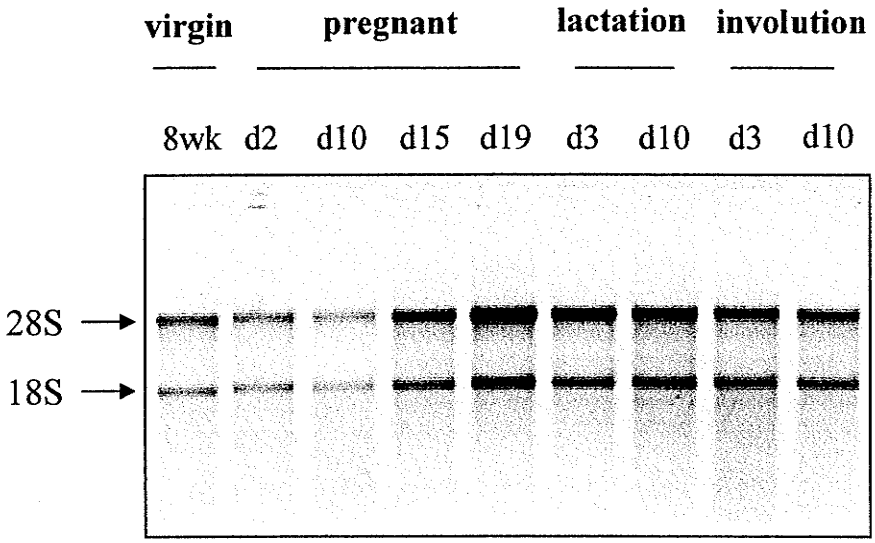

Figure 10. Analysis of RNA. Total RNA (1 μg) from the mouse mammary gland tissues were electrophoresed on a 1.3% agarose gel and analyzed prior to RT-PCR analysis. The results show that the RNA was intact and not denatured. The 28S and 18S ribosomal RNA bands are clearly prominent on the EtBr stained agarose gel visualized by ultraviolet light. Abbreviations: d = day, wk = weeks.

Figure 11. IGF-IR PCR product detection in real time. (A) The PCR amplification plot for the IGF-IR plasmid standard and (B) the amplification plot of the IGF-IR PCR products. The plots show the relative fluorescence units (RFU) versus cycle number. The threshold limit (red line) was set at 10 times the standard deviation of fluorescence over the base line. (C) The standard curve plot shows the log of initial copy number versus the threshold cycle value. The correlation coefficient and the slope and the intercept of the standard curve are indicated. (D) Individual melt curves (at 89°C) of each PCR product amplified with the IGF-IR primers are shown in the -dF/dT versus temperature plot.

A

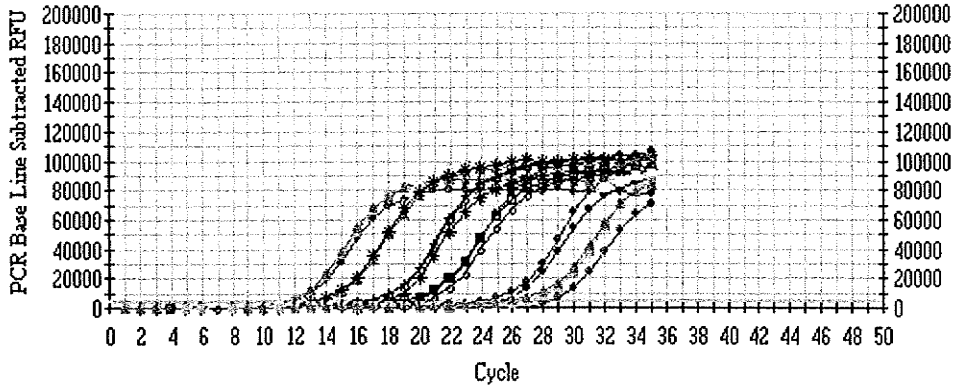
PCR Base Line Subtracted RFU
Cycle

B

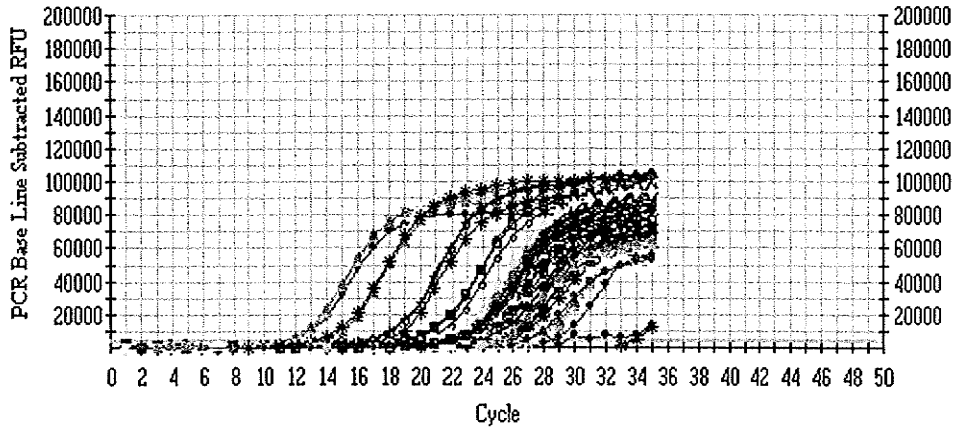
PCR Base Line Subtracted RFU
Cycle

C

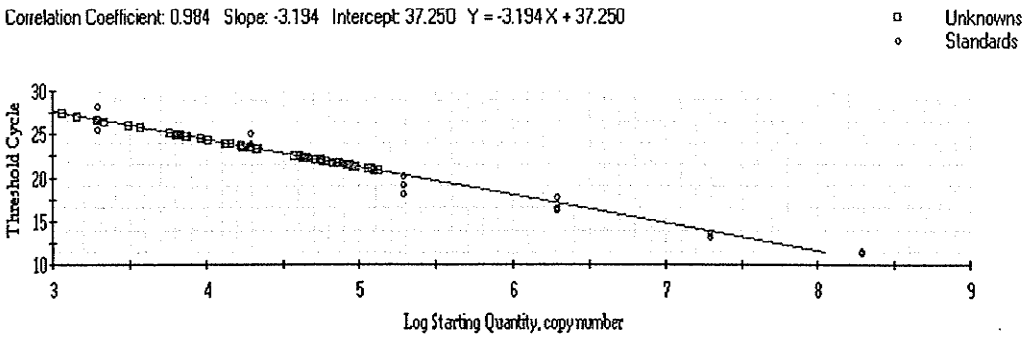
Correlation Coefficient: 0.984 Slope: -3.194 Intercept: 37.250 Y = -3.194 X + 37.250
Unknowns
Standards
Threshold Cycle
Log Starting Quantity, copy number

D

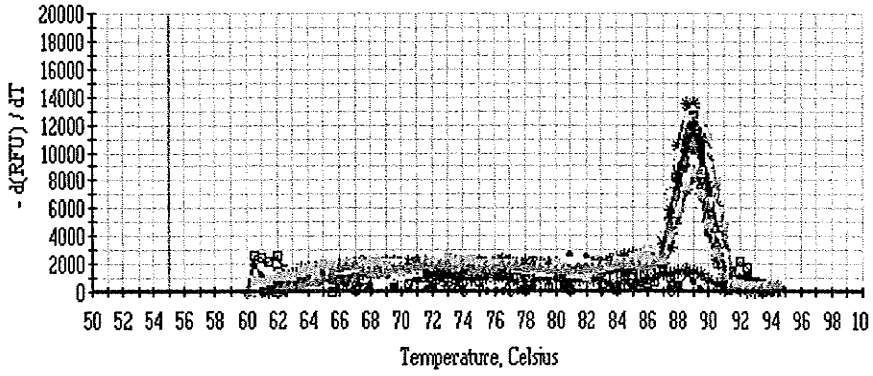
- d(RFU) / dT
Temperature, Celsius

Figure 12. 18S rRNA PCR product detection in real time. (A) The PCR amplification plot for the 18S rRNA plasmid standard and (B) the amplification plot of the 18S rRNA PCR products. The threshold limit was set at 10 times the standard deviation of fluorescence over the base line. (C) The correlation coefficient and the slope and the intercept of the standard curve are indicated. (D) Individual melt curves (at 87°C) of each PCR product amplified with the 18S rRNA primers are shown in the -dF/dT versus temperature plot.

A

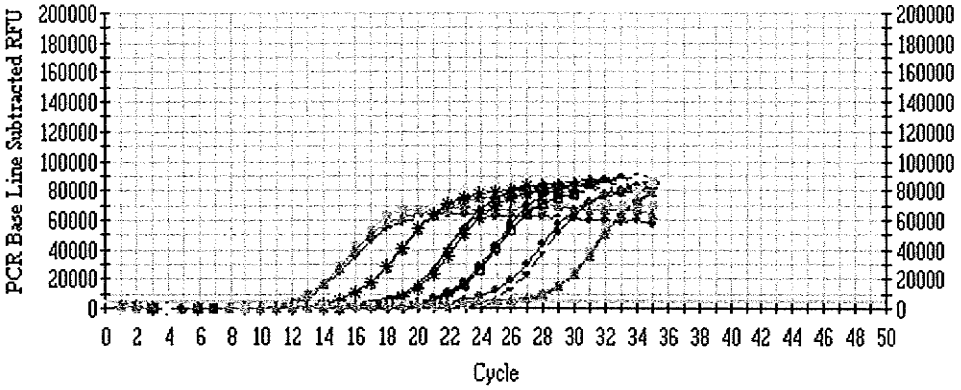
PCR Base Line Subtracted RFU
200000
180000
160000
140000
120000
100000
80000
60000
40000
20000
0
0 2 4 6 8 10 12 14 16 18 20 22 24 26 28 30 32 34 36 38 40 42 44 46 48 50
Cycle

B

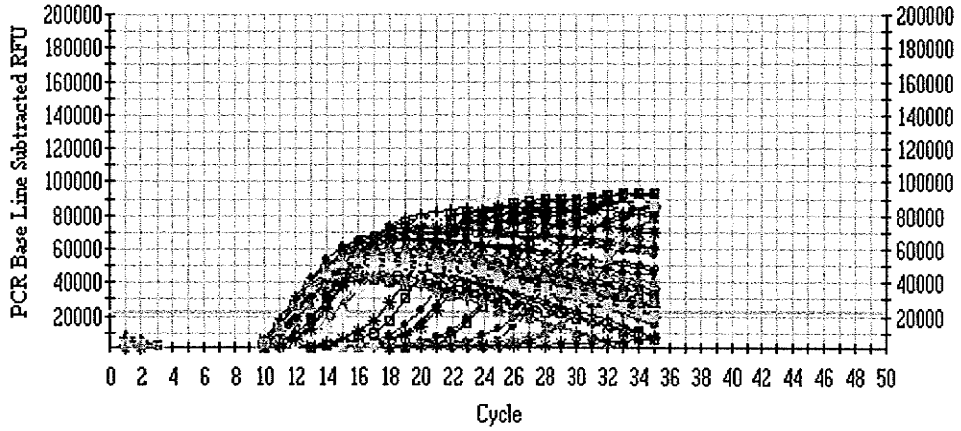
PCR Base Line Subtracted RFU
200000
180000
160000
140000
120000
100000
80000
60000
40000
20000
0 2 4 6 8 10 12 14 16 18 20 22 24 26 28 30 32 34 36 38 40 42 44 46 48 50
Cycle

C

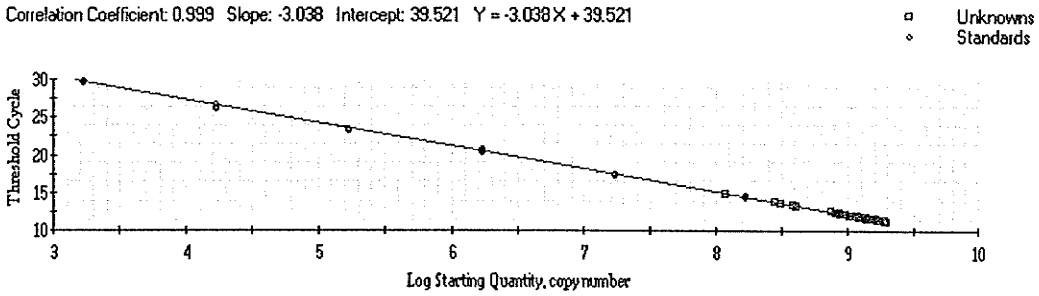
Correlation Coefficient: 0.999 Slope: -3.038 Intercept: 39.521 Y = -3.038 X + 39.521
Unknowns
Standards
Threshold Cycle
30
25
20
15
10
3 4 5 6 7 8 9 10
Log Starting Quantity, copy number

D

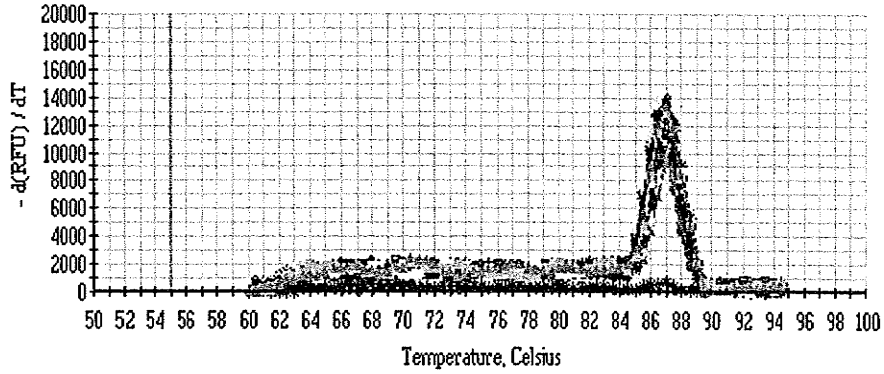
- d(RFU) / dT
20000
18000
16000
14000
12000
10000
8000
6000
4000
2000
0
50 52 54 56 58 60 62 64 66 68 70 72 74 76 78 80 82 84 86 88 90 92 94 96 98 100
Temperature, Celsius

Figure 13. IGF-IR mRNA levels at different stages of normal mouse mammary gland development. (A) IGF-IR gene expression levels decreased significantly (5.4 fold) during day 19 of pregnancy compared to levels in the 8 week virgin mammary gland. IGF-IR gene expression levels were lowest during early (d3; 9.2 fold) and late lactation (d10; 13.1 fold). Following late (d10) lactation, gene expression levels were significantly increased at early (d3; 1.6 fold) and late involution (d10; 2.5 fold). Results are expressed as a percentage of the value determined for the virgin mammary gland. Shown on the graph are the means ± S.D. of three independent RT reactions, each amplified in duplicate (n=6). (B) The results from individual time points were placed into 6 broader groups of mammary gland development. These groups indicated that IGF-IR gene expression was significantly lower during late pregnancy (d19; 5.4 fold) and lactation (d3 and 10; 10.8 fold) compared to that of virgin mice. IGF-IR gene expression was highest during late involution (d10). ***, $P<0.001$ (by Tukey test). Abbreviations: d = day, wk = weeks.

A

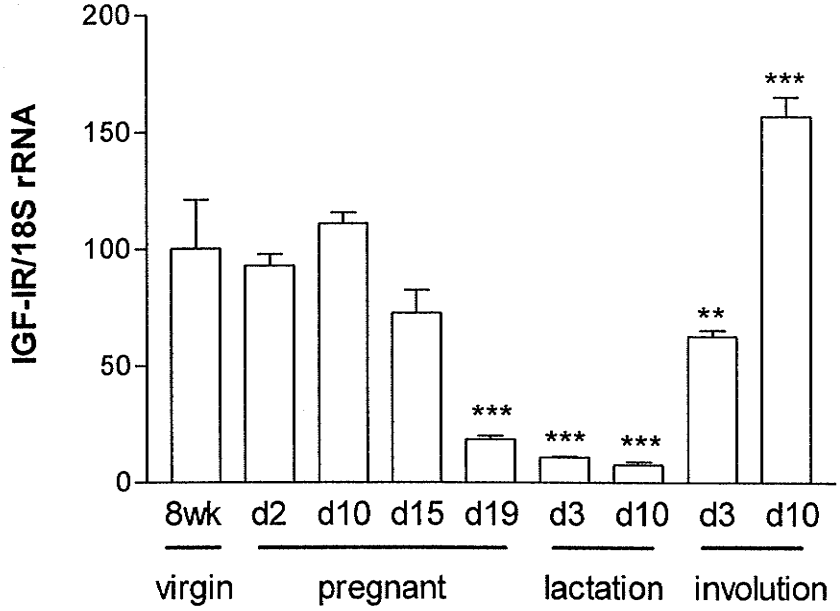
IGF-IR/18S rRNA
200
150
100
50
0
***
**
***
***
***
8wk
d2
d10
d15
d19
d3
d10
d3
d10
virgin
pregnant
lactation
involution

B

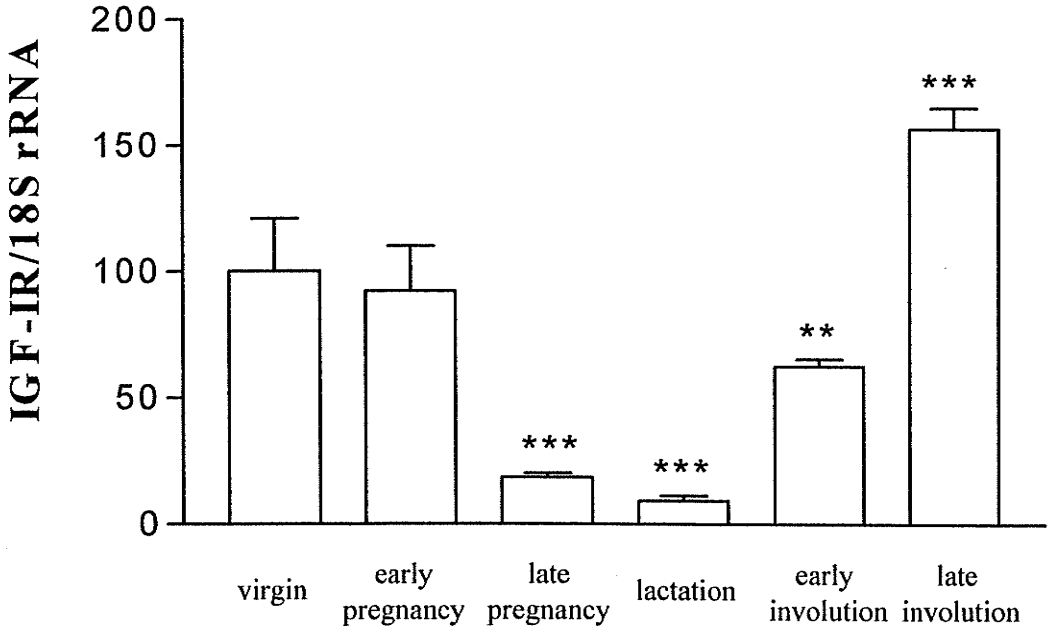
IGF-IR/18S rRNA
200
150
100
50
0
***
***
**
***
virgin
early pregnancy
late pregnancy
lactation
early involution
late involution

Figure 14. *In situ* analysis of spatial and temporal expression of the IGF-IR gene during mouse mammary gland development. The panels on the left (A, C, E, G, I, K) show the results of the hybridization of the 502 bp IGF-IR antisense probe to mammary gland sections and the panels on the right (B, D, F, H, J, L) represent hybridization with the sense probe. In the mammary glands of (A) virgin (20 week) and (C) early pregnant mice (day 8), IGF-IR transcripts were localized to the ductal epithelium and in the terminal end buds. During (E) late pregnancy (day 19) and (G) lactation (day 3) transcripts were detected in the ductal and alveolar epithelium and in the alveolar epithelium, respectively. IGF-IR transcripts were also found in the alveoli during (I) early involution (day 3) and in the ductal epithelium at (K) late involution (day 10). Few non-specific signals were observed with the sense probe. Magnification X 200. Abbreviations: de = ductal epithelium, td = terminal ducts, av = alveoli.

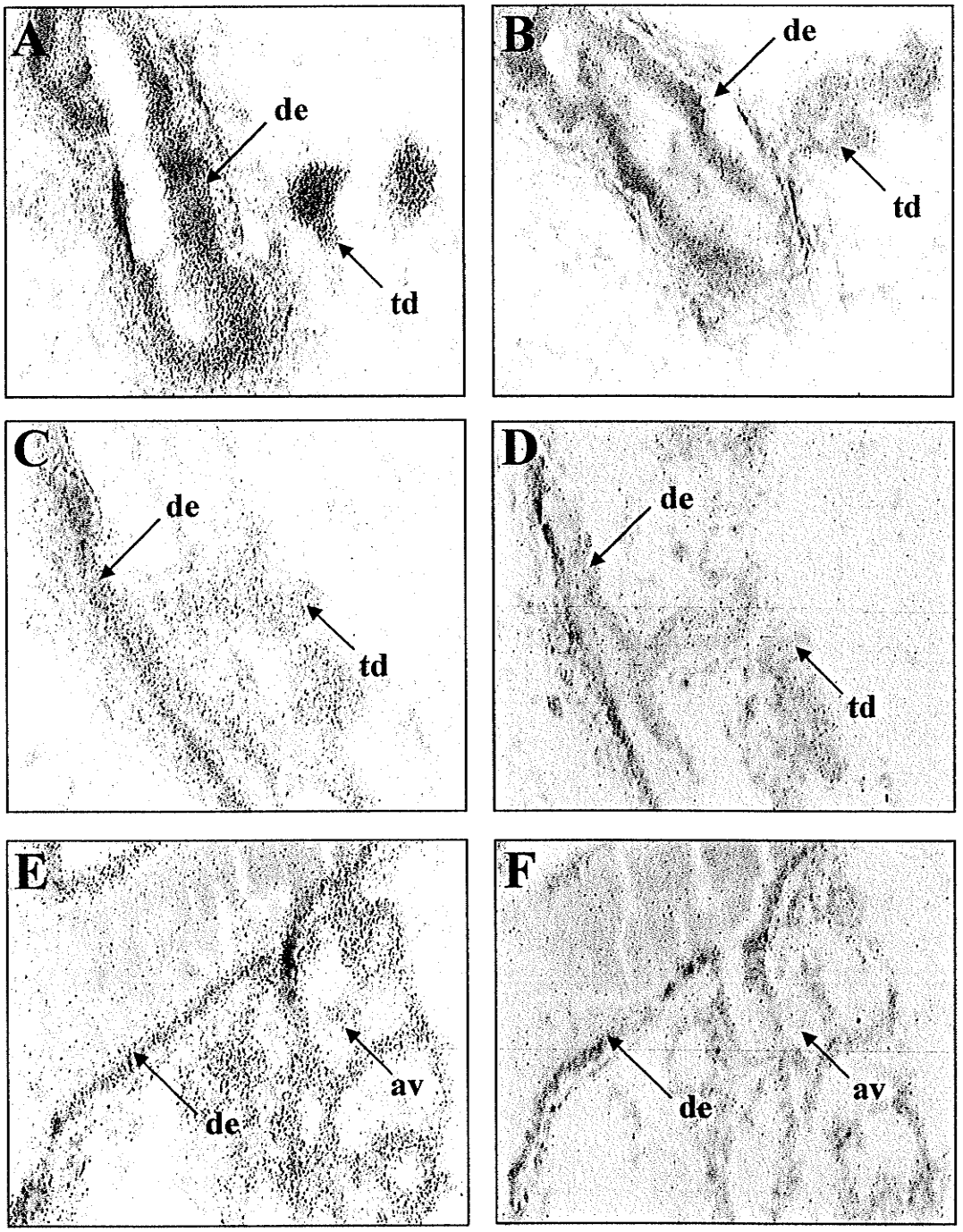
A
de
td
B
de
td
C
de
td
D
de
td
E
de
av
F
de
av

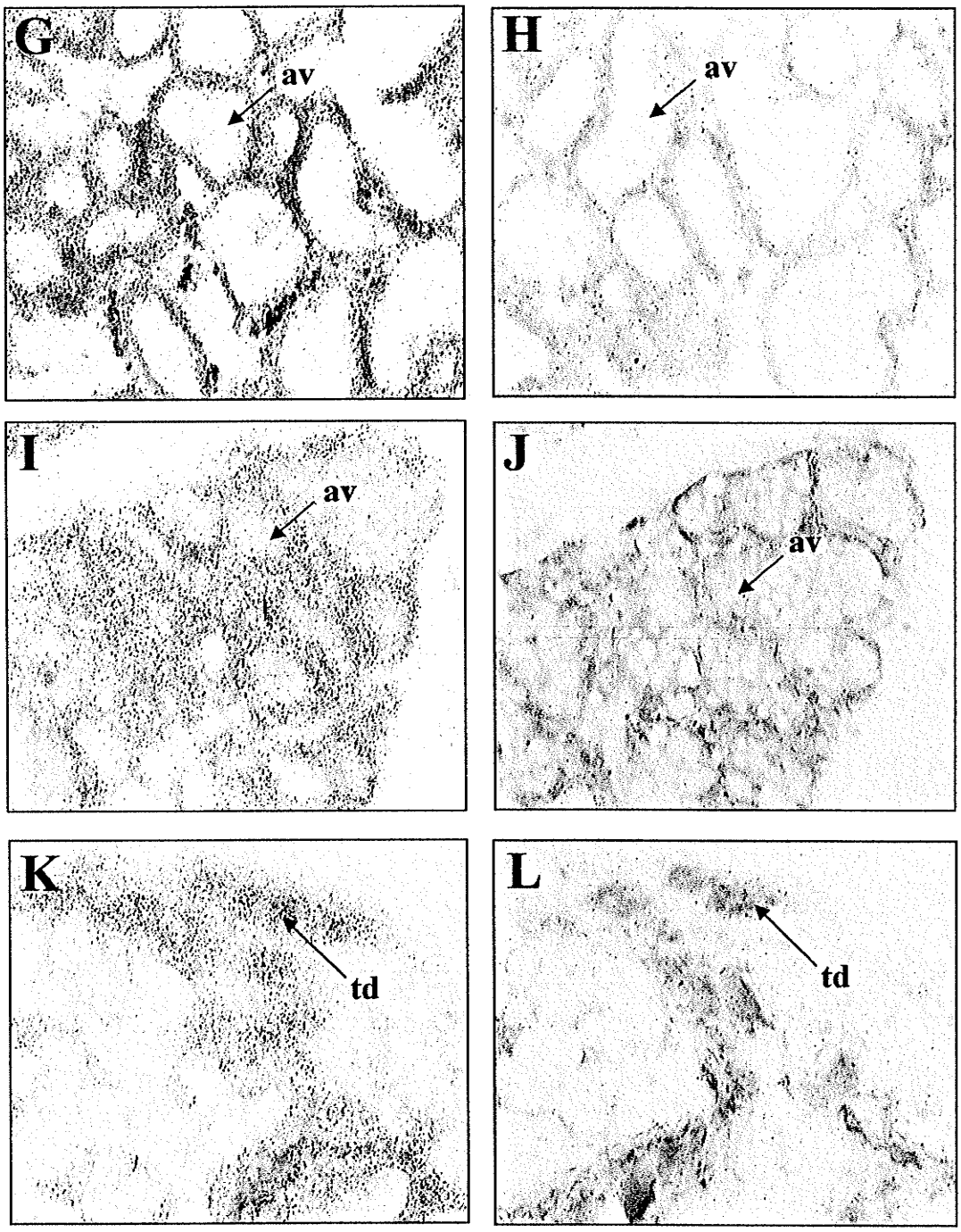
G
av
H
av
I
av
J
av
K
td
L
td

Figure 15. IGF-IR protein expression in the developing mouse mammary gland. (A) Samples (350 μg of total protein extract) were analyzed by Western blot analysis using an antibody, C-20, directed to the carboxy terminus of the β-subunit of the IGF-IR receptor (M_r 90 kDa). Mouse kidney extract was used as a positive control and mouse liver extract as a negative control. Four independent Western blots were performed on each sample. Sample loading is indicated by (B) Ponceau S stained proteins (arrow) on the nitrocellulose membrane (C) and a non-specific protein (arrow) on the Coomassie Blue stained gel.

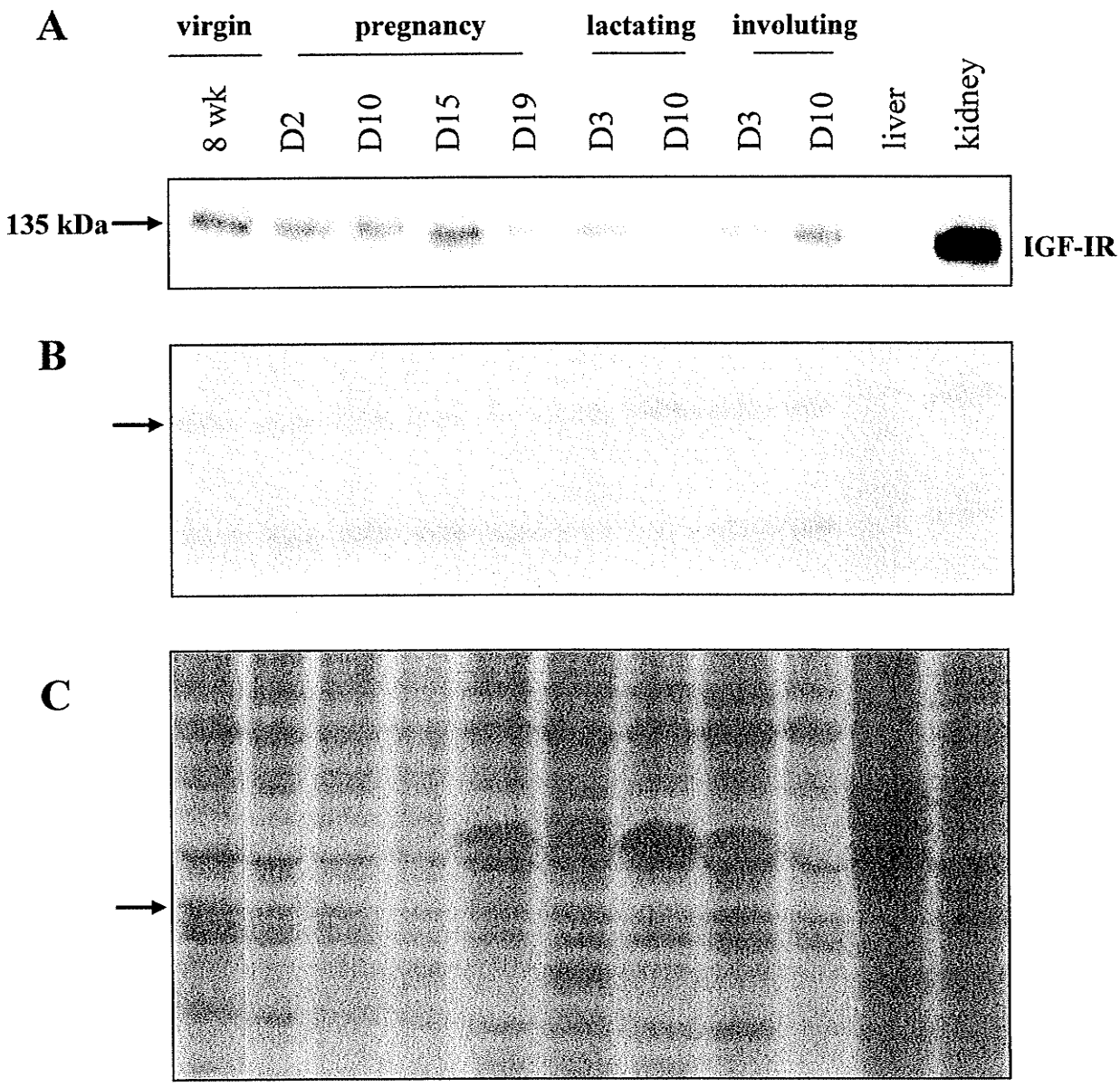
A
virgin
pregnancy
lactating
involuting
8 wk
D2
D10
D15
D19
D3
D10
D3
D10
liver
kidney
135 kDa
IGF-IR
B
C

Figure 16. IGF-IR protein levels at different stages of normal mouse mammary gland development. Image analysis of protein bands was done using the FluorS-MAX MultiImager (Bio-Rad Laboratories) at 10, 30 and 60 second time intervals. The band densities were determined using the Quantity One version 4.2 quantitation software program. (A) Density values of IGF-IR bands were normalized to the density of the positive control band. IGF-IR protein levels decreased significantly (2.3 fold) during day 19 of pregnancy compared to levels in the 8 week virgin mammary gland. These decreases in protein levels continued during early (d3; 2.0 fold) and late lactation (d10; 5.0 fold) and during early (d3; 2.5 fold) involution. Results are expressed as a percentage of the value obtained for the virgin mammary gland. Shown on the graph are the means ± S.D. (n=4). (B) Individual time points were placed in designated groups representing the different stages of mammary gland development. IGF-IR protein expression levels were found to be significantly lower at late pregnancy (d19; 2.3 fold), lactation (d3 and 10; 3.0 fold) and early involution (d3; 2.5 fold) when compared to that of virgin mice. Statistically significant differences between the virgin and the other stages of gland development are illustrated. **, $P<0.01$; ***, $P<0.001$ (by Tukey test). Abbreviations: d= day; wk = weeks.

A

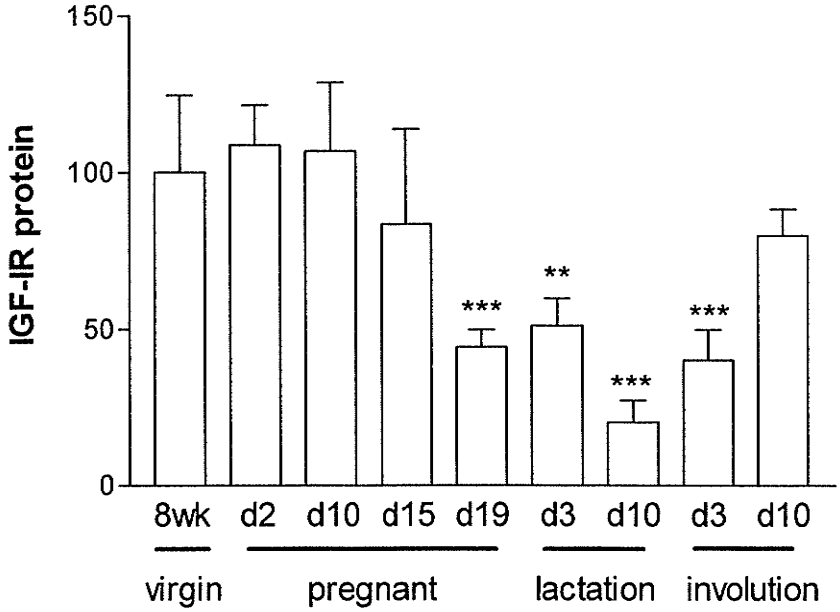
IGF-IR protein
150
100
50
0
***
**
***
***
8wk
d2
d10
d15
d19
d3
d10
d3
d10
virgin
pregnant
lactation
involution

B

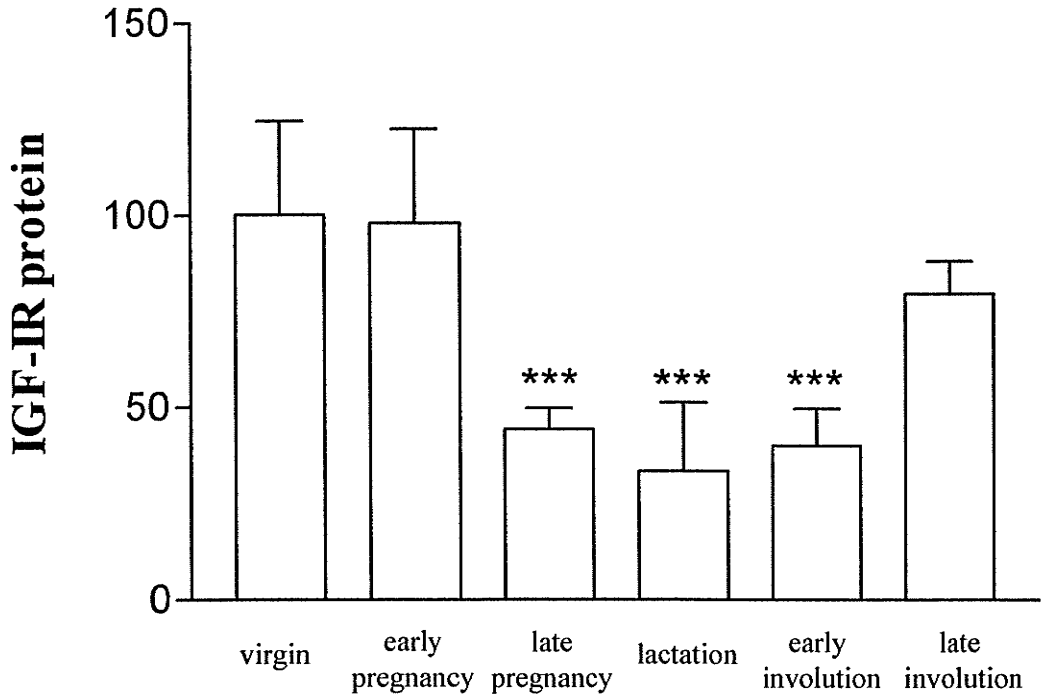
IGF-IR protein
150
100
50
0
***
***
***
virgin
early pregnancy
late pregnancy
lactation
early involution
late involution

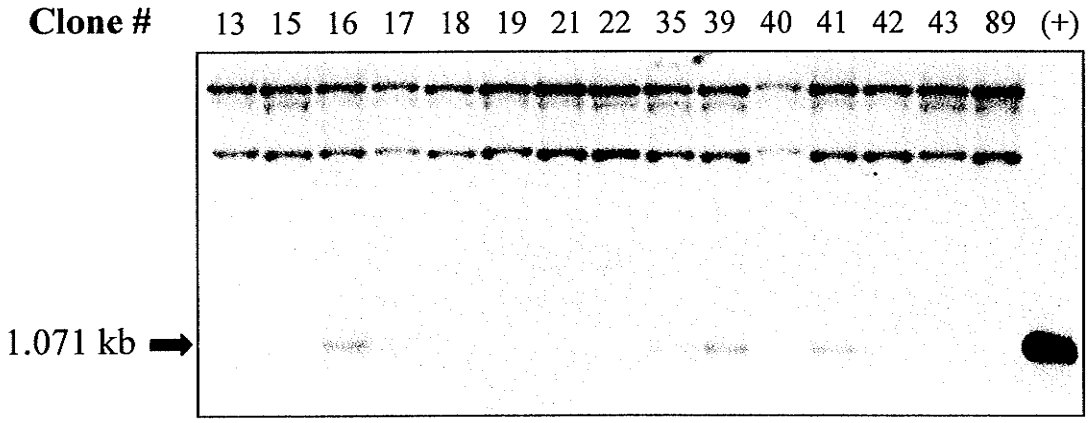

Figure 17. Integration of the IGF-IR-DN gene in stably transfected clonal lines. Southern blot analysis was carried out to examine whether the IGF-IR-DN transgene was integrated into the genome of the cells stably transfected with the tetO-Ph_{CMV}-IGF-IR-DN plasmid. Genomic DNA (10 μg) from 38 clonal cell lines was digested with EcoR V, electrophoresed on a 0.8% gel, transferred and hybridized with a ^{32}P-labeled probe specific for a 1071 bp fragment unique to the IGF-IR-DN cDNA. A total of 10 positive clonal cell lines were identified, of which 5 are shown. The presence of the 1.071 kb band indicated that the transgene was stably integrated. Clone #89 (an rtTA-expressing parental clonal cell line) was used as a negative control. IGF-IR-DN plasmid DNA was used as the positive control.

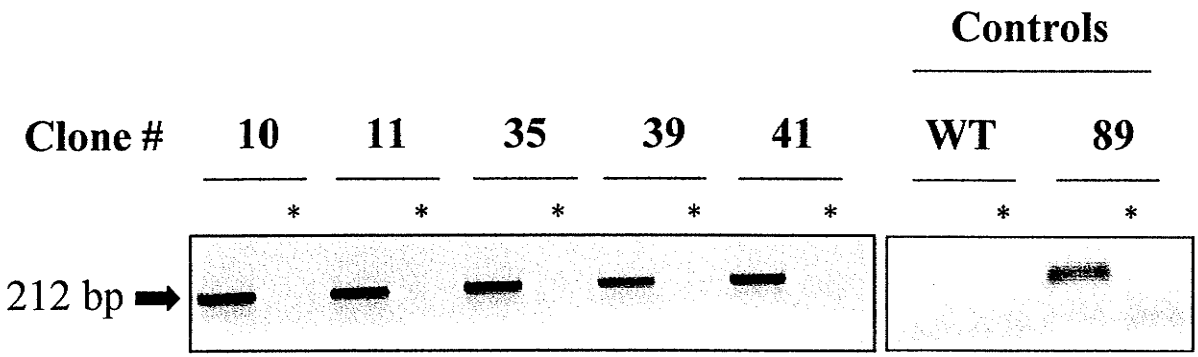

Figure 18. rtTA gene expression in the clonal cell lines. rtTA gene expression in the IGF-IR-DN positive clonal cell lines was confirmed by reverse transcription-polymerase chain reaction (RT-PCR) analysis. The RNA was DNase I treated prior to reverse transcription to remove any contaminating genomic DNA. RT- controls (*) showed that all residual genomic DNA were removed. The rtTA gene was expressed in five different stably transfected MCF-7 clonal cell lines. Clone #89 (an rtTA-expressing parental clonal cell line) was used as a positive control. Reverse transcribed RNA from wild type (WT) MCF-7 cells was used as a negative control.

Figure 19. Determination of doxycycline concentration required to induce optimal expression of the IGF-IR-DN transgene. The stably transfected cells were grown for 24 hours in the presence of doxycycline (0, 0.5, 1, 1.5, 2.0 μg/ml) to determine the dosage required to achieve maximal expression of the IGF-IR-DN gene. Optimal expression was observed with 1.0 μg/ml doxycycline (dox). Ethidium bromide staining was used to reflect RNA loading. The 18S and 28S ribosomal RNA bands are indicated. Clone #1, previously identified as expressing IGF-IR-DN was used as a positive (+) control. Clone #89 (an rtTA-expressing parental clonal cell line) was used as a negative (-) control. Densitometric values from a representative assay are shown in Panel B.

A

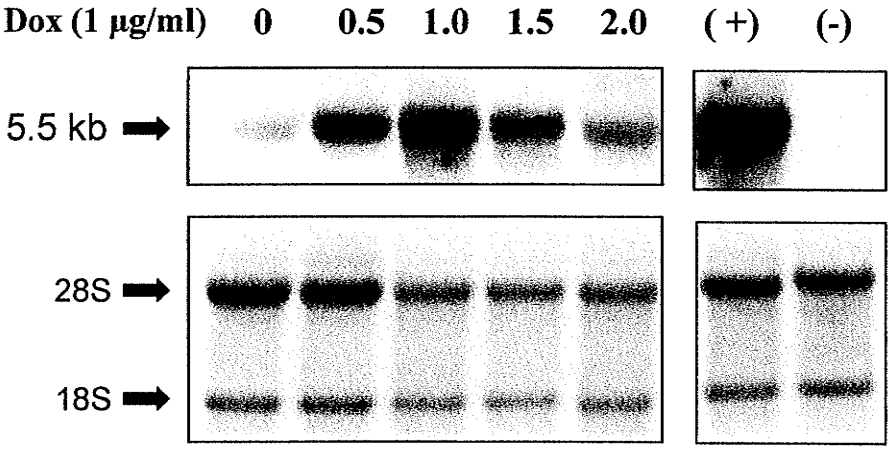
Dox (1 μg/ml) 0 0.5 1.0 1.5 2.0 (+) (-)
5.5 kb
28S
18S

B

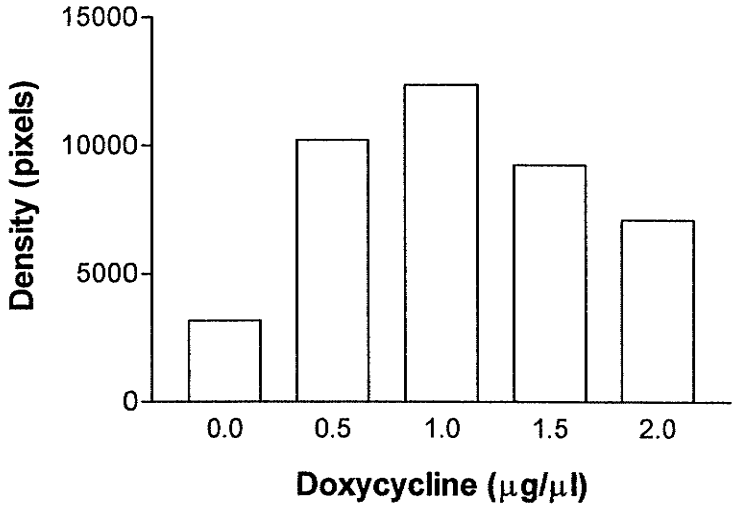
15000
10000
5000
0
Density (pixels)
0.0
0.5
1.0
1.5
2.0
Doxycycline (μg/μl)

Figure 20. Determination of the optimal time course required for doxycycline induced expression of the IGF-IR-DN transgene. The stably transfected cells were grown in the presence of doxycycline (1 μg/ml) for 0, 12, 24 and 48 hours to determine the time required to achieve maximal expression of the IGF-IR-DN gene. Optimal expression was observed after 24 hours. Ethidium bromide staining was used to reflect RNA loading. The 18S and 28S ribosomal RNA bands are indicated. A clone, Clone #1, previously identified as expressing IGF-IR-DN was used as a positive (+) control. Clone #89 (an rtTA-expressing parental clonal cell line) was used as a negative (-) control. Densitometric values from a representative assay are shown in Panel B.

A

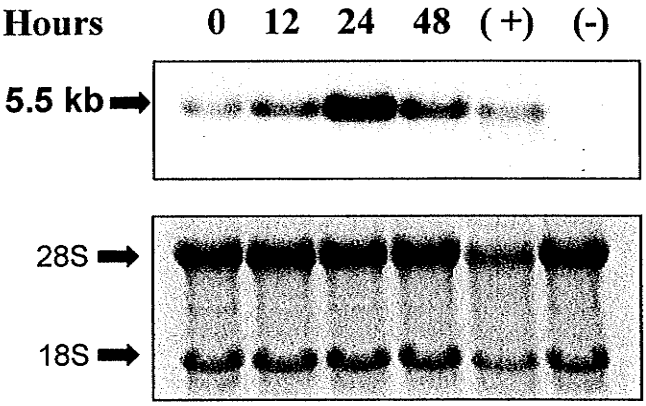
Hours 0 12 24 48 (+) (-)
5.5 kb
28S
18S

B

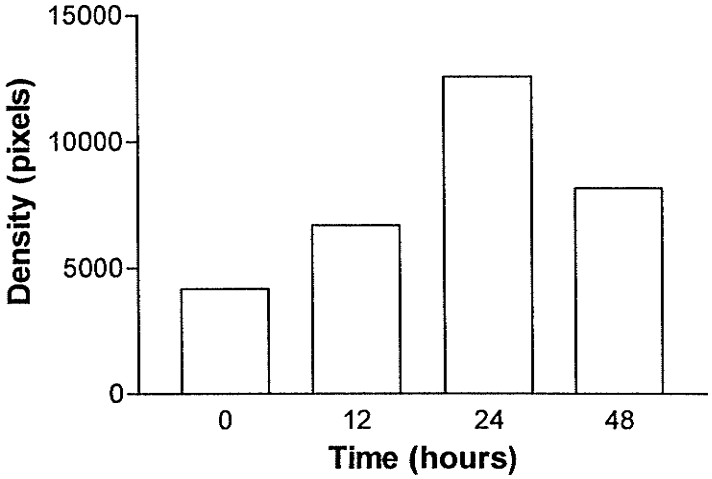
15000
10000
5000
0
Density (pixels)
0
12
24
48
Time (hours)

Figure 21. Northern blot analysis of IGF-IR-DN gene expression in clonal cell lines. (A) Total RNA (30 μg) extracted from doxycycline-induced (+) and uninduced (-) cells was electrophoresed on a 0.8% denaturing agarose-formaldehyde gel, transferred and hybridized with a ^{32}P-labeled IGF-IR-DN cDNA probe. The 5.5 kb IGF-IR-DN transcript was only observed in doxycycline (dox) induced cells. Clone $^{\#}$39, which was positive for IGF-IR-DN gene integration but negative for gene expression, was used as a control. IGF-IR-DN gene expression was greatest in Clone $^{\#}$35 (3.3 fold greater relative to Clone $^{\#}$39). Clone $^{\#}$1, previously identified as expressing IGF-IR-DN, was used as a positive (+) control. The 18S and 28S ribosomal RNA bands are indicated. The membranes were probed with GAPDH cDNA probe to reflect sample loading. The 1.9 kb GAPDH transcripts are indicated in Panel A. Densitometric values from a representative assay are shown in Panel B.

A

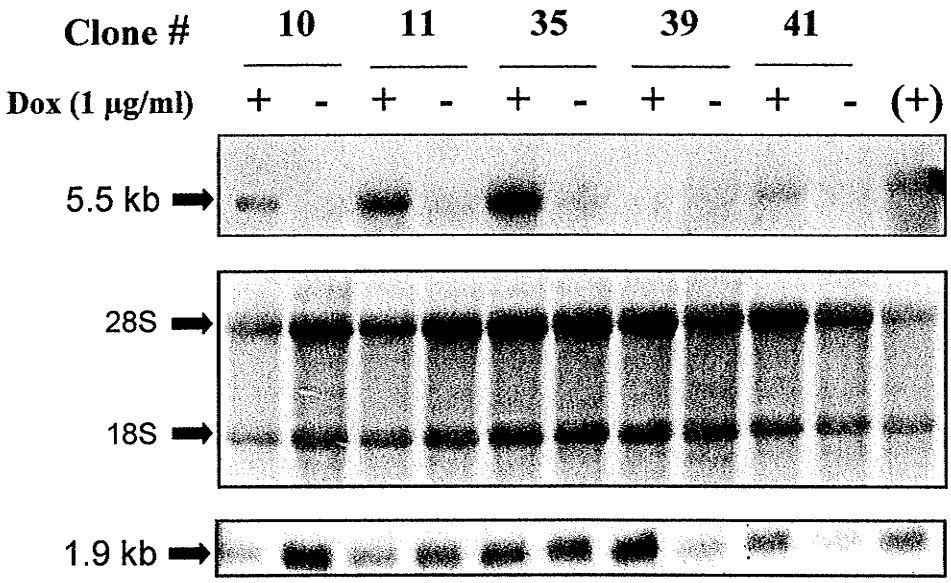
Clone # 10 11 35 39 41
Dox (1 µg/ml) + - + - + - + - + - (+)
5.5 kb
28S
18S
1.9 kb

B

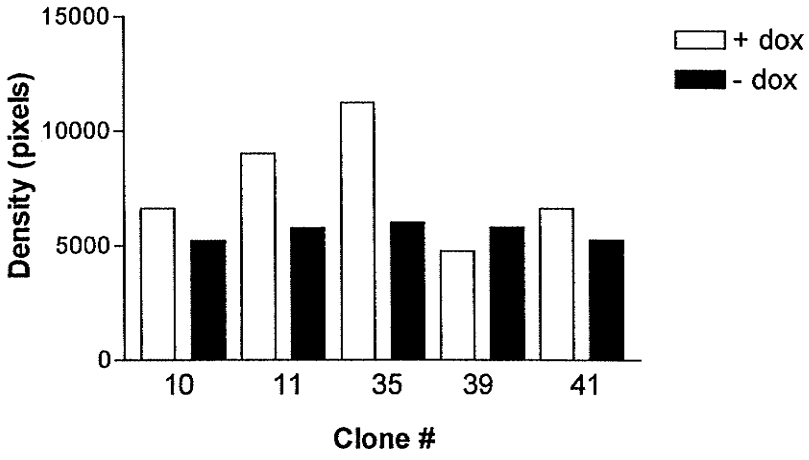
15000
10000
5000
0
Density (pixels)
+ dox
- dox
10
11
35
39
41
Clone #

Figure 22. Determination of IGF-IR-DN gene expression by RT-PCR analysis. A restriction enzyme digest strategy was used to differentiate between the endogenous IGF-IR gene and the mutant IGF-IR transgene. (A) Xba I digestion of the 931bp PCR product results in the presence of two smaller bands confirming the presence of the transgene. This was apparent for clones 10, 11, 35 and 41. Only one band (931 bp) was present in the uninduced cells (-dox) and in Clone $^{\#}$39. Clone $^{\#}$89 (an rtTA-expressing parental clonal cell line) was used as a negative (-) control and genomic DNA from a transgenic mouse expressing the IGF-IR-DN was used as a positive (+) control. The sizes of the PCR products after (+Xba I) and prior to (-Xba I) restriction enzyme digestion are demonstrated in Panel B.

A

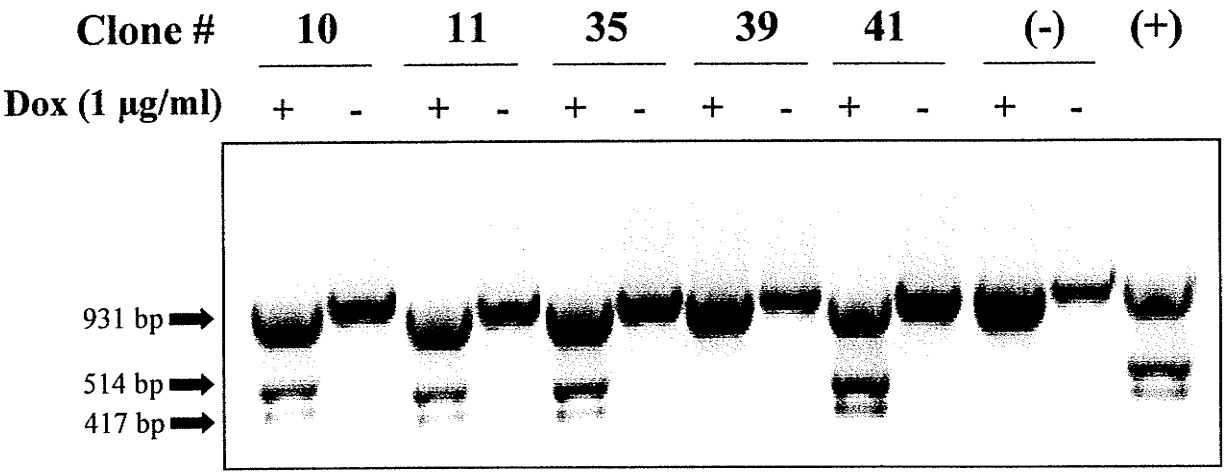
Clone # 10 11 35 39 41 (-) (+)
Dox (1 µg/ml) + - + - + - + - + - + -
931 bp
514 bp
417 bp

B

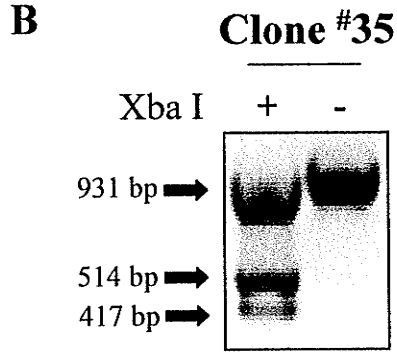
Clone #35
Xba I + -
931 bp
514 bp
417 bp

Figure 23. IGF-IR-DN protein expression in the stably transfected clonal cell lines. Cell lysates were collected from doxycycline-induced and uninduced stably transfected MCF-7 cells, analyzed by SDS-PAGE and immunoblotted with antibodies specific to the IGF-I receptor. (A) Using an antibody against the α subunit (N-20) of the IGF-I receptor, the results showed that doxycycline (dox) induced IGF-IR protein (135 kDa) expression. (B) This result demonstrates that the endogenous IGF-IR (90 kDa) was present in both induced (+) and uninduced (-) cells. The antibody used (H-60) was directed against the β-subunit. (C) The mutant receptor (50 kDa), present in the stably transfected cells treated with doxycycline, was recognized by the same antibody (H-60). Low levels of the mutant receptor were seen in the non-induced cells. The mutant receptor was absent in the clonal cell line, $^{\#}$39, which was negative for gene expression. (D) The membranes were stripped and immunoblotted with an antibody against actin (45 kDa) to reflect the loading of the samples. Densitometric values from a representative assay are shown.

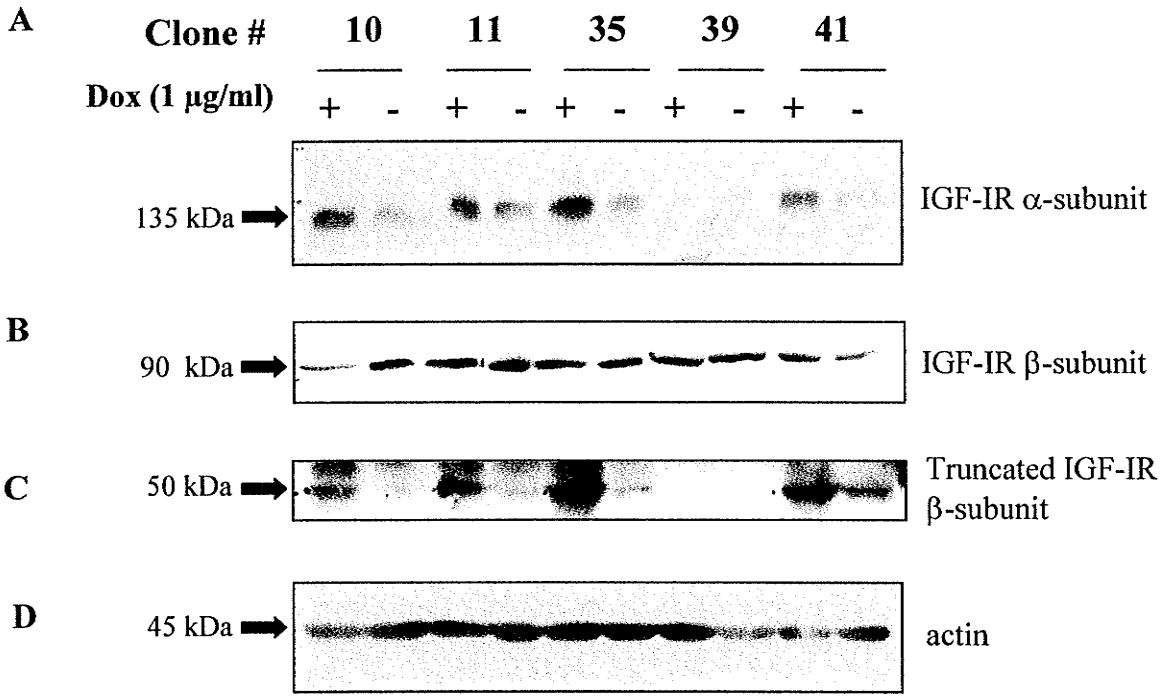
A
Clone #
10
11
35
39
41
Dox (1 µg/ml)
+ - + - + - + - + -
135 kDa
IGF-IR α-subunit
B
90 kDa
IGF-IR β-subunit
C
50 kDa
Truncated IGF-IR β-subunit
D
45 kDa
actin

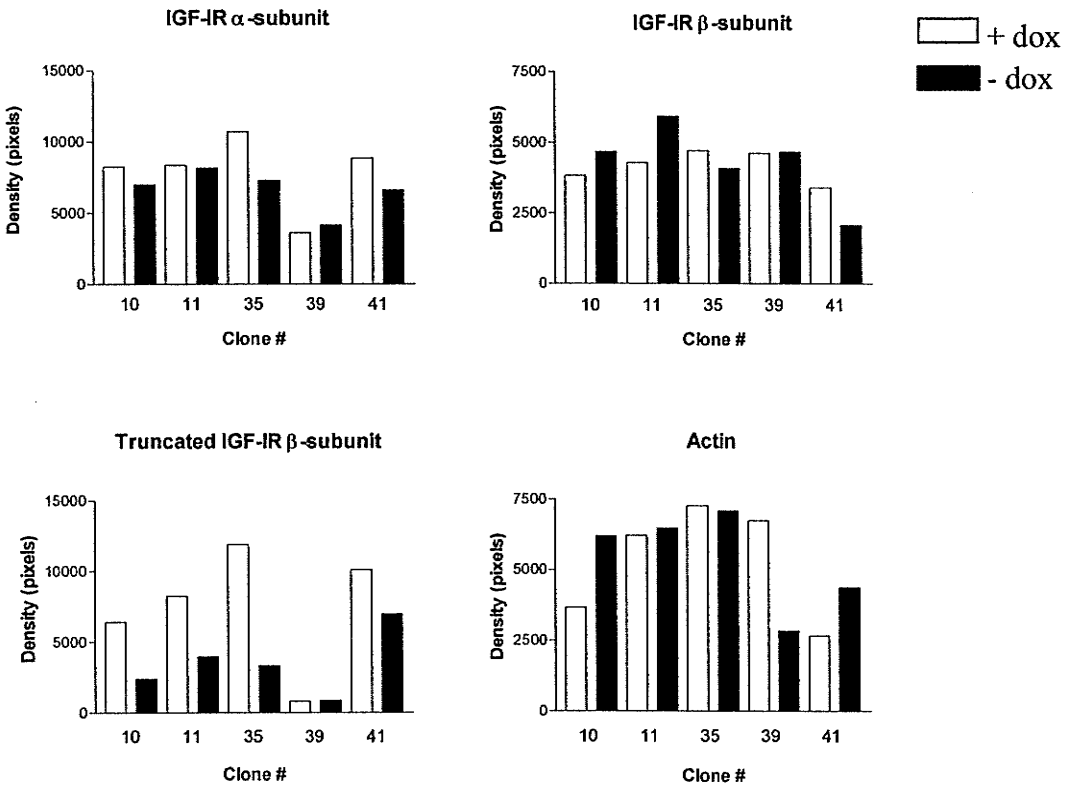
IGF-IR α-subunit
IGF-IR β-subunit
+ dox
- dox
Density (pixels)
15000
10000
5000
0
7500
2500
10
11
35
39
41
Clone #
Truncated IGF-IR β-subunit
Actin

Figure 24. The truncated IGF-I receptor does not inhibit autophosphorylation of the IGF-I receptor and phosphorylation of the downstream substrate, insulin receptor substrate 1 (IRS-1). Tyrosine phosphorylation studies were carried out as described in Materials and Methods. Cell lysates were collected and subjected to SDS-PAGE (6.5% gel) and analyzed by Western blotting with an anti-phosphotyrosine antibody (PY-20). Autophosphorylation of the IGF-IR and the phosphorylation of the IRS-1 was not inhibited by the IGF-IR-DN in clonal cell lines #11 (Panel A) and #35 (Panel B). Autophosphorylation of the IGF-IR β subunit (90 kDa) and phosphorylation of the IRS-1 (185 kDa) was detected both in IGF-I stimulated cells grown in the presence and absence of doxycycline. Two clonal cell lines, #39 (Panel C; that was negative for IGF-IR-DN gene expression) and #89 (Panel D; an rtTA-expressing parental clonal cell line) were used as negative controls. The mobility of the molecular mass standard is indicated on the left. Densitometric values from a representative assay from three independent experiments are shown.

A

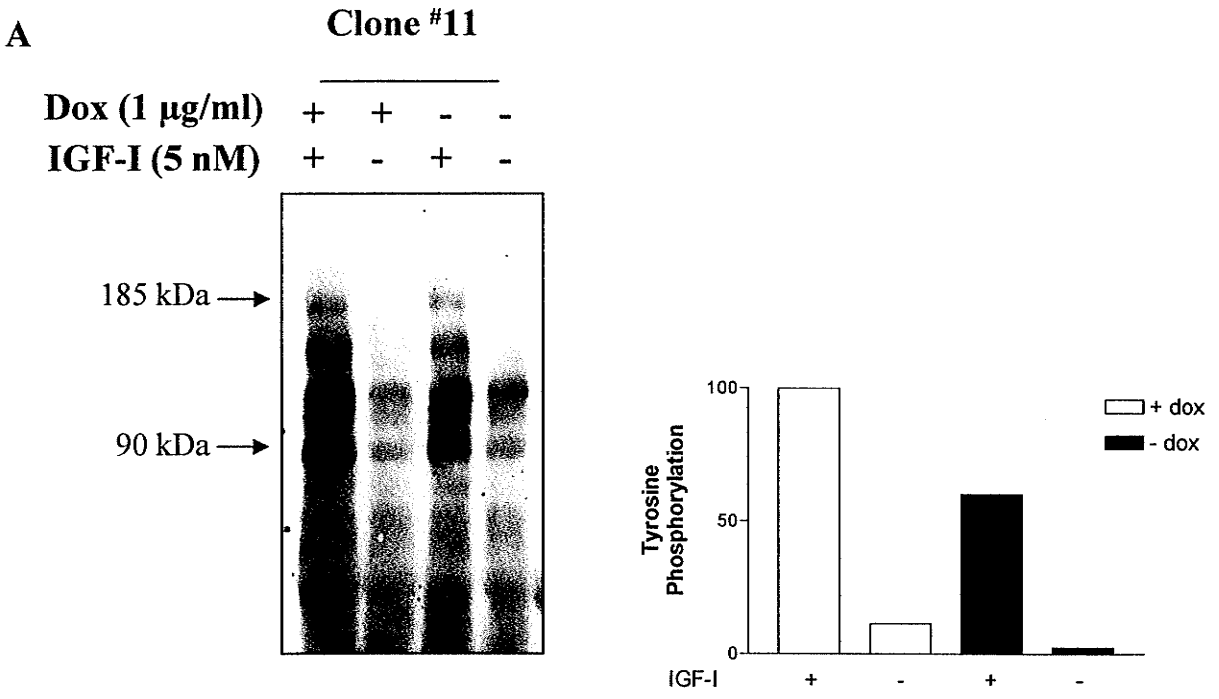
Clone #11
Dox (1 μg/ml) + + - -
IGF-I (5 nM) + - + -
185 kDa
90 kDa
Tyrosine Phosphorylation
100
50
0
+ dox
- dox
IGF-I + - + -

B

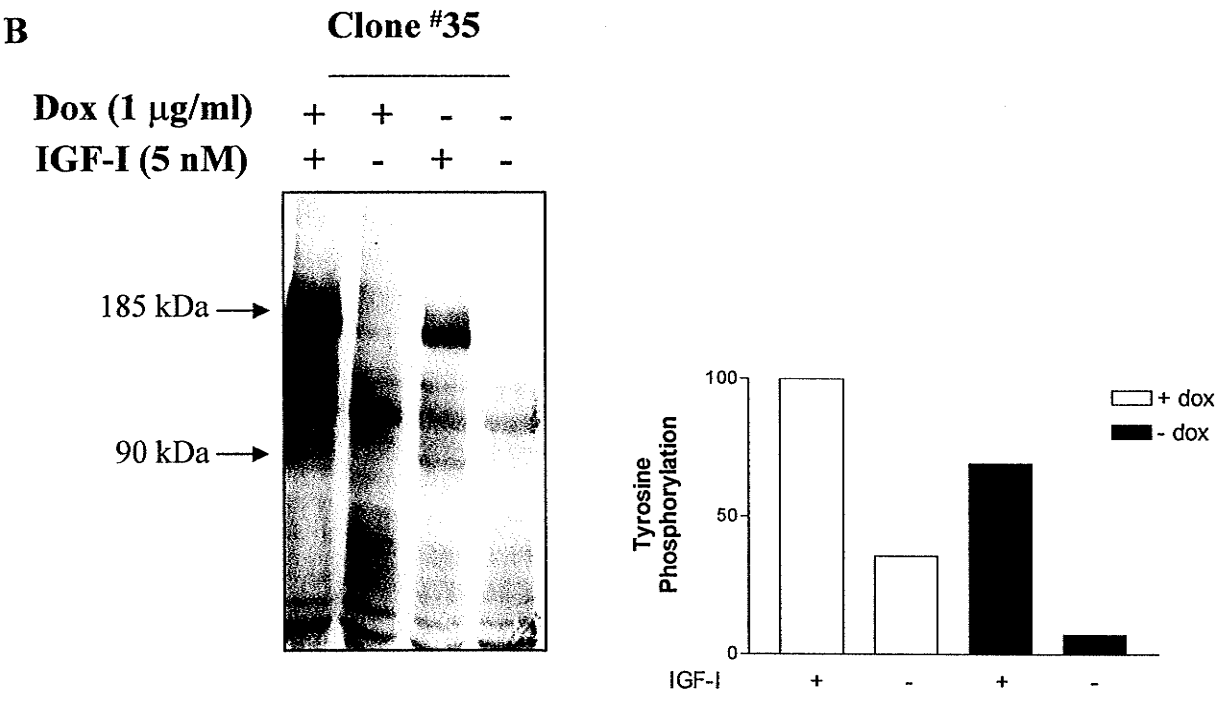
Clone #35
Dox (1 μg/ml) + + - -
IGF-I (5 nM) + - + -
185 kDa
90 kDa
Tyrosine Phosphorylation
100
50
0
+ dox
- dox
IGF-I + - + -

C

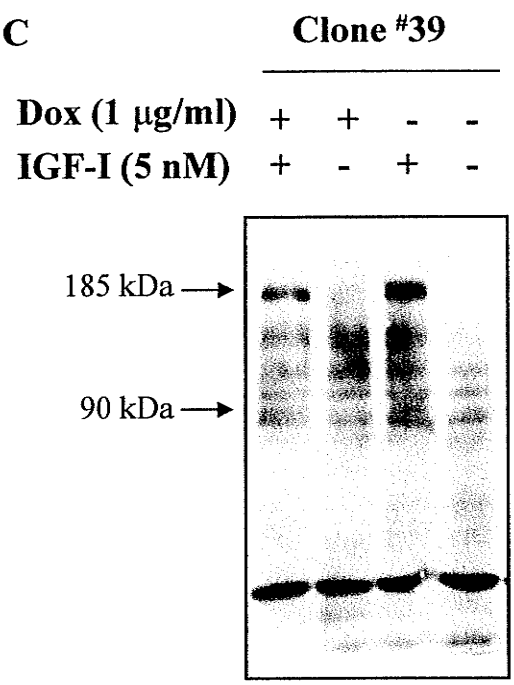
Clone #39
Dox (1 μg/ml) + + - -
IGF-I (5 nM) + - + -
185 kDa
90 kDa

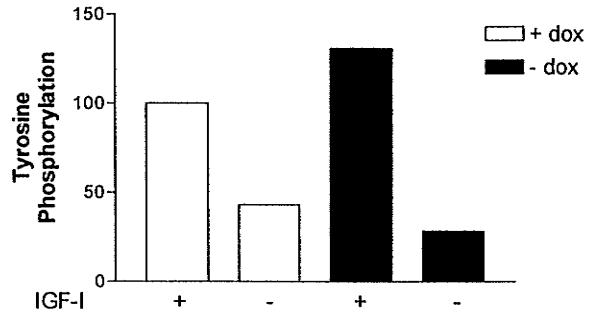
Tyrosine Phosphorylation
150
100
50
0
+ dox
- dox
IGF-I
+ - + -

D

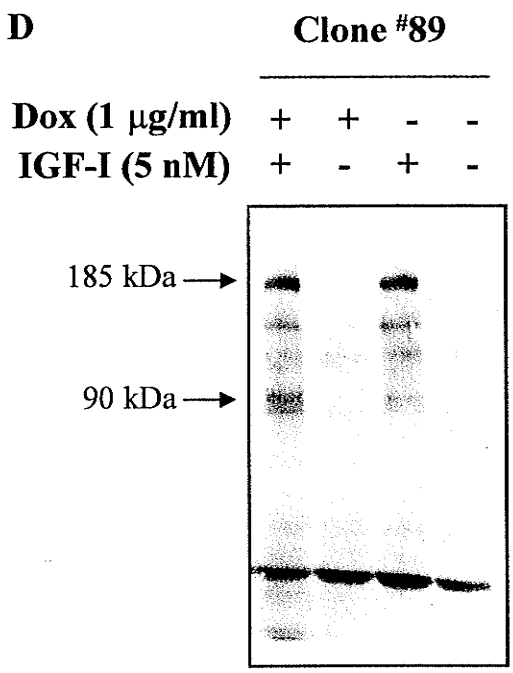
Clone #89
Dox (1 μg/ml) + + - -
IGF-I (5 nM) + - + -
185 kDa
90 kDa

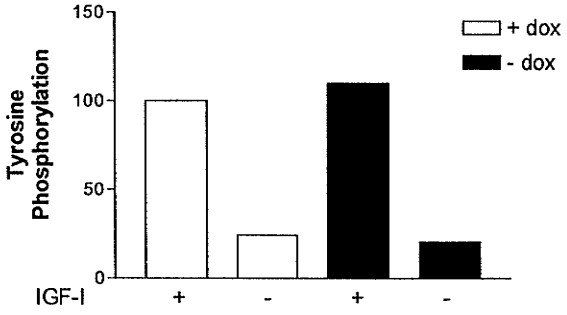
Tyrosine Phosphorylation
150
100
50
0
+ dox
- dox
IGF-I
+ - + -

Figure 25. Autophosphorylation of the IGF-I receptor and phosphorylation of the IRS-1 substrate. IGF-I, at concentrations ranging from 2.5 to 10 nm was added to the doxycycline-induced (+) and uninduced (-) cells for 10 minutes in order to determine the optimal concentration of the ligand required for phosphorylation of the tyrosine residues on the IRS-1. Cell lysates were collected, subjected to SDS-PAGE (6.5% gel) and analyzed by Western blotting with an anti-phosphotyrosine antibody (PY-20). Autophosphorylation of the IGF-IR β subunit (90 kDa) and phosphorylation of the IRS-1 (185 kDa) was detected in both IGF-I stimulated cells grown in the presence and absence of doxycycline. Cells that were not treated with IGF-I served as a negative control. Densitometric values from a representative assay from two independent experiments are shown.

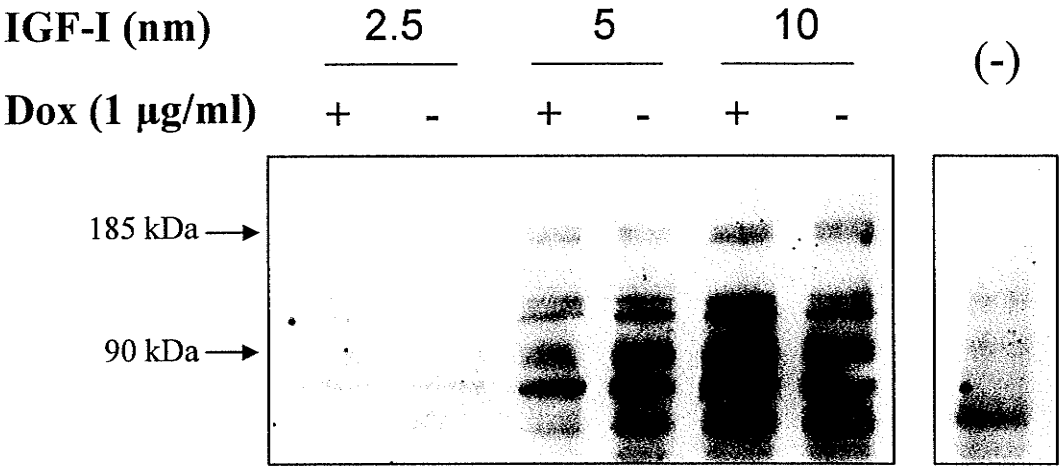
IGF-I (nm)
2.5
5
10
(-)
Dox (1 µg/ml)
+ - + - + -
185 kDa
90 kDa

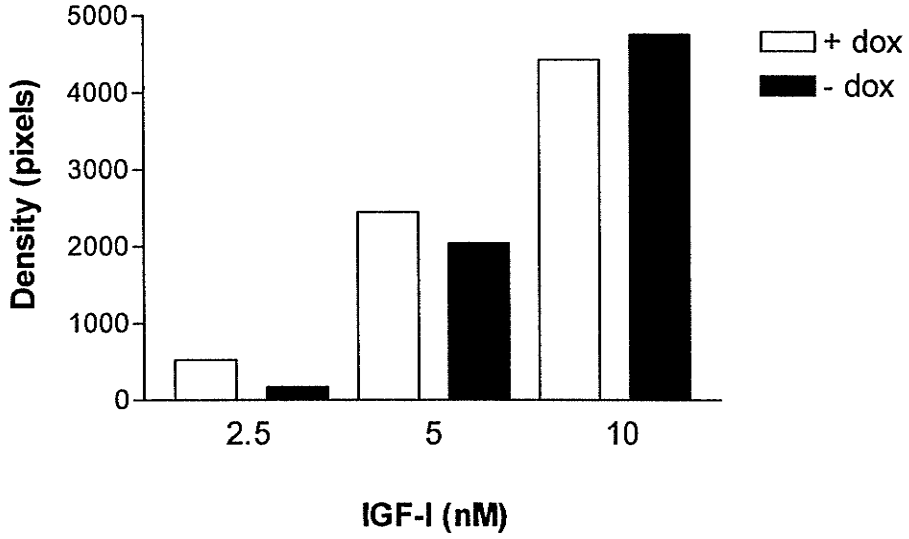
5000
4000
3000
2000
1000
0
Density (pixels)
2.5
5
10
IGF-I (nM)
+ dox
- dox

Figure 26. IRS-1 phosphorylation and IRS-1 protein expression in the stably transfected clonal cell lines. To confirm the identify of the 185 kDa tyrosine phosphorylated protein in the IGF-I stimulated cells, the same nitrocellulose membranes were stripped and immunoblotted with the antibody against the phospho-insulin receptor substrate-I (Oncogene Research Products). The membranes were also immunoblotted with an antibody against the IRS-1 (Upstate Biotechnology). The IRS-I protein (185 kDa) expression was observed in all samples, irrespective of treatment condition. The membranes were immunoblotted with an antibody against actin (45 kDa) to reflect the loading of samples. Densitometric values from a representative assay are shown.

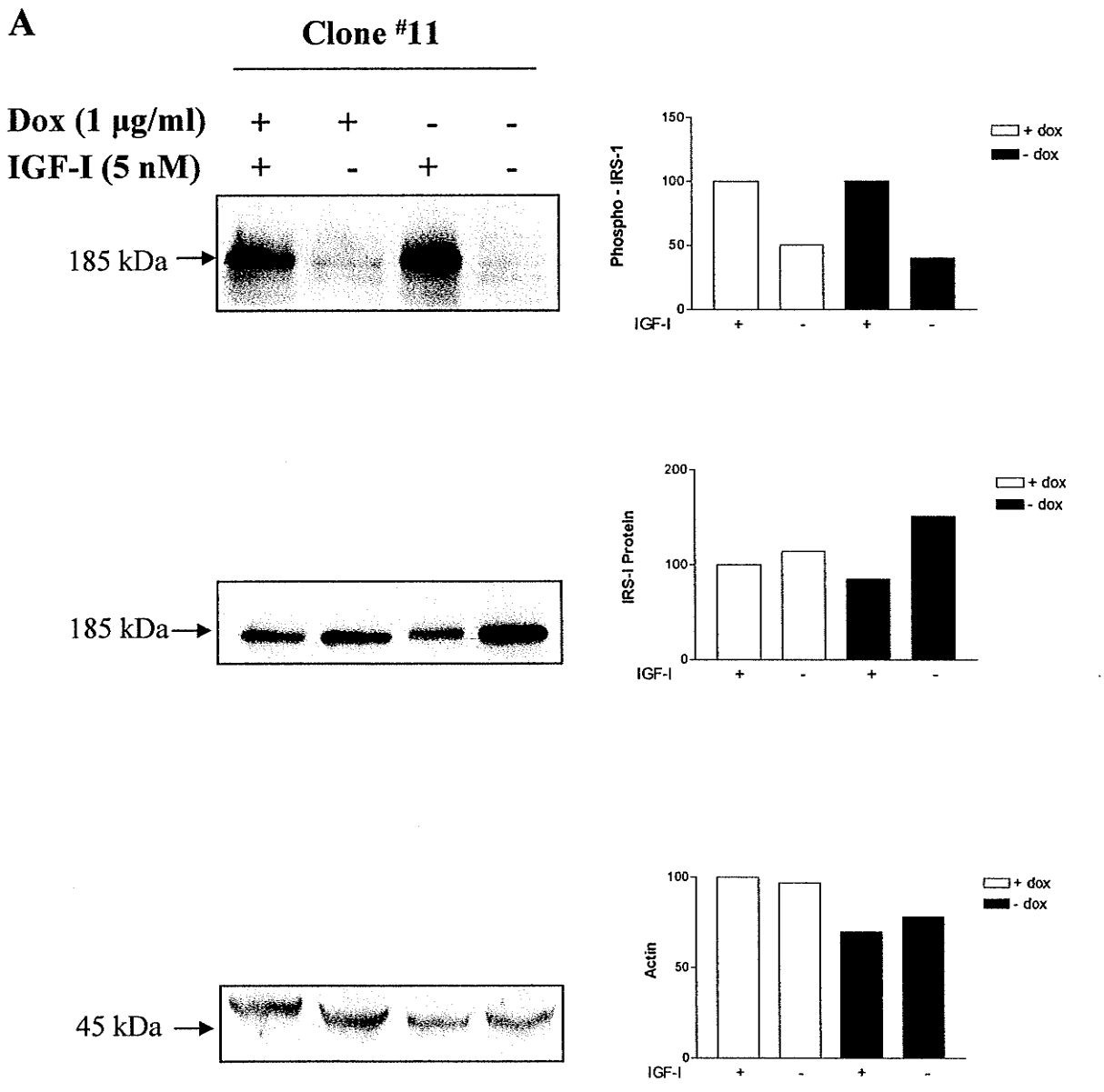
A
Clone #11
Dox (1 µg/ml) + + - -
IGF-I (5 nM) + - + -
185 kDa
Phospho - IRS-1
150
100
50
0
IGF-I + - + -
+ dox
- dox
185 kDa
IRS-I Protein
200
100
0
IGF-I + - + -
+ dox
- dox
45 kDa
Actin
100
50
0
IGF-I + - + -
+ dox
- dox

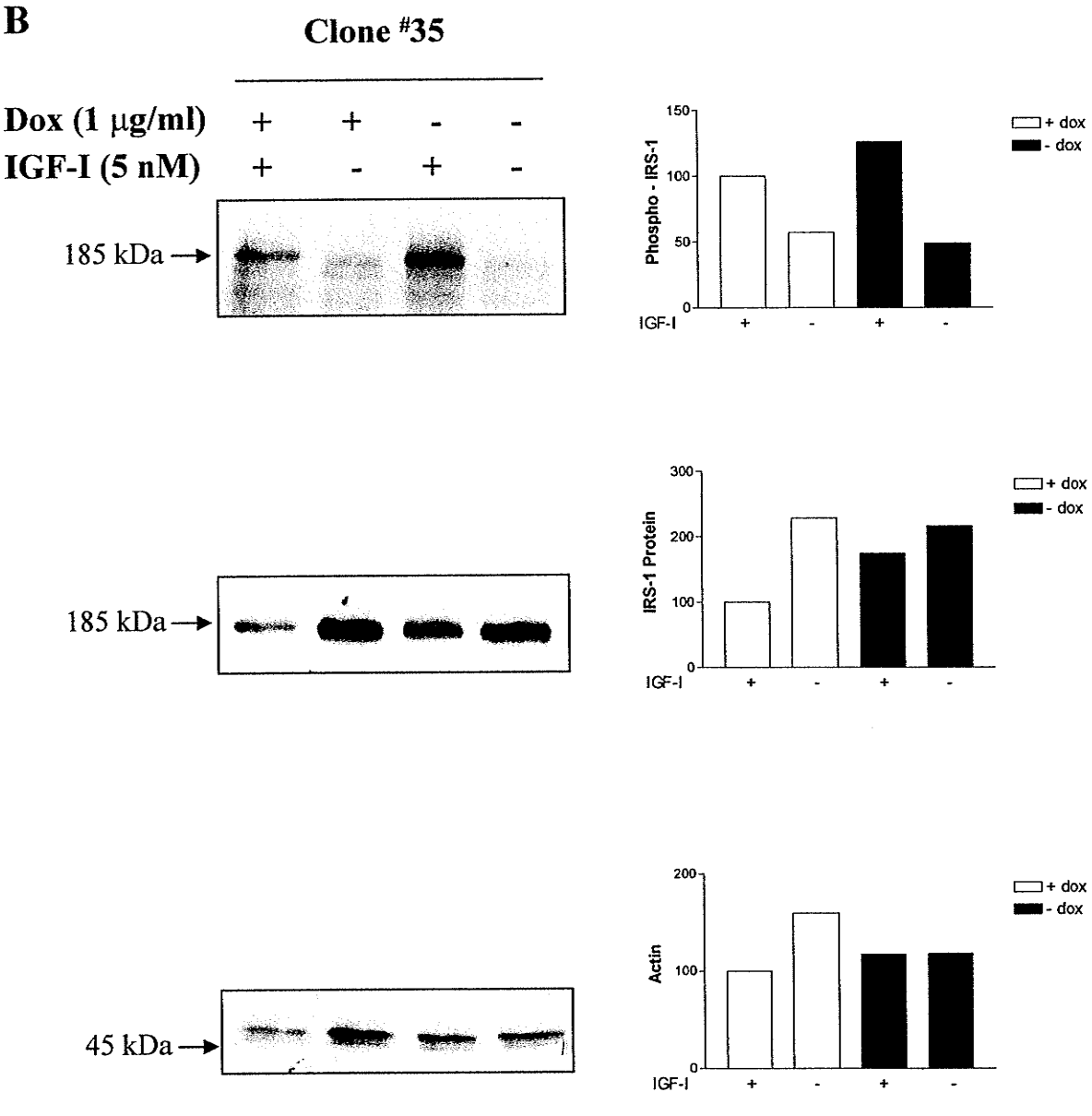
B
Clone #35
Dox (1 μg/ml) + + - -
IGF-I (5 nM) + - + -
185 kDa
Phospho - IRS-1
150
100
50
0
IGF-I + - + -
+ dox
- dox
185 kDa
IRS-1 Protein
300
200
100
0
IGF-I + - + -
+ dox
- dox
45 kDa
Actin
200
100
0
IGF-I + - + -
+ dox
- dox

Figure 27. The presence of the mutant IGF-I receptor protein in the IGF-I stimulated cells. To demonstrate the presence of the mutant IGF-I receptor in the IGF-I stimulated cells, the blots that were immunoblotted with the anti-phosphotyrosine antibody were stripped and reprobed with IGF-IR specific antibodies. Using an antibody against the α subunit (N-20) of the IGF-I receptor, an increase in IGF-IR protein (135 kDa) expression was observed in (A) Clone #11 (2.7 fold) and (B) Clone #35 (5.6 fold) cells treated with doxycycline (dox) compared to uninduced cells. No difference in IGF-IR α subunit expression levels was observed in doxycycline-induced cells treated with or without IGF-I. The endogenous IGF-IR (90 kDa), detected with the antibody against the β-subunit (H-60), was present in all cells, despite the treatment. The mutant receptor (50 kDa), also detected with the H-60 antibody was detected only in the stably transfected cells treated with doxycycline, whether stimulated with IGF-I or not. The mutant receptor protein was absent in uninduced cells. The same membranes were immunoblotted with an antibody against actin (45 kDa) to indicate sample loading. Densitometric values representing the levels of the endogenous and mutant IGF-I receptors in doxycycline induced and uninduced cells from representative assays are shown. (C and D) Two clonal cell lines, #39 (that was negative for IGF-IR-DN gene expression) and #89 (an rtTA-expressing parental clonal cell line) were used as negative controls. The mutant IGF-I receptor was absent in the doxycycline-induced control cell lines. In addition, the observed levels of the IGF-IR α-subunit in the doxycycline-induced control cells were not different from those observed in the uninduced cells.

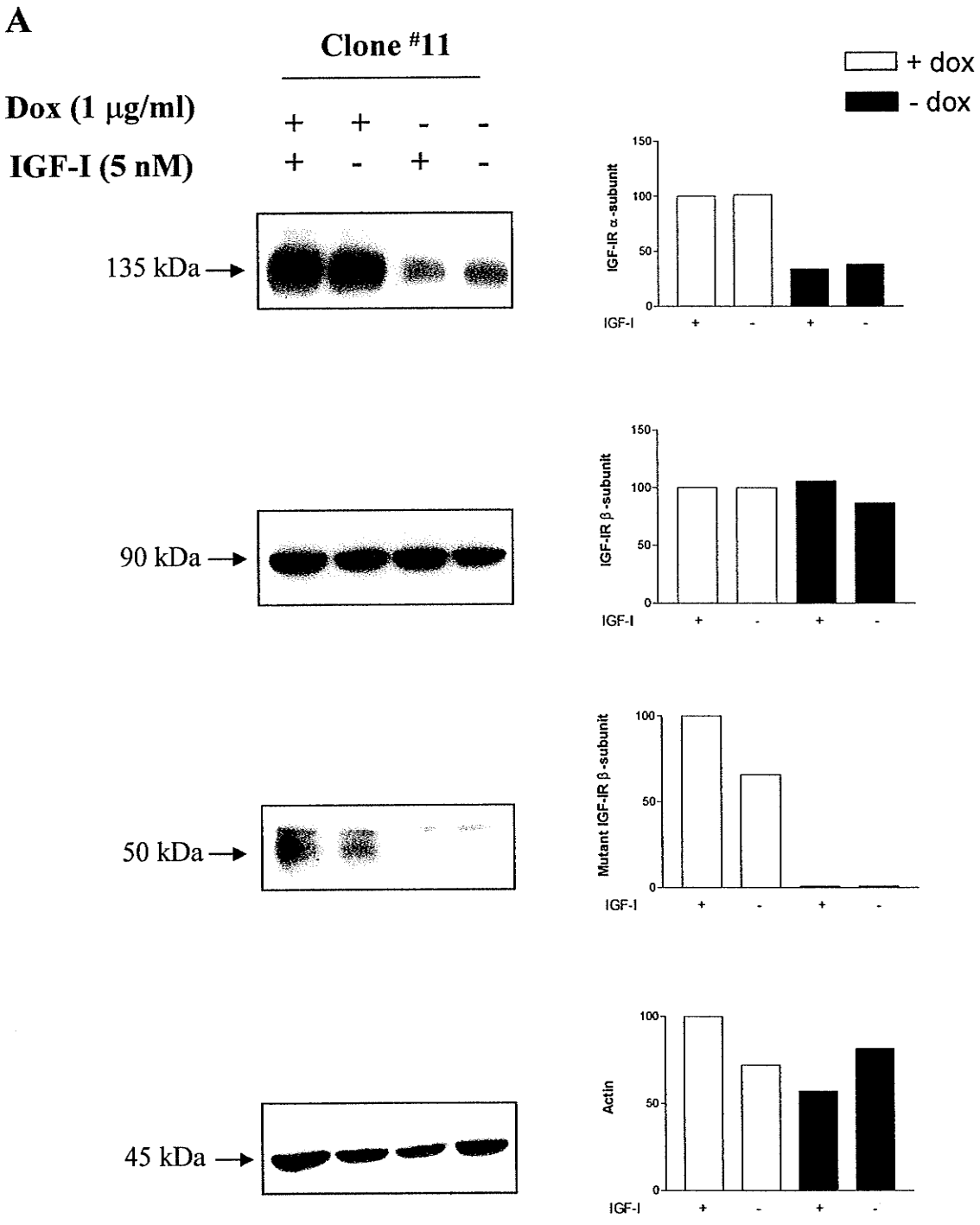
A
Clone #11
Dox (1 μg/ml)
IGF-I (5 nM)
+ + - -
+ - + -
135 kDa
90 kDa
50 kDa
45 kDa
+ dox
- dox
IGF-IR α-subunit
IGF-IR β-subunit
Mutant IGF-IR β-subunit
Actin
150
100
50
0
IGF-I
+ - + -

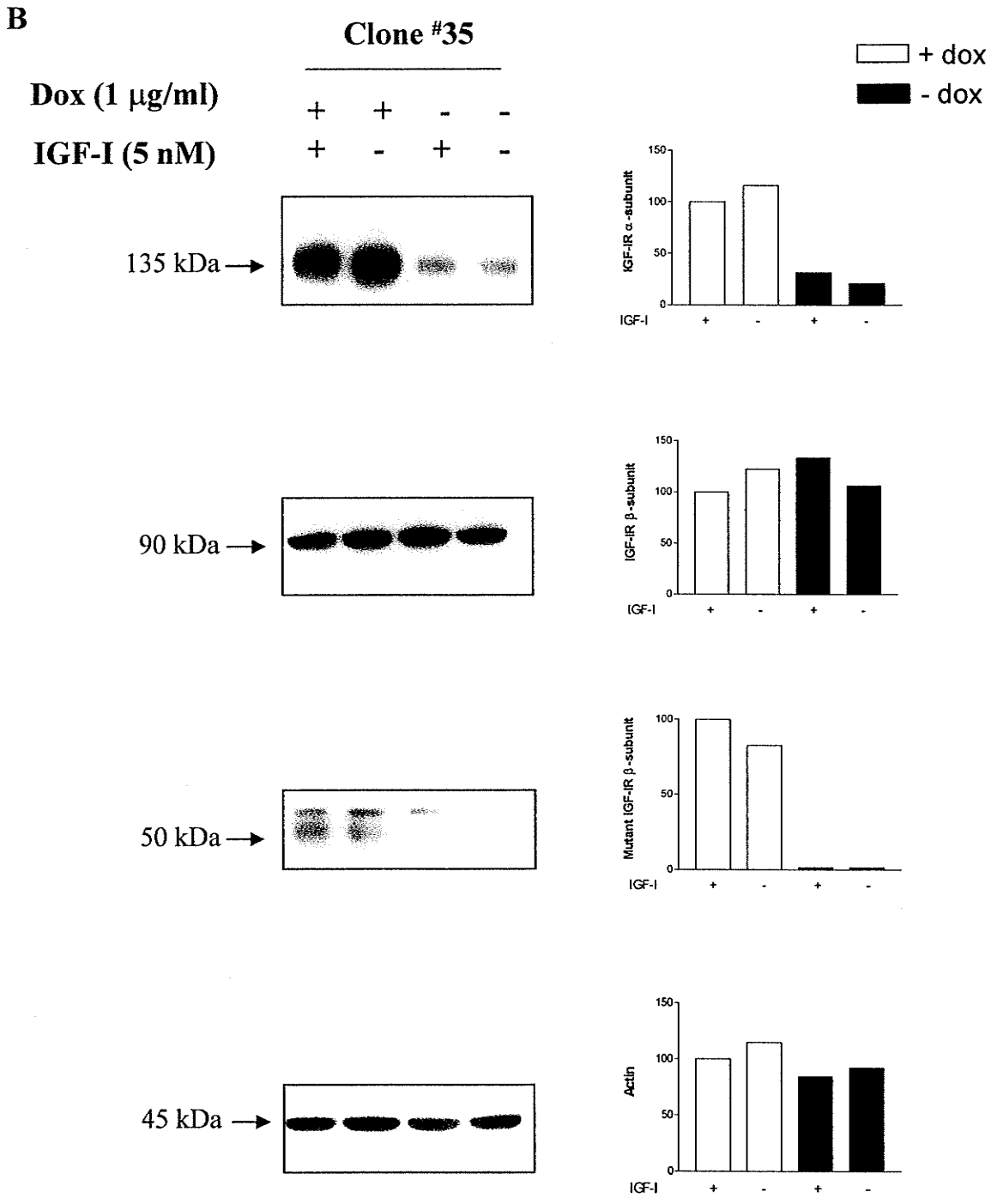
B
Clone #35
+ dox
- dox
Dox (1 μg/ml)
IGF-I (5 nM)
+ + - -
+ - + -
135 kDa
90 kDa
50 kDa
45 kDa
IGF-IR α-subunit
IGF-IR β-subunit
Mutant IGF-IR β-subunit
Actin
150
100
50
0
IGF-I
+ - + -

C

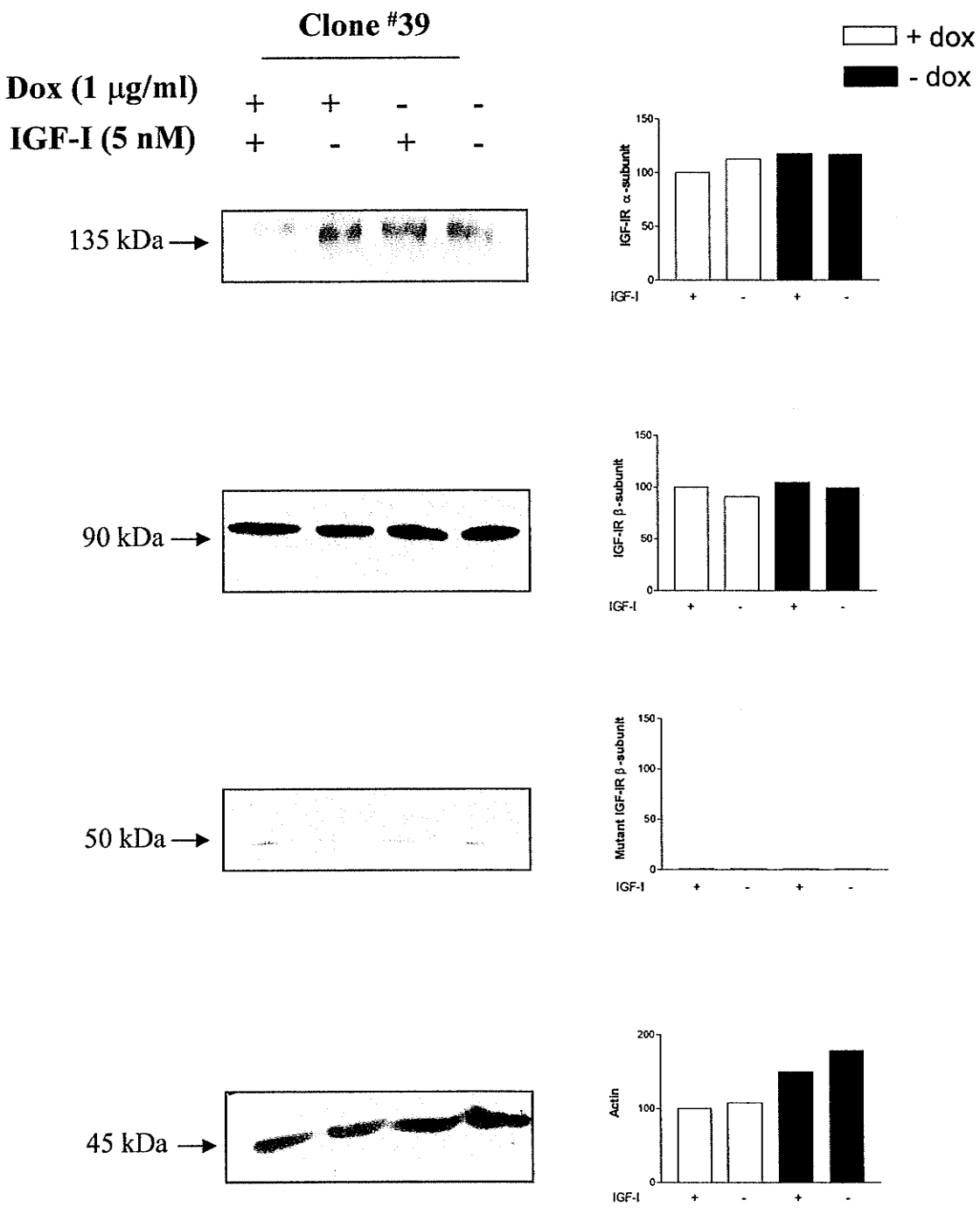
Clone #39
+ dox
- dox
Dox (1 μg/ml) + + - -
IGF-I (5 nM) + - + -
135 kDa
90 kDa
50 kDa
45 kDa
IGF-IR α-subunit
IGF-IR β-subunit
Mutant IGF-IR β-subunit
Actin
IGF-I
150
100
50
0
200

D

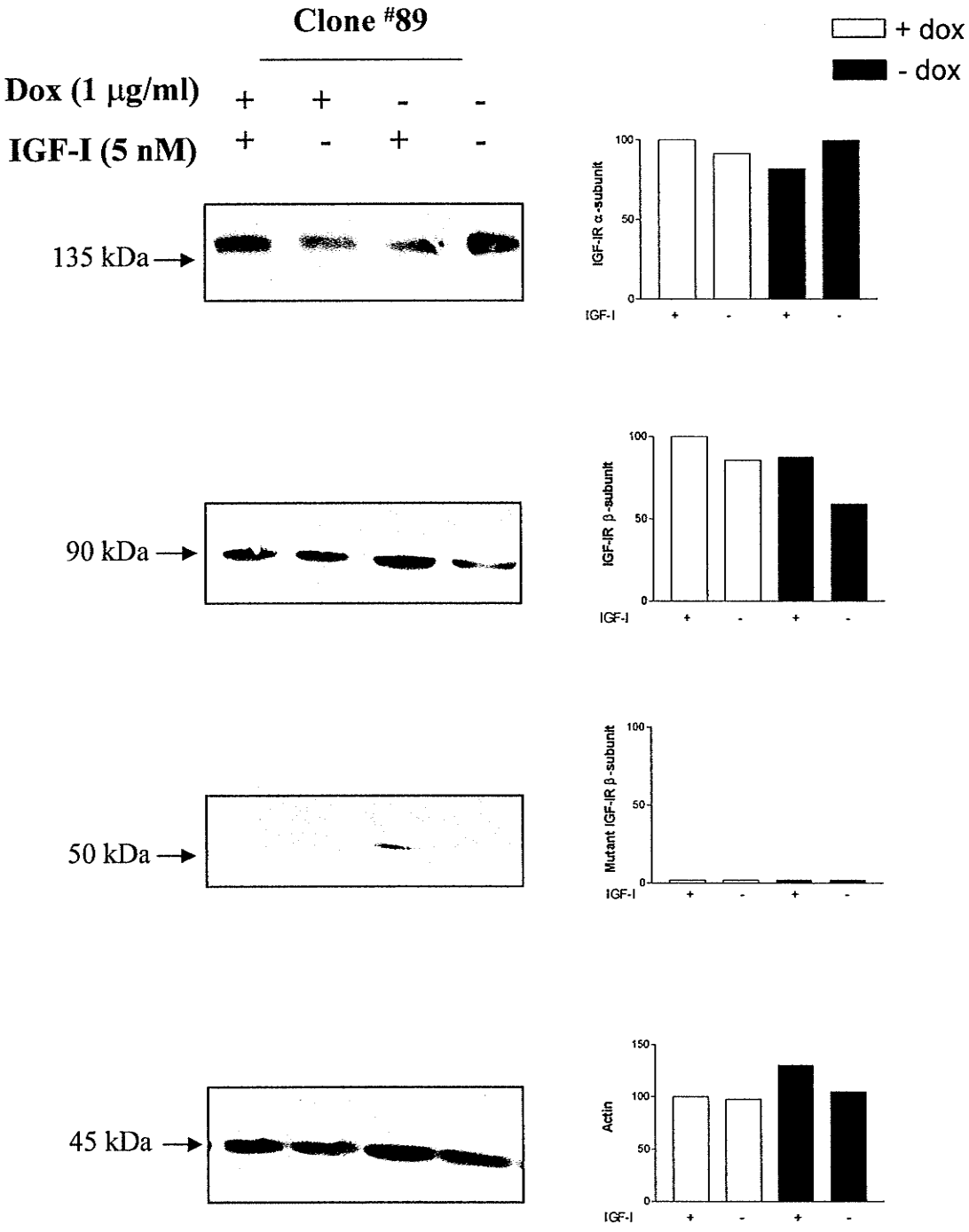
Clone #89
+ dox
- dox
Dox (1 μg/ml) + + - -
IGF-I (5 nM) + - + -
135 kDa
90 kDa
50 kDa
45 kDa
IGF-IR α-subunit
IGF-IR β-subunit
Mutant IGF-IR β-subunit
Actin
IGF-I
100
50
0
150

Figure 28. Effect of IGF-I on cell growth. Stably transfected MCF-7 cells were seeded on 96-well cell clusters in phenol-red free DMEM supplemented with 5% fetal bovine serum. The media was replaced with serum-free, phenol-red free DMEM, supplemented with 200 μg/ml bovine serum albumin and 10 μg/ml transferrin for 24 hours. The cells were then treated with 1 μg/ml doxycycline and 5 nM recombinant human IGF-I and the media replaced every two days. Cell proliferation was measured using the Crystal Violet staining assay. Cell growth was assessed in clonal lines 11, 35, 39 and 89 at Days 0, 2, 4 and 6 of IGF-I treatment. IGF-I stimulated growth in clonal lines 11 and 35 was evident in uninduced cells (▼), whereas cell growth was lower in doxycycline-induced cells (■). No cell proliferation was observed in either doxycycline-induced (Δ) or uninduced cells in the absence of IGF-I (◊). Doxycycline treatment did not prevent IGF-I induced cell growth in Clones $^{\#}$39 and $^{\#}$89, which were used as negative controls. Data collected from two independent experiments (with six measurements per experiment for each condition; n=12) were combined and are represented as means ± S.D.

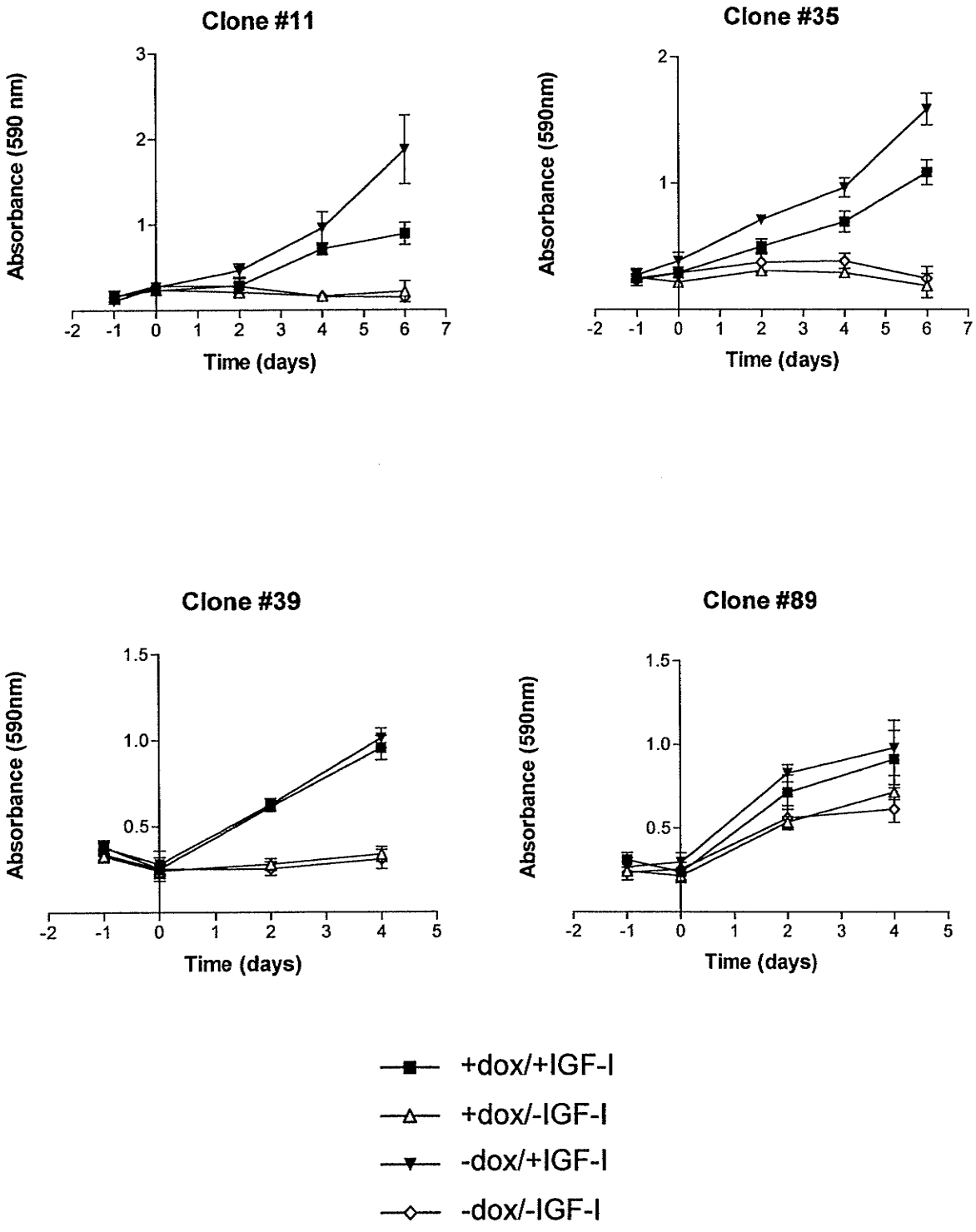
Clone #11
Absorbance (590 nm)
Time (days)
Clone #35
Absorbance (590nm)
Time (days)
Clone #39
Absorbance (590nm)
Time (days)
Clone #89
Absorbance (590nm)
Time (days)
+dox/+IGF-I
+dox/-IGF-I
-dox/+IGF-I
-dox/-IGF-I

Figure 29. A graphical representation of IGF-I stimulated cell growth in the presence and absence of doxycycline. Growth data expressed as a percentage of the value for the IGF-I stimulated cells grown with doxycycline (+dox/+IGF-I) at day 4 are shown. (A) IGF-I stimulated growth in the doxycycline-induced Clone #11 cells was lower (1.3 fold) than in uninduced cells. Similarly, IGF-I stimulated growth in the doxycycline-induced Clone #35 cells was lower (1.4 fold) than in uninduced cells. (B) No difference in cell growth was observed between the doxycycline-induced and uninduced control cell lines (Clones #39 and #89). Data collected from two experiments (with six measurements per experiment for each condition) were combined and are represented as means ± S.D. (n=12). Significant differences between the +dox/+IGF-I treatment group and the other treatment groups are illustrated. *, $P<0.05$; **, $P<0.01$; ***, $P<0.001$ (by Tukey test).

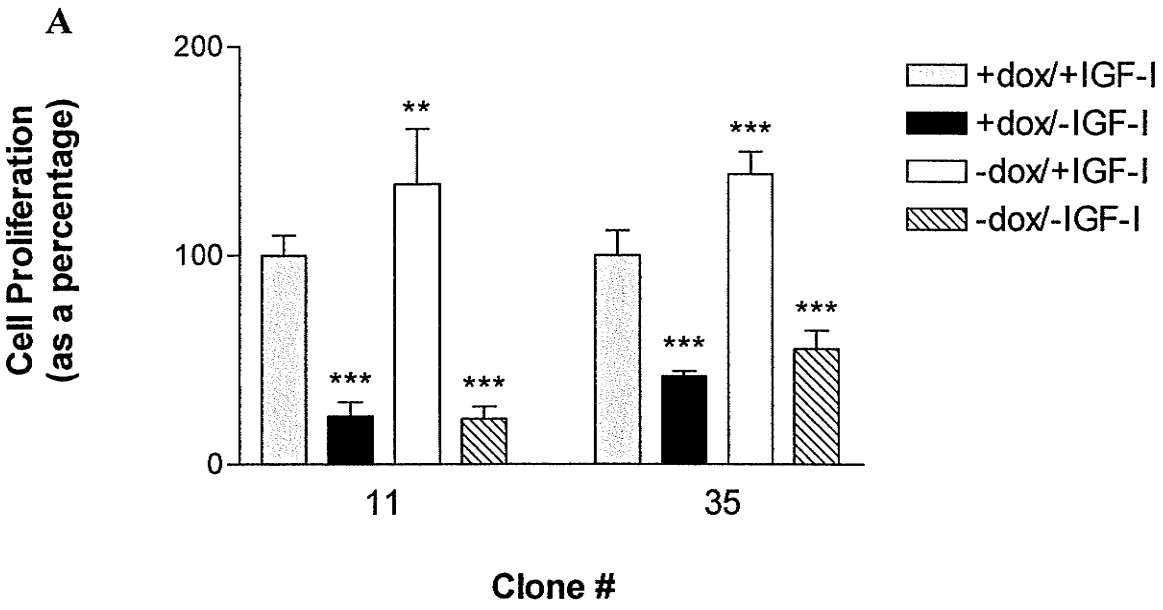
A
Cell Proliferation (as a percentage)
200
100
0
**
***
***
***
***
***
11
35
Clone #
+dox/+IGF-I
+dox/-IGF-I
-dox/+IGF-I
-dox/-IGF-I

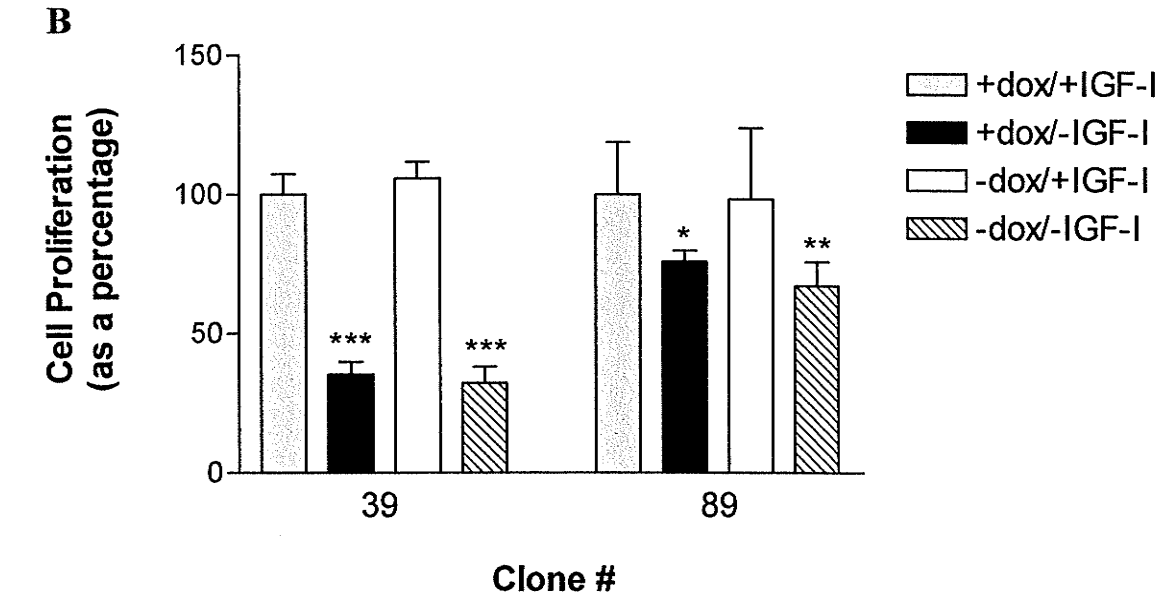
B
Cell Proliferation (as a percentage)
150
100
50
0
***
***
*
**
39
89
Clone #
+dox/+IGF-I
+dox/-IGF-I
-dox/+IGF-I
-dox/-IGF-I

Figure 30. Morphological studies of the stably transfected MCF-7 cells. Cell morphology was observed following doxycycline treatment and following IGF-I stimulation in the MCF-7 cells. Throughout the treatment period (Days 0, 2, 4, 6), the cells were flat and polygonal, exhibiting typical epithelial-like features. The doxycycline (dox) treated cells did not demonstrate an altered morphology. Shown here are representative photographs of Clone $^{\#}$35.

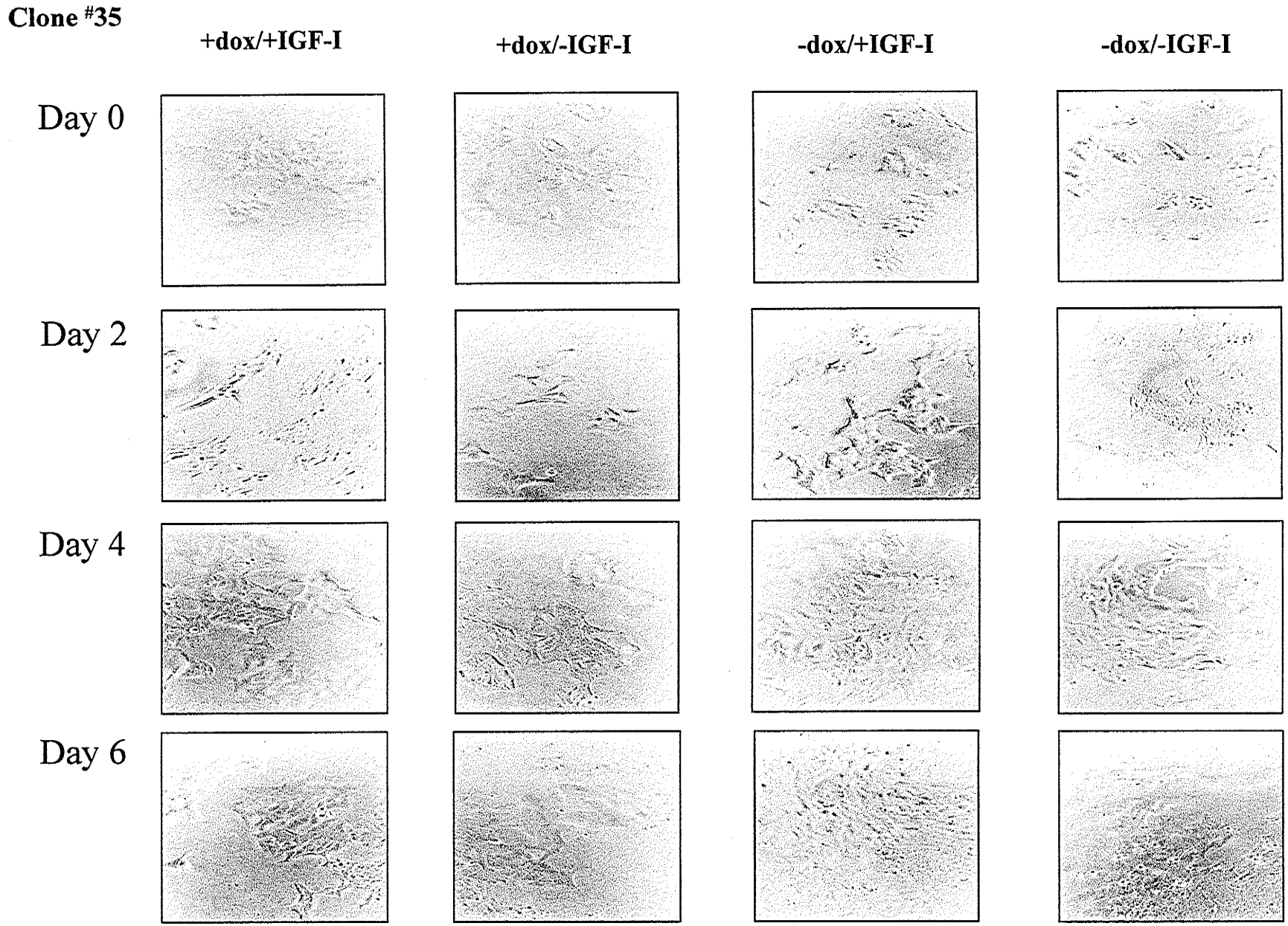
Clone #35
+dox/+IGF-I
+dox/-IGF-I
-dox/+IGF-I
-dox/-IGF-I
Day 0
Day 2
Day 4
Day 6

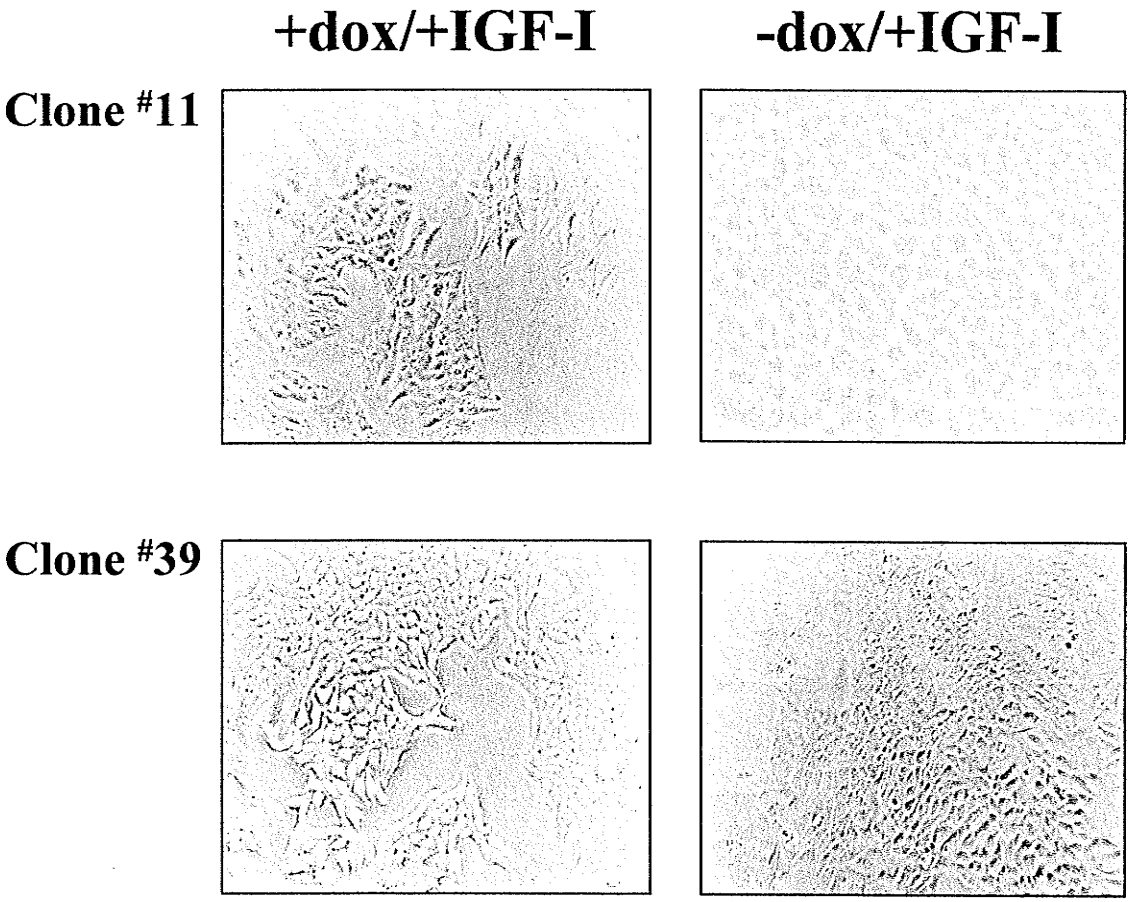

Figure 31. IGF-I stimulated growth of the stably transfected MCF-7 cells in the presence and absence of doxycycline. After 6 days, Clone #11 cells grown for 6 days with IGF-I in the absence of doxycycline visually appeared denser than those grown with doxycycline and IGF-I. Cell density was low in the doxycycline-induced Clone #11 cells. Clonal cell line, #39 (that was negative for IGF-IR-DN gene expression) was used as a negative control to demonstrate that IGF-I stimulated cell growth was not affected by the doxycycline treatment. These observations are consistent with findings from the cell growth assays (See Figure 28).

TABLES

Table 1. The primer sets for PCR amplification of cDNA derived from both mouse mammary glands and from the stably transfected MCF-7 human breast epithelial cells.

Target		Sequence (5′-3′)	Product Size (bp)	Concentration used
IGF-IR	Forward	CAC GAG GCT GAG AAG CT	502	200 nM
	Reverse	AGG CAT ACA GCA CTC CA		200nM
IGF-IR-R2	Reverse	CTC CGG CCA TCT GAA T	931	200nM
18S rRNA	Forward	GTA ACC CGT TGA ACC CCA TT	151	200 nM
	Reverse	CCA TCC AAT CGG TAG TAG CG		200 nM
rtTA	Forward	CTT AAT GAG GTC GGA ATC	250	200 nM
	Reverse	GTA GGC CGT GTA TCT GA		200 nM

Table 2. Profiles used for PCR amplification of cDNA derived from mouse mammary glands and MCF-7 human breast epithelial cells, using the PTC-100 Programmable Thermal Controller (MJ Research, Inc.).

	IGF-IR/IGF-IR-R2		18S rRNA		rtTA	
Step	**Temp (°C)**	**Time**	**Temp (°C)**	**Time**	**Temp (°C)**	**Time**
Initial	94	10 min	94	10 min	94	10 min
Denaturation (1 cycle)	94	1 min	94	30 sec	94	1 min
Annealing (1 cycle)	57	1 min	60	30 sec	52	1 min
Elongation (1 cycle)	72	1 min	72	30 sec	72	1 min
Final	72	10 min	72	10 min	72	5 min
Number of Cycles	40		35		45	

Table 3. PCR and Melt Curve Profiles for IGF-IR and 18S rRNA gene amplification, using the iCycler iQ Multi-Color Real Time PCR Detection System (Bio-Rad Laboratories).

Primers	IGF-IR and 18S rRNA			
Cycle	**Repeat**	**Step**	**Time**	**Temp (°C)**
1	1	1	4 min	95
2	35	**Denaturation** **Annealing** **Elongation**	15 sec 15 sec 30 sec	95 60 72
Melt Curve				
3	1	1	1 min	95
4	1	1	1 min	60
5	71	1	10 sec	60
6	1	1		25

Table 4. Antibodies used for Western Blot Analysis.

Target Protein	Primary Antibody (1° Ab)	Dilution of 1° Ab used	Primary Antibody (2° Ab)	Dilution of 2° Ab used
IGF-IR α-subunit	Polyclonal Rabbit anti-human[1]	1:200*	Polyclonal Goat anti-rabbit[8]	1:2500*
IGF-IR β-subunit	Polyclonal Rabbit anti-human[2]	1:200*	Polyclonal Goat anti-rabbit[8]	1:2500*
IGF-IR β-subunit	Polyclonal Rabbit anti-human[3]	1:200*	Polyclonal Goat anti-rabbit[8]	1:2500*
Phosphorylated IRS-1 & IGF-IR	Monoclonal Mouse anti-human[4]	1:500**	Polyclonal Goat anti-mouse[9]	1:2500**
Phospho-IRS-1	Polyclonal Rabbit anti-human[5]	1:200**	Polyclonal Goat anti-rabbit[8]	1:2500**
IRS-1	Polyclonal Rabbit anti-human[6]	1:200*	Polyclonal Goat anti-rabbit[8]	1:2500*
Actin	Polyclonal Goat anti-human[7]	1:500*	Polyclonal Bovine anti-goat[10]	1:2500*

*Diluted in 1X TBST (0.05% Tween 20) with 5% skim milk powder

**Diluted in 1X TBST (0.1% Tween 20) with 1% BSA

[1]IGF-IRα (N-20) (Santa Cruz Biotechnology, Inc., Santa Cruz, CA, USA)

[2]IGF-IRβ (C-20) (Santa Cruz Biotechnology, Inc.)

[3]IGF-IRβ (H-60) (Santa Cruz Biotechnology, Inc.)

[4]Phophotyrosine (PY-20) (BD BioSciences, Mississauga, Ontario, Canada)

[5]Phospho-IRS-1 (Ab-1) (Oncogene Research Products, Boston, MA, USA)

[6]IRS-1 (Upstate Biotechnology, Lake Placid, NY, USA)

[7]Actin (I-19) (Santa Cruz Biotechnology, Inc.)

[8, 9, 10]BioRad EIA grade affinity purified IgG (H+L) horse radish peroxidase conjugate secondary antibody (Bio-Rad Laboratories, Hercules, CA, USA)

Table 5. Real time RT-PCR analysis of IGF-IR gene expression using DNase I treated and untreated RNA extracted from mouse mammary gland tissues. DNase I treated and untreated RNA were reverse transcribed and real time PCR was performed in triplicate for each sample. Representative data from two independent experiments are shown. The standard errors in copy number values were greater in the PCR products generated using DNase I treated RNA compared to that of the products generated from DNase I untreated RNA. The copy number was also 10 fold less in the PCR products generated using the DNase I treated RNA. Real time quantitative data from RT-PCR products amplified from untreated RNA were used to determine IGF-IR gene expression during mouse mammary gland development.

Sample	DNase I treated RNA	Untreated RNA
IGF-IR		
8 week virgin	7.51×10^2	4.94×10^4
	1.26×10^3	4.44×10^4
	8.20×10^2	4.39×10^4
Mean	$\mathbf{9.43 \times 10^2}$	$\mathbf{4.59 \times 10^4}$
S.E.	$\mathbf{1.59 \times 10^2}$	$\mathbf{1.76 \times 10^3}$
day 10 involuting	1.25×10^4	2.24×10^4
	4.03×10^3	2.80×10^4
	1.79×10^3	2.89×10^4
Mean	$\mathbf{6.11 \times 10^3}$	$\mathbf{2.64 \times 10^4}$
S.E.	$\mathbf{3.26 \times 10^3}$	$\mathbf{2.03 \times 10^3}$
18S rRNA		
8 week virgin	9.98×10^7	1.43×10^9
	9.48×10^7	1.44×10^9
	1.05×10^8	1.31×10^9
Mean	$\mathbf{9.99 \times 10^7}$	$\mathbf{1.39 \times 10^9}$
S.E.	$\mathbf{2.95 \times 10^6}$	$\mathbf{4.18 \times 10^7}$
day 10 involuting	1.35×10^8	1.29×10^9
	1.24×10^8	1.19×10^9
	1.56×10^8	1.37×10^9
Mean	$\mathbf{1.38 \times 10^8}$	$\mathbf{1.28 \times 10^9}$
S.E.	$\mathbf{9.39 \times 10^6}$	$\mathbf{5.21 \times 10^7}$

Table 6. IGF-I stimulated growth in doxycycline-induced and uninduced cells. Growth data collected from cells treated with IGF-I was assessed by statistical analysis. Data were compared by Tukey tests at Days 0, 2, 4 and 6. IGF-I stimulated growth was significantly higher in (C) uninduced cells compared to (A) doxycycline-induced cells in clonal cell lines #11 and #35 at days 2, 4 and 6 of IGF-I treatment. Doxycycline treatment (A vs. C) did not prevent IGF-I induced cell growth in Clones #39 and #89, which were used as negative controls. Cell growth was not significantly different in (B) doxycycline-induced or (D) uninduced cells in the absence of IGF-I in all clonal cell lines. Data collected from two independent experiments (with six measurements per experiment for each condition; n=12) were combined and analyzed for statistical significance.

Abbreviations:

A = Supplemented serum-free media + doxycycline + IGF-I

B = Supplemented serum-free media + doxycycline - IGF-I

C = Supplemented serum-free media - doxycycline + IGF-I

D = Supplemented serum-free media - doxycycline - IGF-I

	IGF-I Treatment			
	Day 0	**Day 2**	**Day 4**	**Day 6**
Clone #11				
A vs. B	P > 0.05	P > 0.05	P < 0.001	P < 0.001
A vs. C	**P > 0.05**	**P < 0.001**	**P < 0.01**	**P < 0.001**
A vs. D	P > 0.05	P > 0.05	P < 0.001	P < 0.001
B vs. C	P > 0.05	P < 0.001	P < 0.001	P < 0.001
B vs. D	P > 0.05	P > 0.05	P > 0.05	P > 0.05
C vs. D	P > 0.05	P < 0.001	P < 0.001	P < 0.001
Clone #35				
A vs. B	P < 0.05	P < 0.001	P < 0.001	P < 0.001
A vs. C	**P > 0.05**	**P < 0.001**	**P < 0.001**	**P < 0.001**
A vs. D	P > 0.05	P < 0.01	P < 0.001	P < 0.001
B vs. C	P < 0.001	P < 0.001	P < 0.001	P < 0.001
B vs. D	P < 0.05	P > 0.05	P > 0.05	P > 0.05
C vs. D	P < 0.05	P < 0.001	P < 0.001	P < 0.001
Clone #39				
A vs. B	P > 0.05	P < 0.001	P < 0.001	-
A vs. C	**P > 0.05**	**P > 0.05**	**P > 0.05**	-
A vs. D	P > 0.05	P < 0.001	P < 0.001	-
B vs. C	P > 0.05	P < 0.001	P < 0.001	-
B vs. D	P > 0.05	P > 0.05	P > 0.05	-
C vs. D	P > 0.05	P < 0.001	P < 0.001	-
Clone #89				
A vs. B	P > 0.05	P < 0.05	P < 0.05	-
A vs. C	**P > 0.05**	**P > 0.05**	**P > 0.05**	-
A vs. D	P > 0.05	P > 0.05	P < 0.01	-
B vs. C	P > 0.05	P < 0.01	P < 0.01	-
B vs. D	P > 0.05	P > 0.05	P > 0.05	-
C vs. D	P > 0.05	P < 0.01	P < 0.001	-

REFERENCES

Abbott AM, Buenos R, Pedrini MT, Murray JM, Smith RJ (1991) Insulin-like growth factor I receptor gene structure. *Journal of Biological Chemistry* **179:** 10759-10763.

Adams TE, Epa VC, Garrett PJ, Ward CW (2000) Structure and function of the type 1 insulin-like growth factor receptor. *Cellular and Molecular Life Sciences* **57:** 1050-1093.

Alberts B, Bray D, Lewis J, Raff M, Roberts K, Watson JD (1989) The Molecular Biology of the Cell 2nd edition. Garland Publishing Inc. New York, NY.

Alfa MJ and Jay FT (1988) Distinct domains of recombinant human IFN-γ responsible for anti-viral effector function. *Journal of Immunology* **141:** 2472-2479.

Ambion's QuantumRNA 18S Internal Standards 1999. Manual Version 9907.

Arteaga CL and Osborne CK (1989) Growth inhibition of human breast cancer cells *in vitro* with an antibody against the type I somatomedin receptor. *Cancer Research* **49:** 6237-6241.

Baik MG, Lee MJ, Choi YJ (1998) Gene expression during involution of mammary gland (Review) *International Journal of Molecular Medicine* **2:** 39-44.

Bailyes EM, Naveacute BT, Soos MA, Orr SR, Hayward Ac, Siddle K (1997) Insulin receptor/IGF-I hybrids are widely distributed in mammalian tissues: quantification of insulin receptor species by selective immunoprecipitation and immunoblotting. *Biochemistry Journal* **327:** 209-215.

Baker J, Liu JP, Robertson EJ, Efstraiadis A (1993) Role of insulin-like growth factors in embryonic and postnatal growth. *Cell* **75:** 73-82.

Barbu V and Dautry F (1989) Northern blot normalization with a 28S rRNA oligonucleotide probe. *Nucleic Acids Research* **17:** 7115.

Baserga R (1985) The Biology of Cell Reproduction. Harvard University Press, Cambridge, MA.

Baserga R (1994) Oncogenes and the strategy of growth factors. *Cell* **79:** 927-930.

Baserga R (2000) The contradictions of the insulin-like growth factor 1 receptor. *Oncogene* **19:** 5574-5581.

Beitner-Johnson D and LeRoith D (1995) Insulin-like growth factor-I stimulated tyrosine phosphorylation of endogenous c-Crk. *The Journal of Biological Chemistry* **270:** 5187-5190.

Beitner-Johnson D, Blakesley VA, Shen-Orr Z, Jimenez M, Stannard B, Wang LM, Pierce J, LeRoith D (1996) The proto-oncogene product c-Crk associates with insulin receptor substrate-1 and 4PS. Modulation by insulin growth factor-I (IGF) and enhanced IGF-I signaling. *Journal of Biological Chemistry* **271:** 9287-90.

Blakesley VA, Scrimgeour A, Esposito D, LeRoith D (1996) Signaling via insulin-like growth factor-I receptor: Does it differ from insulin receptor signaling? *Cytokine & Growth Factor Reviews* **7:** 153-159.

Bondy CA, Werner H, Roberts Jr CT, LeRoith D (1990) Cellular pattern of insulin-like growth factor-I (IGF-I) and type I IGF receptor gene expression in early organogenesis: comparison with IGF-II gene expression. *Molecular Endocrinology* **4:** 1386-1398.

Buhler TA, Dale TC, Kieback C, Humphreys RC, Rosen JM (1993) Localization and quantification of the Wnt-2 gene expression in mouse mammary development. *Developmental Biology* **155:** 87-96.

Bustin SA (2000) Absolute quantification of mRNA using real-time reverse transcription polymerase chain reaction assays. *Journal of Molecular Endocrinology* **25:** 169-193.

Butler AA, Blaskesley VA, Koval A, deJong A, Groffen J, LeRoith D (1997) *In vivo* regulation of CrkII and CrkL proto-oncogenes in the uterus by insulin-like growth factor-I. *The Journal of Biological Chemistry* **44:** 27660-27664.

Butler AA and LeRoith D (2001) Minireview: tissue-specific *versus* generalized gene targeting of the *igf1* and *igf1r* genes and their roles in insulin-like growth factor physiology. *Endocrinology* **142:** 1685-1688.

Butler AA, Yakar S, Gewolb IH, Karas M, Okubo Y, LeRoith D (1998) Insulin-like growth factor-I receptor signal transduction: at the interface between physiology and cell biology. *Comparative Biochemistry and Physiology* **121:** 19-26.

Campbell PG and Baumrucker CR (1986) Characterization of insulin-like growth factor-1/somatomedin C receptors in the bovine mammary gland. *Journal of Dairy Science* **69:** 218A.

Campochiaro PA, Chang M, Ohsato M, Vinores SA, Nie Z, Hjelmeland L, Mansukhani A, Basiliso C, Zach DJ (1996) Retinal degeneration in transgenic mice with photoreceptor-specific expression of a dominant-negative fibroblast growth factor receptor. *The Journal of Neuroscience* **16:** 1679-1688.

Clarke RB, Howell A, Anderson E (1997) Type I insulin-like growth factor receptor gene expression in normal human breast tissue treated with oestrogen and progesterone. *British Journal of Cancer* **75:** 251-257.

Coleman-Krnacik S and Rosen JM (1994) Differential temporal and spatial gene expression of fibroblast growth factor family members during mouse mammary gland development. *Molecular Endocrinology* **8:** 218-229.

Coppola D, Ferber A, Miura M, Sell C, D'Ambrosia C, Rubin R, Baserga R (1994) A functional insulin-like growth factor I receptor is required for the mitogenic and transforming activities of the epidermal growth factor receptor. *Molecular and Cellular Biology* **14:** 11663-11669.

Cullen KJ, Yee D, Sly WS, Perdue J, Hampton B, Lippman ME, Rosen N (1990) Insulin-like growth factor receptor expression and function in human breast cancer. *Cancer Research* **50:** 48-53.

Daniel CW and Silberstein GB (1987) Postnatal development of the rodent mammary gland. *In* The Mammary Gland: Development, Regulation and Function, edited by MC Neville and CW Daniel. Plenum Press, New York, NY, pp. 1-36.

DeChiara TM, Efstratiadis A, Robertson EJ (1990) A growth-deficiency phenotype in heterozygous mice carrying an insulin-like growth factor II receptor gene disrupted by targeting. *Nature* **345:** 78-80.

Dehoff MH, Elgin RG, Collier RJ, Clemmons DR (1988) Both type I and II insulin-like growth factor receptor binding increase during lactogenesis in bovine mammary tissue. *Endocrinology* **122:** 2412-2417.

DeLeeuw WJ, Slagboom PE, and Viij J (1989) Quantitative comparison of mRNA levels in mammalian tissues: 28S ribosomal RNA levels as an accurate internal control. *Nucleic Acids Research* **17:** 10137-10138.

Di Fiore MSH (1987) Atlas of Normal Histology, 6th Edition, edited by VP Eroschecnko. Lea & Febiger, Philadelphia, PA.

Dudek H, Datta SR, Franke TF, Birnbaum MJ, Yao R, Cooper GM, Segal RA, Kaplan DR, Greenberg ME (1997) Regulation of neuronal survival by the serine-threonine protein kinase Akt. *Science* **275:** 661-665.

Dufourny B, Alblas J, van Teeffelen HA, van Schaik FM, Van Der Burg B, Steenbergh PH, Sussenbach JS (1997) Mitogenic signaling of insulin-like growth factor I in MCF-7 human breast cancer cells requires phosphatidylinositol 3-kinase and is independent of mitogen-activated protein kinase. *Journal of Biological Chemistry* **272:** 31163-31171.

Dunbar ME and Wysolmerski JJ (2001) Mammary ductal and alveolar development: lesson learned from genetically manipulated mice. *Microscopy Research and Technique* **52:** 163-170.

Dupont J and LeRoith D (2001) Insulin and Insulin-like growth factor I receptors: similarities and differences in signal transduction. *Hormone Research* **55:** 22-26.

Dupont J and LeRoith D (2001) Insulin-like growth factor I and oestradiol promote cell proliferation of MCF-7 breast cancer cells: new insights into their synergistic effects. *Journal of Clinical Pathology: Molecular Pathology* **54:** 149-154.

Dupont J, Karas M, LeRoith D (2000) The potentiation of estrogen on insulin-like growth factor I action in MCF-7 human breast cancer cells includes cell cycle components. *Journal of Biological Chemistry* **275:** 35893-901.

Eshet R, Werner B, Klinger B, Silbergeld A, Laron Z, LeRoith D, Roberts Jr CT (1993) Up-regulation of insulin-like growth factor-I (IGF-I) receptor gene expression in patients with reduced serum IGF-I levels. *Journal of Molecular Endocrinology* **10:** 115-120.

Federici M, Porzio O, Zucaro L, Fusco A, Borboni P, Lauro D, Sesti G (1997) Distribution of insulin/insulin-like growth factor-I hybrid receptors in human tissues. *Molecular and Cellular Endocrinology* **129:** 121-126.

Fife RS and Sledge Jr GW (1998) Effects of doxycycline on cancer cells *in vitro* and *in vivo*. *Advancements in Dental Research* **12:** 94-96.

Fisher DE (1994) Apoptosis in cancer therapy: crossing the threshold. *Cell* **78:** 539-542.

Forsyth IA (1989) Growth factors in mammary gland function. *Journal of Reproduction and Fertility* **85:** 759-770.

Frattali AL and Pessin JE (1993) Relationship between α subunit ligand occupancy and β subunit autophosphorylation in insulin/insulin-like growth factor-I hybrid receptors. *Journal of Biological Chemistry* **268:** 7393-7400.

Freundlieb S, Baron U, Bonin AL, Gossen M, Bujard H (1997) Use of tetracycline-controlled gene expression systems to study mammalian cell cycle. *Methods in Enzymology* **283:** 159-172.

Furlanetto RW and DiCarlo JN (1994) Somatomedin-C receptors and growth effects in human breast cancer cells maintained in long-term tissue culture. *Cancer Research* **44:** 2122-2128.

Gebauer G, Jager W, Lang N (1998) mRNA expression of components of the insulin-like growth factor system in breast cancer cell lines tissues and metastatic breast cancer cells. *Anticancer Research* **18:** 1191-1196.

Geier A, Haimshon M, Beery R, Hemi R, Lunenfeld B (1992) Insulin-like growth factor-1 inhibits cell death induced by cycloheximide in MCF-7 cells: a model system for analyzing control of cell death. *In Vitro Cell Developmental Biology* **28A:** 725-729.

Gossen M and Bujard H (1992) Tight control of gene expression in mammalian cells by tetracycline-responsive promoters. *Proceedings of the National Academy of Sciences of the United States of America* **89:** 5547-5551.

Gossen M, Freundlieb S, Bender G, Müller G, Hillen W, Bujard H (1995) Transcriptional activation by tetracyclines in mammalian cells. *Science* **268:** 1766-1769.

Grimberg A and Cohen P (2000) Role of insulin-like growth factors and their binding proteins in growth control and carcinogenesis. *Journal of Cellular Physiology* **183:** 1-9.

Gunther EJ, Belka GK, Wertheim GBW, Wang J, Hartman JH, Boxer RB, Chodosh LA (2002) A novel doxycycline-inducible system for the transgenic analysis of mammary gland biology. *The FASEB Journal* **16:** 283-292.

Guvakova MA and Surmacz E (1997) Overexpressed IGF-I receptors reduce estrogen growth requirements, enhance survival and promote cell-cell adhesion in human breast cancer cells. *Experimental Cell Research* **231:** 149-162.

Hadsell DL and Bonnette SG (2000) IGF and insulin action in the mammary gland: lessons from transgenic and knockout models. *Journal of Mammary Gland Biology and Neoplasia* **5:** 19-30.

Hadsell DL, Greenberg NM, Fligger JM, Baumrucker RR, Rosen JM (1996) Targeted expression of des (1-3) human insulin-like growth factor I in transgenic mice influences mammary gland development and IGF-binding protein expression. *Endocrinology* **137:** 321-330.

Herskowitz I (1987) Functional inactivation of genes by dominant negative mutations. *Nature* **329:** 219-222.

Jackson D, Bresnick J, Roswell I, Crafton T, Poulsom R, Stamp G, Dickson C (1997) Fibroblast growth factor receptor signaling has a role in lobuloalveolar development of the mammary gland. *Journal of Cell Science* **110:** 1261-1268.

Jones JI and Clemmons DR (1995) Insulin-like growth factors and their binding proteins: biological actions. *Endocrine Reviews* **16:** 3-34.

Kaleko M, Rutter WG, Miller AD (1990) Overexpression of the human insulin-like growth factor 1 receptor promotes ligand-dependent neoplastic transformation. *Molecular and Cellular Biology* **10:** 464-473.

Karey KP and Sirbasku DA (1988) Differential responsiveness of human breast cancer cell lines MCF-7 and T47-D to growth factors and 17-β estradiol. *Cancer Research* **48:** 4083-4092.

Khandwala HM, McCuthcheon IE, Flyvbjerg A, Friend KE (2000) The effects of insulin-like growth factors on tumorigenesis and neoplastic growth. *Endocrine Reviews* **21:** 215-244.

Kleinberg DL (1998) Role of IGF-I in normal mammary development. *Breast Cancer Research and Treatment* **47:** 201-208.

Kleinberg DL, Feldman M, Ruan W (2000) IGF-I: an essential factor in terminal end bud formation and ductal morphogenesis. *Journal of Mammary Gland Biology and Neoplasia* **5:** 7-17.

Kleinberg DL, Ruan WF, Catanese V, Newman CB, Feldman M (1990) Non-lactogenic effects of growth hormone on growth, and insulin-like growth factor-I messenger ribonucleic acid of rat mammary gland. *Endocrinology* **126:** 3274-3276.

Kleinman D, Karas M, Roberts Jr CT, LeRoith D, Phillip M, Segev Y, Levy J, Sharoni Y (1995) Modulation of insulin-like growth factor I (IGF-I) receptors and membrane-associated IGF-binding proteins in endometrial cancer cells by estradiol. *Endocrinology* **136:** 2531-7.

Kulik G, Klippel A, Weber MJ (1997) Antiapoptotic signaling by the insulin-like growth factor I receptor, phosphatidylinositol 3-kinase and Akt. *Molecular and Cellular Biology* **17:** 1595-1606.

Lee AV and Yee D (1995) Insulin-like growth factors and breast cancer. *Biomedicine and Pharmacotherapy* **49:** 415-421.

Leeson RL, Leeson SL, Paparo AA (1985) The female reproductive system. *In* Textbook of Histology 5th edition. W.B. Saunders Company, Philadelphia, PA, pp. 462-491.

LeRoith D, Werner H, Beitner-Johnson D, Roberts Jr CT (1995) Molecular and cellular aspects of the insulin-like growth factor 1 receptor. *The Endocrine Society* **16:** 143-163.

Liu J, Baker J, Perkins AS, Robertson EJ, Efstratiadis A (1993) Mice carrying null mutations of the genes encoding insulin-like growth factor 1 (*igf-1*) and type 1 IGF receptor (*igf-1r*). *Cell* **75:** 59-72.

Lorenzino L (1998) Structure and function of the insulin-like growth factor I receptor. *Breast Cancer Research and Treatment* **47:** 235-253.

Ludwig T, Eggenschwiler J, Fisher P, D'Ercole AJ, Davenport ML, Efstratiadis A (1996) Mouse mutants lacking the type 2 IGF receptor (IGF2R) are rescued from perinatal lethality in Igf1 and Igf1r null backgrounds. *Developmental Biology* **177:** 517-535.

Lund LR, Romer J, Thomasset N, Solberg H, Pyke C, Bissell MJ, Dano K, Werb Z (1996) Two distinct phases of apoptosis in mammary gland involution: proteinase-independent and dependent pathways. *Development* **122:** 181-193.

Marti A, Lazar H, Ritter P, Jaggi R (1999) Transcription factor activities and gene expression during mouse mammary gland involution. *Journal of Mammary Gland Biology and Neoplasia.* **4:** 145-152.

Maniatis T, Fritstch EF, Sambrook J (1982) Molecular Cloning: a laboratory manual. Cold Spring Harbor Laboratory, Cold Spring Harbor, NY.

Matsuda M, Tanaka S, Nagata S, Kojima A, Kurata T, Shibuya M (1992) Two species of human CRK cDNA encode proteins with distinct biological activities. *Molecular and Cellular Biology* **12:** 3482-3489.

Mauro L, Salerno M, Panno ML, Bellizzi D, Sisci D, Miglietta A, Surmacz E, Ando S (2001) Estradiol increases IRS-1 gene expression and insulin signaling in breast cancer cells. *Biochemistry and Biophysical Research and Communication* **288:** 685-689.

McCormack JT and Greenwald GS (1974) Evidence for a preimplantation rise in oestradiol-17 beta levels on day 4 of pregnancy in the mouse. *Journal of Reproduction and Fertility* **41:** 297-301.

Myal Y, Shiu R, Bhaumick B, Bala B (1984) Receptor binding and growth-promoting activity of insulin-like growth factors in human breast cancer cells (T-47D) in culture. *Cancer Research* **44:** 5486-5490.

Myers Jr MG, Xun XJ, Cheatham B, Jachna BR, Glasheen EM, Backer JM, White MF (1993) IRS-I is a common element in insulin and insulin-like growth factor-I signaling to the phophatidylinositol 3′ kinase. *Endocrinology* **132:** 1421-1430.

Neuenshwander Jr SRCT, Schwartz A, Wood TL, Roberts Jr CT, Hennighausen L, LeRoith D (1996) Involution of the lactating mammary gland is inhibited by the IGF system in a transgenic mouse model. *Journal of Clinical Investigation* **97:** 2225-2232.

Nilsson A, Isgaard J, Lindahl A, Dahlstrom A, Skottner A, Isaksson OJP (1986) Regulation by growth hormone of number of chondrocytes containing IGF-1 in rat growth plate. *Science* **233:** 571-574.

Peruzzi F, Prisco M, Dews M, Salomoni P, Grassilli E, Romano G, Calabretta B, Baserga M (1999) Multiple signaling pathways of the insulin-like growth factor 1 receptor in protection from apoptosis. *Molecular and Cellular Biology* **19:** 7203-7215.

Peyrat JP and Bonneterre J (1992) Type I IGF receptor in human breast diseases. *Breast Cancer Research and Treatment* **22:** 59-67.

Pollak MN (1998) Endocrine effects of IGF-I on normal and transformed breast epithelial cells: potential relevance to strategies for breast caner treatment and prevention. *Breast Cancer Research and Treatment* **47:** 209-217.

Pollak MN, Polychronakos C, Yousefi S, Richard M (1988) Characterization of insulin-like growth factor I receptors of human breast cancer cells. *Biochemical and Biophysical Research Communications* **154:** 326-331.

Prager D, Li H, Asa S, Melmed S (1994) Dominant-negative inhibition of tumorigenesis *in vivo* by human insulin-like growth factor 1 receptor mutant. *Proceedings of the National Academy of Sciences of the United States of America* **91:** 2181-2185.

Prager D, Yamasaki H, Weber MM, Gebremedhin S, Melmed S (1992) Human insulin-like growth factor I receptor in pituitary cells is suppressed by a dominant negative mutant. *Journal of Clinical Investigation* **990:** 2117-2122.

Resnicoff M, Burgaud JL, Rotman HL, Abraham D, Baserga R (1995) The insulin-like growth factor I receptor protects tumor cells from apoptosis *in vivo*. *Cancer Research* **55:** 2463-2469.

Richert MM and Wood TL (1999) The insulin-like growth factors (IGF) and IGF type I receptor during postnatal growth of the murine mammary gland: sites of messenger ribonucleic acid expression and potential functions. *Endocrinology* **140:** 454-461.

Rillema JA (1994) Development of the mammary gland and lactation. *Trends in Endocrinology Metabolism* **5:** 149-154.

Roth RA, Yonezawa K, Pierce S, Steele-Perkins G (1991) Substrates of the insulin and insulin-like growth factor 1. *In* Modern Concepts of Insulin-like Growth Factors, edited by EM Spencer. Elsevier, Amsterdam, pp. 505-515.

Ruan W and Kleinberg DL (1999) Insulin-like growth factor is essential for terminal end bud formation and ductal morphogenesis during mammary development. *Endocrinology* **140:** 5075-5081.

Ruan W, Newman CB, Kleinberg DL (1992) Intact and amino-terminally shortened forms of insulin-like growth factor I induce mammary gland differentiation and development. *Proceedings of the National Academy of Sciences of the United States of America* **89:** 10872-10876.

Rubini M, Hongo A, D'Ambrosia C, Baserga R (1997) The IGF-I receptor in mitogenesis and transformation of mouse embryo cells: role of receptor number. *Experimental Cell Research* **230:** 284-292.

Rubin R and Baserga R (1995) Biology of disease - insulin-like growth factor-1 receptor - its role in cell proliferation apoptosis and tumorigenecity. *Laboratory Investigation* **73:** 311-331.

Ryding ADS, Sharp MGF, Mullins JJ (2001) Conditional transgenic technologies. *Journal of Endocrinology* **171:** 1-14.

Saji S, Sakaguchi H, Andersson S, Warner M, Gustafsson, J (2001) Quantitative analysis of estrogen receptor proteins in rat mammary gland. *Endocrinology* **142:** 3177-3186.

Samani AA and Brodt P (2001) The receptor for the type I insulin-like growth factor and its ligands regulate multiple cellular functions that impact on metastasis. *Surgical Oncology Clinics of North America* **10:** 289-312.

Sasaoka T, Ishiki M, Sawa T, Ishihara H, Takata Y, Imamura T, Usui I, Olefsky JM, Kobayashi M (1996) Comparison of the insulin and insulin-like growth factor 1 mitogenic intracellular signaling pathways. *Endocrinology* **137:** 4427-4434.

Schmittegen TD and Zakrajsek BA (2000) Effect of experimental treatment on housekeeping gene expression: validation by real-time quantitative RT-PCR. *Journal of Biochemical and Biophysical Methods* **46:** 69-81.

Sell C, Dumenil G, Deveaud C, Miura M, Coppola D, Deanelis T, Rubin R, Efstratiadis A, Baserga R (1994) Effect of a null mutation of the insulin-like growth factor I receptor gene on growth and transformation of mouse embryo fibroblasts. *Molecular and Cellular Biology* **14:** 3604-3612.

Siddle K, Soos MA, Field CE, Nave BT (1994) Hybrid and atypical insulin/insulin-like growth factor I receptors. *Hormone Research* **41:** 56-65.

Silberstein GB (2001) Postnatal mammary gland morphogenesis. *Microscopy Research and Technique* **52:** 155-162.

Snedeker S, Brown C, Di Augustine R (1991) Expression and functional properties of transforming growth factor α and epidermal growth factor during mouse mammary gland ductal morphogenesis. *Developmental Biology* **88:** 276-280.

Soos MA, Field CE, Siddle K (1993) Purified hybrid insulin/insulin-like growth factor-I receptors bind insulin-like growth factor-I, but not insulin, with high affinity. *Biochemistry Journal* **290:** 419-425.

Soule HD, Vazguez J, Long A, Albert S, Brennan M (1973) A human cell line from a pleural effusion derived from a breast carcinoma. *Journal of the National Cancer Institute* **51:**1409-16.

Stewart A, Johnson M, May F, Westley B (1990) Role of insulin-like growth factors and the type 1 insulin-like growth factor receptor in the estrogen-stimulated proliferation of human breast cancer cells. *Journal of Biological Chemistry* **265:** 21172-21178.

Strange R, Feng L, Saurer S, Burkhardt A, Friss RR (1992) Apoptotic cell death and tissue remodeling during mouse gland involution. *Development* **115:** 49-58.

Surmacz E (2000) Function of the IGF-I receptor in breast cancer. *Journal of Mammary Gland Biology and Neoplasia* **5:** 95-105.

Tamm I and Kikuchi T (1990) Insulin-like growth factor-1 (IGF-1), insulin, and epidermal growth factor (EGF) are survival factors for density inhibited, quiescent BALB/c-3T3 murine fibroblasts. *Journal of Cell Physiology* **143:** 494-500.

Ten Hoeve J, Morris C, Heisterkamp H, Groffen J (1993) Isolation and chromosomal localization of CRKL, a human Crk-like gene. *Oncogene* **8:** 2469-2474.

Thellin O, Zorzi W, Lakaye B, DeBorman B, Coumans B, Hennen G, Grisar T, Igout A, Heinen E (1999) Housekeeping genes as internal standards: use and limits. *Journal of Biotechnology* **75:** 291-295.

Topper YJ and Freeman CS (1980) Multiple hormone interactions in the developmental biology of the mammary gland. *Physiological Reviews* **60:** 1049-1106.

Ullrich A, Gray A, Tam AW, Yang-Feng T, Tsubokawa M, Collins C, Henzel W, Le Bon T, Kathuria S, Chen E, Jacons S, Francke U, Ramachandran J, Fujita-Yamaguchi (1986) Insulin-like growth factor I receptor primary structure: comparison with insulin receptor suggests structural determinant that define functional specificity. *EMBO Journal* **5:** 2503-2512.

Valentinis B and Baserga R (2001) IGF-I receptor signaling in transformation and differentiation. *Journal of Clinical Pathology: Molecular Pathology* **54:**133-137.

Van Der Berg B, Rutteman GR, Blankenstein MA, De Laat SW, Van Zoelen EJJ (1988) Mitogenic stimulation of human breast cancer cells in a growth factor-defined medium: synergistic action of insulin and estrogen. *Journal of Cellular Physiology* **134:** 101-108.

Varma H and Conrad SE (2002) Antiestrogen ICI 182,780 decreases proliferation of insulin-like growth factor I (IGF-I)-treated MCF-7 cells without inhibiting IGF-I signaling. *Cancer Research* **62:** 3985-3991.

Venditti M, Iwasiow B, Orr FW, Shiu RPC (2002) C-myc gene expression alone is sufficient to confer resistance to antiestrogen in human breast cancer cells. *International Journal of Cancer* **99:** 35-42.

Wada J, Liu ZZ, Alvares K, Kumar A, Wallner E, Makino H, Kanwar YS (1993) Cloning of cDNA for the alpha subunit of mouse insulin-like growth factor 1 receptor and the role of the receptor in metanephric development. *Proceedings of the National Academy of Sciences of the United States of America* **90:** 10360-10364.

Walker NI, Bennett RE, Kerr JF (1989) Cell death by apoptosis during involution of the lactating breast in mice and rats. *American Journal of Anatomy* **185:** 19-26.

Ward CW, Garrett TPJ, McKern NM, Lou M, Cosgrove LJ, Sparrow LG, Frenkel MJ, Hoyne PA, Elleman TC, Adams TE, Lovrecz GO, Lawrence LJ, Tulloch PA (2001) The three dimensional structure of the type I insulin-like growth factor receptor. *Journal of Clinical Pathology: Molecular Pathology* **54:** 125-132.

Werner H (1999) Molecular biology of the type I IGF receptor. *In* Contemporary Endocrinology: The IGF System, edited by R Rosenfield and C Roberts Jr. Humana Press Inc., Totowa, NJ, pp. 63-88.

Werner H and LeRoith D (2000) New concepts in regulation and function of the insulin-like growth factors: implications for understanding normal growth and neoplasia. *Cellular and Molecular Life Sciences* **57:** 932-942.

Werner H, Woloschak M, Adamo M, Shen-Orr Z, Roberts Jr CT, LeRoith D (1989) Developmental regulation of the rat insulin-like growth factor I receptor gene. *Proceedings of the National Academy of Sciences of the United States of America* **86:** 7451-7455.

White MF and Yenush L (1998) The IRS-signaling system: a network of docking proteins that mediate insulin and cytokine action. *Current Topics in Microbiology and Immunology* **228:** 179-208.

Xie W, Patterson A, Chin E, Nabell LM, Kudlow JE (1997) Targeted expression of a dominant-negative epidermal growth factor in the mammary gland of transgenic mice inhibits pubertal mammary duct development. *Molecular Endocrinology* **11:** 1766-1781.

Zhang X and Yee D (2000) Tyrosine kinase signaling in breast cancer insulin-like growth factors and their receptors in breast cancer. *Breast Cancer Research* **2:** 170-175.